2013

CYCLIC RESISTANCE - SHEAR WAVE VELOCITY RELATIONSHIPS FOR MONTEREY AND CABO ROJO CARBONATE SAND

Michael Lowell Dobling
University of Rhode Island, michael_dobling@my.uri.edu

CYCLIC RESISTANCE - SHEAR WAVE VELOCITY RELATIONSHIPS FOR MONTEREY AND CABO ROJO CARBONATE SAND

BY

MICHAEL LOWELL DOBLING

A THESIS SUBMITTED IN PARTIAL FULFILLMENT OF THE

REQUIREMENTS FOR THE DEGREE OF

MASTER OF SCIENCE

IN

OCEAN ENGINEERING

UNIVERSITY OF RHODE ISLAND

2013

MASTER OF SCIENCE THESIS

OF

MICHAEL LOWELL DOBLING

APPROVED:

Thesis Committee:

Major Professor Chris Baxter

Aaron Bradshaw

Gopu Potty

Nasser Zawia

DEAN OF THE GRADUATE SCHOOL

UNIVERSITY OF RHODE ISLAND

2013

Abstract

The current state-of-the-practice for estimating the liquefaction potential of a site is to use correlations with the in situ tests such as the Standard Penetration Test (SPT), Cone Penetration Test (CPT), and shear wave velocity (V_s). In each method, field data has been collected from sites where either liquefaction or no liquefaction was observed following earthquakes.

These methods assume that the in situ measurement (SPT, CPT, or V_s) captures the liquefaction resistance of all coarse-grained soils. This has been shown to be true for the SPT and CPT, where resistance is related to the relative density of the soil. In contrast, shear wave velocity is a function of a soils' void ratio, and soils with the same void ratio can have very different soil behavior. There is some evidence in the literature that the relationship between cyclic resistance and shear wave velocity may be soil specific, meaning that using a field-based V_s approach for liquefaction resistance for all sands may not be appropriate.

The objective of this study is to evaluate whether the Cyclic Resistance (CRR) - Shear Wave Velocity (V_s) relationship is soil specific for two soils. A laboratory program was developed and twenty-nine undrained cyclic triaxial tests were conducted with shear wave velocity measurements taken using bender elements.

Eleven cyclic triaxial tests were conducted on Monterey sand and eighteen cyclic triaxial tests were conducted on a calcareous sand from Cabo Rojo, Puerto Rico. Three

different void ratios were chosen for each sand and the data was compared against published data on comparable soils.

The results suggest that the liquefaction resistance of both the Monterey and Cabo Rojo calcareous sand is lower than predicted by the field-based approaches of Andrus and Stokoe (2000) and Kayen et al. (2013). In this case, using the field-based shear wave velocity approach would significantly overestimate the liquefaction resistance of the Cabo Rojo and Monterey sands. More research is needed, however, the results of this study support the hypothesis that the Cyclic Resistance - Shear Wave Velocity relationship is soil specific.

Acknowledgements

This thesis would not be possible without the help of so many people in so many ways.

Dr. Christopher P. Baxter for exciting my interest in soil mechanics and guiding me from initiation to completion of this thesis. Without his help and guidance, this research would still be ongoing.

Dr. Aaron Bradshaw for letting me use his laboratory equipment and providing advice and assistance during my laboratory testing.

My fellow students for developing the equipment and procedures used for this research, along with constant support and assistance. Kevin Broccolo and Fred Pease for their technical assistance throughout the duration of my research.

My mother, Barbara Dobling, because without her I would be still lost in the cornfields of Iowa.

Most importantly my best friend and wife, Jenna, for her continuous support and encouragement with all matters. Thank you.

Table of Contents

List of Tables

List of Figures

1. Introduction

1.1 Statement of the Problem

Liquefaction is a phenomenon that describes the loss of strength and significant deformation of cohesionless soils following undrained loading. The most common manifestation of liquefaction occurs in loose saturated sands during earthquakes.

The current state-of-the-practice for determining the liquefaction potential of a site with high seismicity is based on in situ tests. The Standard Penetration Test (SPT), the Cone Penetration Test (CPT) and shear wave velocity (V_s) test are examples of the in situ tests most commonly used.

All field based approaches follow these three steps: 1) in situ data (blow counts, tip resistance, shear wave velocity) is collected from sites following earthquakes, 2) cyclic shaking, Cyclic Stress Ratio (CSR), at each site is approximated using the simplified approach, and 3) a boundary line is drawn between the sites of liquefaction occurrence and no occurrence, this boundary line is called the Cyclic Resistance Ratio (CRR).

The CSR was originally developed by Seed and Idriss (1971) with the following expression:

$$CSR = \frac{\tau_{av}}{\sigma`_v} = 0.65 \left(\frac{a_{max}}{g}\right)\left(\frac{\sigma_v}{\sigma`_v}\right) r_d \qquad 1.1$$

where τ_{av}= average equivalent uniform cyclic shear stress caused by the earthquake and is assumed to be 0.65 of the maximum induced stress; a_{max}= peak horizontal ground surface acceleration; g = acceleration of gravity; $\sigma`_v$ =initial effective vertical (overburden) stress at the depth in question; σ_v = total overburden stress at the same depth; and r_d = shear stress reduction coefficient to adjust for the flexibility in the soil profile.

The SPT approach is based on evidence of liquefaction occurrence (sand boils, lateral spreading, and sand expulsion) and non-occurrence. For each site where an earthquake was known to occur, a correlation was made between the CSR and $(N_1)_{60}$, defined as the blow count corrected to an overburden stress of approximately 100 kPa and a hammer efficiency of 60%. These correlations assumed an effective stress of 100 kPa and used magnitude scaling factors to an earthquake magnitude (M) of 7.5.

The resultant data point from each site was plotted in Figure 1-1 and a best fit line was created to show the boundary of liquefaction and non-liquefaction occurrence.

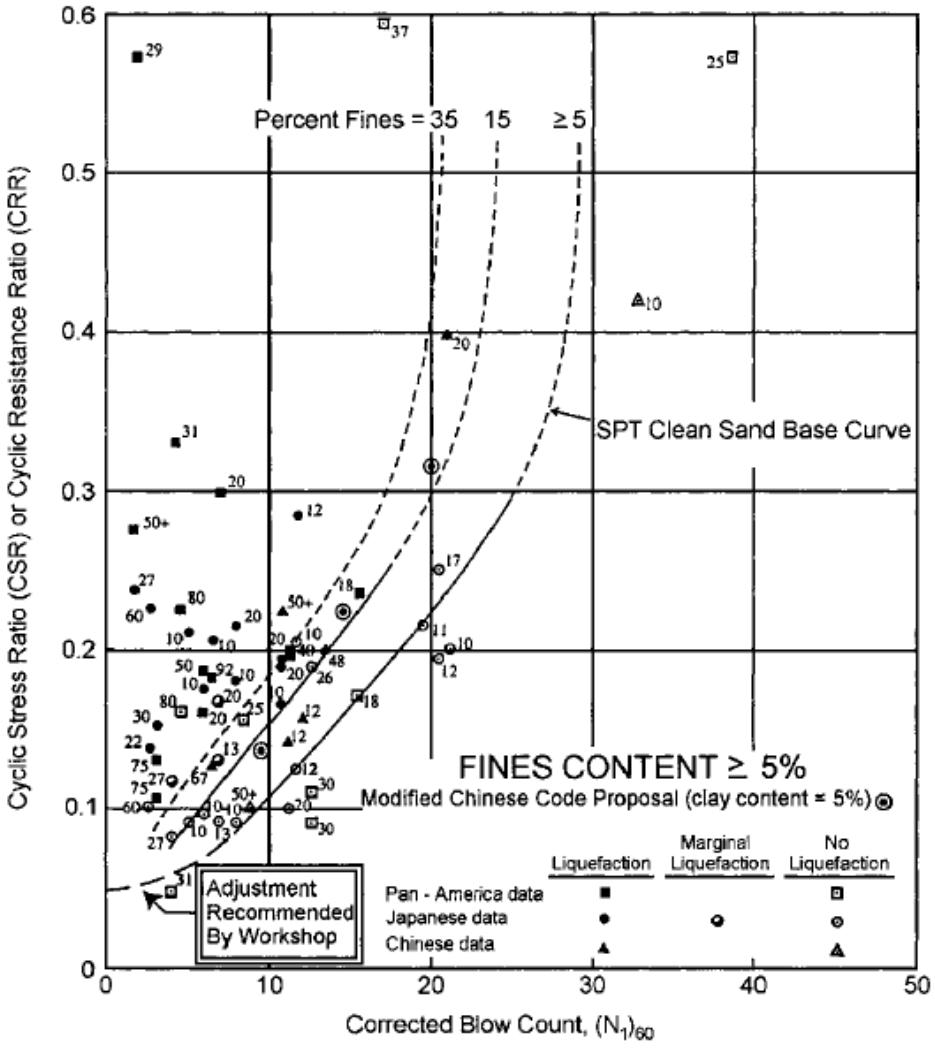

Figure 1-1: Correlation between CRR and $(N_1)_{60}$ for a vertical effective stress of 100 kPa and an earthquake moment magnitude of 7.5 (Seed et al. 1985; Youd et al. 2001).

The Cone Penetration Test (CPT) procedure was developed by Robertson and Wride (1998) and is the current standard-of-practice for evaluating liquefaction potential using the CPT (Youd et al. 2001). This method correlates CRR from the tip-resistance normalized (q_{c1N}) to an effective overburden stress of approximately 100kPa. Similar

to the SPT-based method, field observations of liquefaction and non-liquefaction occurrence were made, a CSR was calculated for each site, and a CRR - (q_{c1N}) boundary line was made. These data points were then plotted in Figure 1-2 and a best fit line was drawn to determine the liquefaction potential boundary.

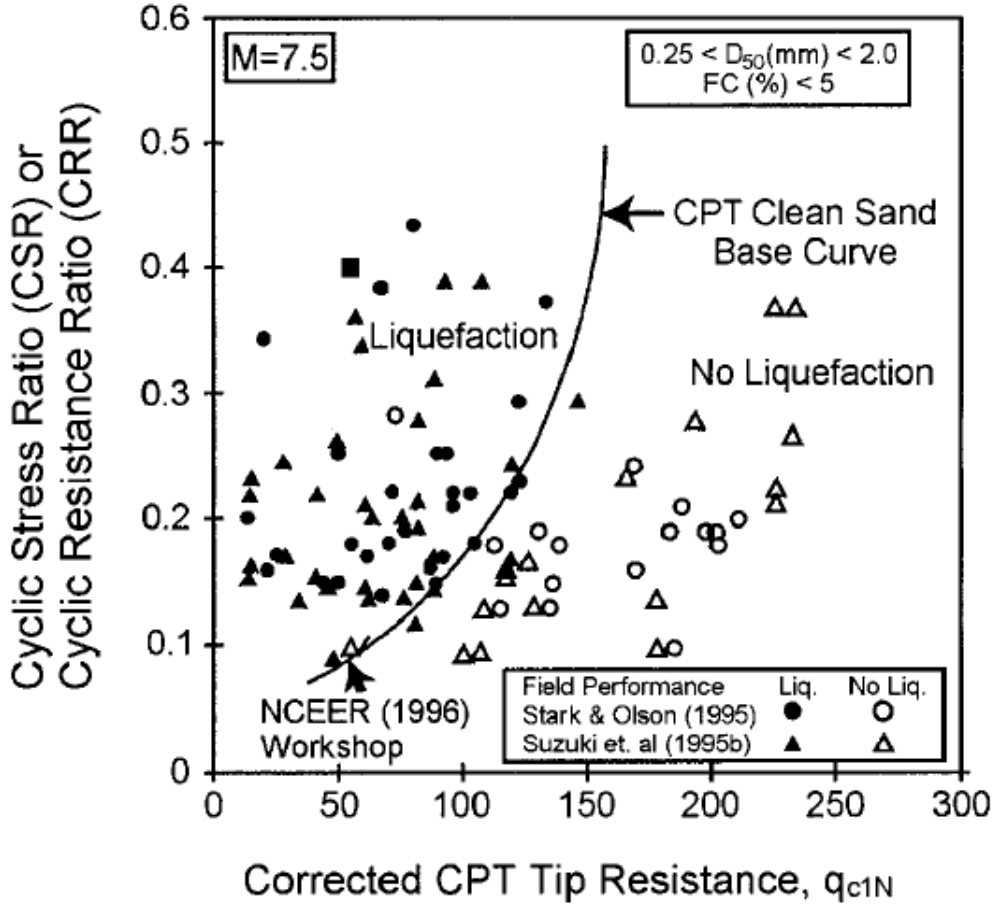

Figure 1-2: CPT- based cyclic resistance correlation (Robertson and Wride 1998; Youd et al. 2001)

The shear wave velocity (V_s) based method was developed by Andrus and Stokoe (2000) and is the current standard-of-practice for evaluating liquefaction potential using V_s. In this method, the CSR is calculated for each site and a correlation made with the

measured shear wave velocity normalized to an effective stress of 100 kPa (V_{s1}). Similar to the SPT and CPT correlations, sites were selected by field observations of liquefaction occurrence and no occurrence and then plotted in Figure 1-3.

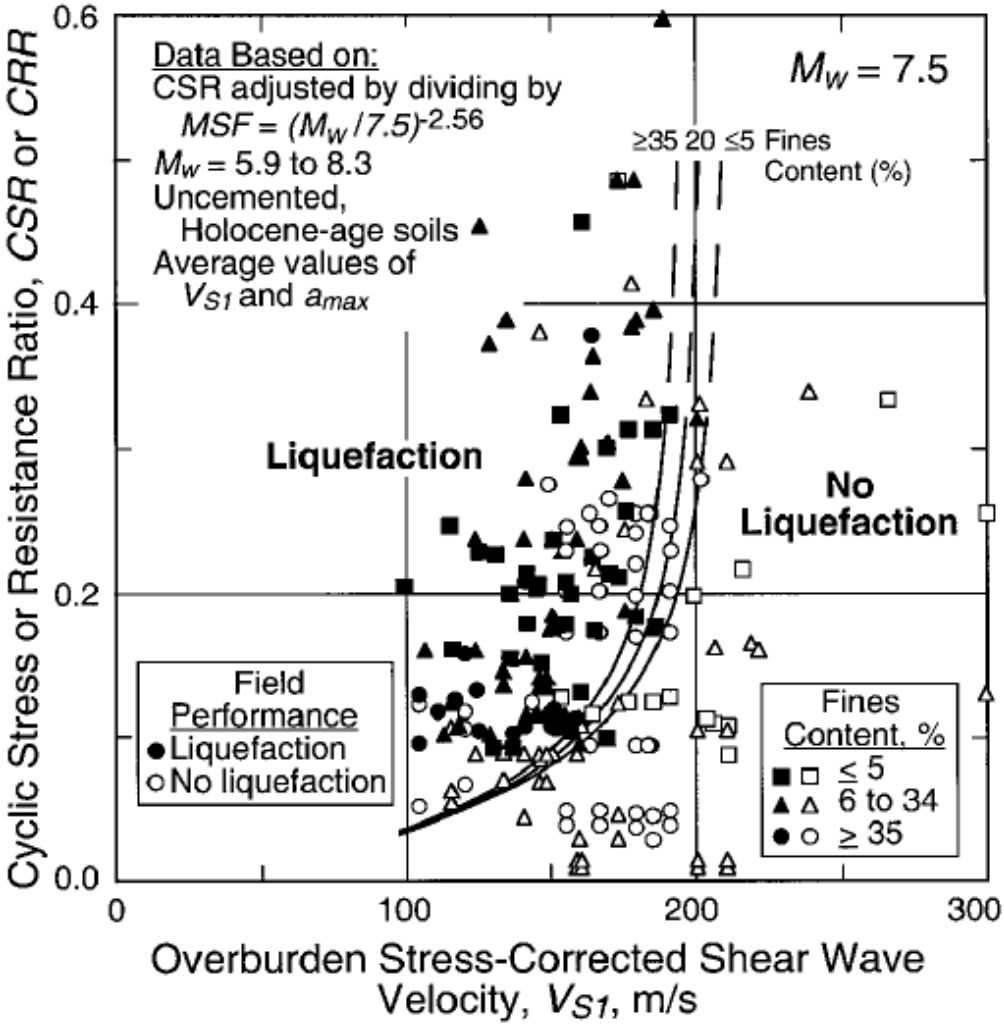

Figure 1-3: V_{s1} – based cyclic resistance correlation for clean sands (Andrus and Stokoe 2000)

Previous researchers, Andrus and Stokoe (2000) and Kayen et al. (2004 and 2013) have made correlations for the CRR – V_{s1} relationships based on in situ testing of sites with

liquefaction and non-liquefaction, however these databases need to be expanded. A more economical alternative to in situ testing is to expand these databases with cyclic triaxial testing in the laboratory.

Baxter et al. (2008) and Tokimatsu et al. (1986) conducted cyclic triaxial testing of various soil types and those studies showed the CRR $-V_S$ correlations are independent of stress history and sample preparation methods, but highly dependent on soil types.

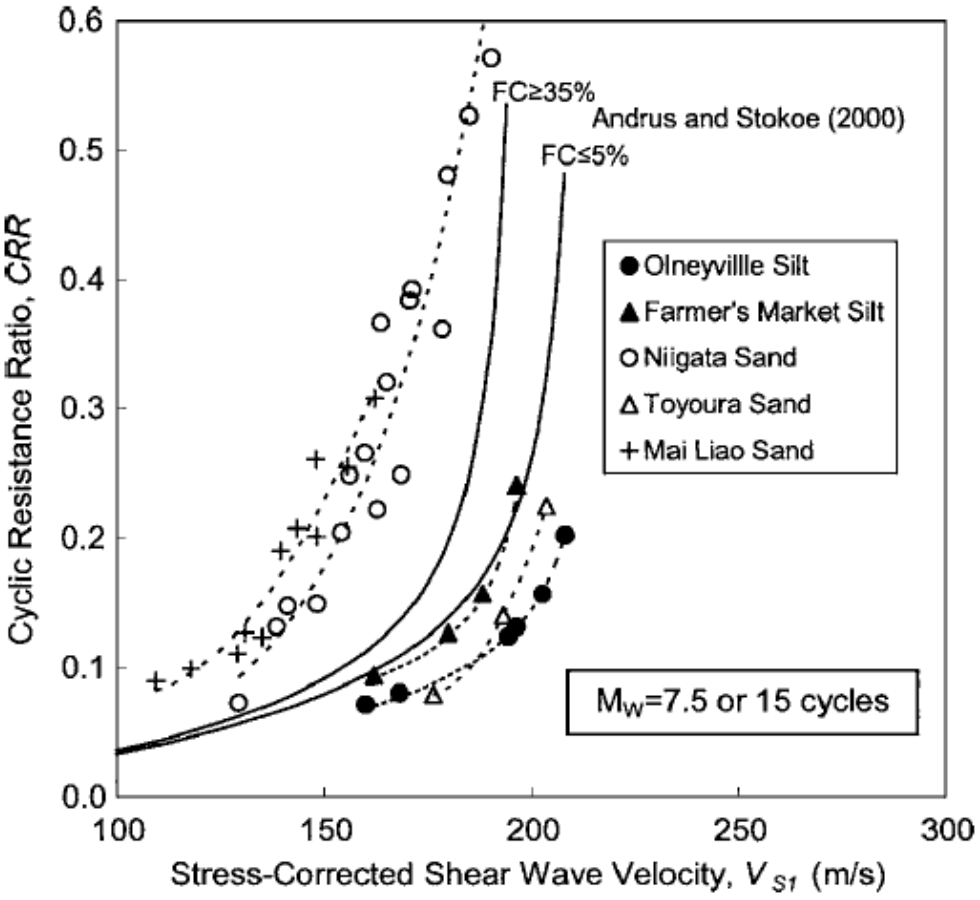

Figure 1-4: Comparison between the existing field-based correlations of Andrus and Stokoe (2000) and laboratory-based correlations from two silts and three clean sands (Baxter et al. 2008)

1.2 Objective of thesis

The objective of this study is to evaluate whether the relationship between Cyclic Resistance Ratio (CRR) - Shear Wave Velocity (V_s) is soil specific for two soils.

To study this problem, a detailed laboratory testing program was developed for conducting undrained stress controlled cyclic triaxial tests with shear wave velocity measurements. Samples of a calcareous sand from Cabo Rojo, Puerto Rico and Monterey silica sand were prepared to various relative densities and values of shear wave velocity.

This thesis is divided into five chapters. This chapter provides a statement of the problem and the objective of the thesis. Chapter two is a literature review of published studies on correlations between cyclic resistance ratio and shear wave velocity, including research on calcareous sands. Chapter three is a description of the laboratory testing program developed for determining the cyclic resistance ratio-shear wave velocity relationships. The results of the laboratory testing program and presented and discussed in Chapter four, along with a comparison with published data and recommendations for future work. Chapter five is a conclusion of the research and recommendations for future studies.

2. Literature Review

2.1 Field-based Approach to Assessment of Liquefaction Potential Using Shear Wave Velocity

The use of shear wave velocity (V_s) as a field based approach for the assessment of liquefaction resistance is soundly based because both V_s and CRR are similarly influenced by the void ratio, effective confining stresses, stress history, and geologic age. Some advantages of V_s measurements include: (1) V_s measurements can be made in soils hard to penetrate with CPT and SPT or extract undisturbed samples and (2) V_s is a basic mechanical property of soil materials and measurements can be performed on laboratory samples, allowing direct comparisons between laboratory and field behavior.

Andrus and Stokoe (2000) were the first to document a field-based correlation between a soils' shear wave velocity and liquefaction resistance. They evaluated shear wave velocity measurements from cases of liquefaction and non-liquefaction for 26 earthquakes and more than 70 different sites using analytical studies, laboratory studies and field performance data.

From this study, they recommended categorizing the soils into three groups: sands and gravels with average fines content less than or equal to 5%; sands and gravels with average fines content of 6% to 34%; and sands and silts with average fines content greater than or equal to 35%.

Kayen et al. (2004) collected a database of in situ shear wave velocity measurements using surface wave techniques at more than 300 sites worldwide of liquefaction occurrence and non-liquefaction. More recently Kayen et al. (2013) expanded this global database to 422 cases of V_s liquefaction performance.

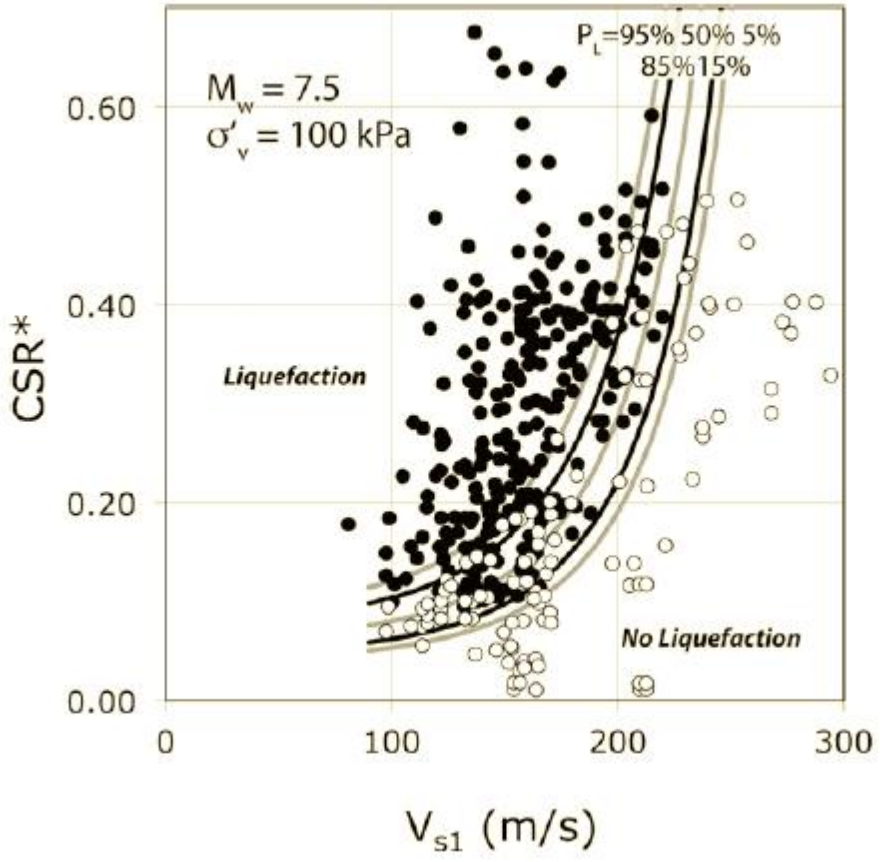

Figure 2-1: Plot showing means of field case histories of liquefaction (solid circles) and non-liquefaction (open circles) and new probabilistic curves (Kayen et al. 2013)

From their analysis shown in Figure 2-1, they recommended a deterministic curve with a factor of safety (FS) = 1.7 and corresponding with a P_L = 15% while the P_L = 50% corresponds with an FS of = 1.0.

This expanded database aids practicing engineers in determining liquefaction potential for specific locations, but the database needed to be further expanded to cover more soil types and locations. In situ tests can be expensive and time consuming, however a more economical option to in situ measurements is laboratory testing.

2.2 Laboratory Studies of the Relationship between Cyclic Resistance and Shear Wave Velocity

Shear wave velocity is a basic mechanical property of soil materials and measurements can easily be performed on laboratory samples, allowing direct comparisons between laboratory and field behavior. This advantage of shear wave velocity measurements can eliminate the need for in situ measurements or collection of undisturbed samples of loose granular material, which is very challenging and expensive.

Undrained cyclic triaxial tests are commonly used to measure the cyclic stress ratio (CSR_{tx}) and shear wave velocity (V_s), where the CRR_{tx} is defined as the cyclic stress ratio causing liquefaction in a given number of cycles. The number of cycles is determined by using an equivalent number of cycles concept, which for an earthquake magnitude of 7.5 is fifteen cycles as initially proposed by Seed (1979). The equivalent number of cycles concept replicates the duration of an earthquake to an equivalent number of cyclic loading cycles.

Shear wave velocity can be measured in the laboratory with a variety of different methods with the most common being the use of bender elements. A shear wave is generated from a bender element mounted on one end of the sample, and the received wave is detected at the other end of the sample (Baxter et al. 2008). The shear-wave velocity is then calculated by either the tip-to-tip distance or point of first arrival and then divided by the travel time of the wave.

Robertson et al. (1995) and Chillarige (1977) compared the results of shear wave measurements made in the laboratory with bender elements to shear wave measurements made in the field with seismic cone equipment. They showed that the results are comparable when corrections are used for overburden stress and anisotropic conditions (Baxter et al. 2008).

Baxter et al. (2008) demonstrated that the liquefaction resistance of reconstituted samples is equal to the undisturbed samples if they are prepared to the same initial shear wave velocity of in situ samples. In their study, a comparison was made between undisturbed block samples of Olneyville silt and reconstituted samples prepared using modified moist tamping. Reconstituted samples prepared to a saturation of 55% demonstrated very good agreement of the $CRR_{tx} - V_s$ correlation as shown in Figure 2-2.

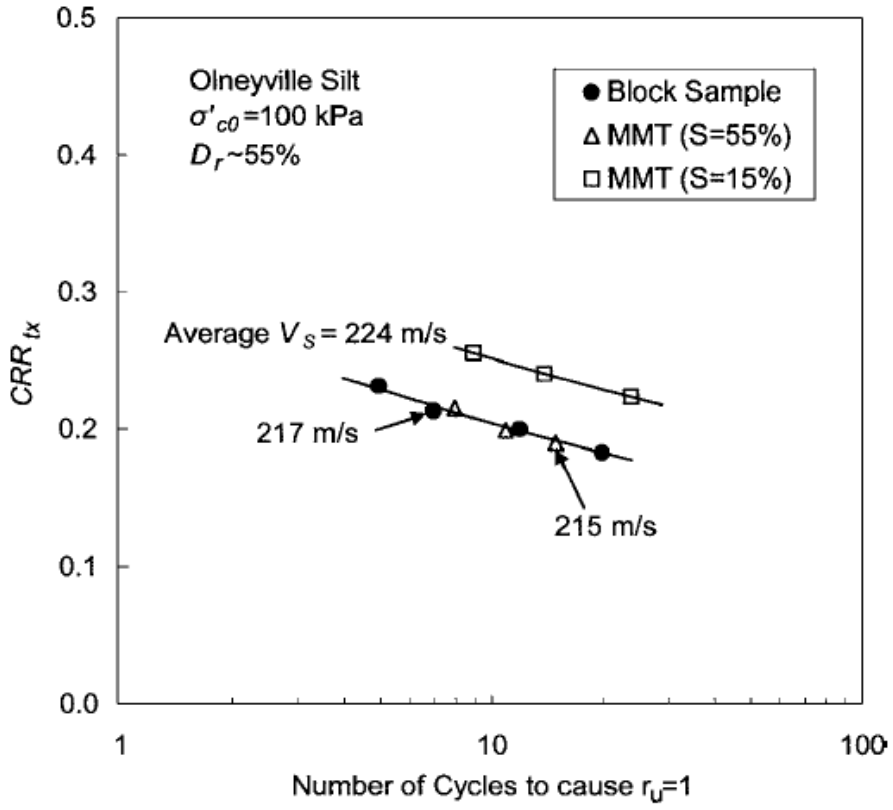

Figure 2-2: Comparison of Cyclic Resistance of undisturbed block sample to reconstituted samples (Baxter et al. 2008)

Their efforts have eliminated the need for the costly collecting of undisturbed samples because similar shear wave velocity measurements can be made on reconstituted samples in the laboratory. Additionally, the lack of sufficient in situ databases for liquefaction resistance of soils makes controlled laboratory testing using shear wave velocity measurements very important in creating a larger liquefaction resistance database (Zhou and Chen 2007).

De Alba et al. (1984) performed the first laboratory study to investigate the relationship between shear wave velocity and the cyclic resistance of sand, since then Tokimatsu et

al. (1986), Tokimatsu and Uchida (1990), Huang et al. (2004), Zhou et al. (2005), Wang et al. (2006), Baxter et al. (2008), have all evaluated cyclic resistance of soils shear wave velocity in the laboratory.

Baxter et al. (2008) compared the CSR_{tx} - V_s relationship for Niigata sand and Olyneyville silt using different sample preparation methods. Their conclusion, consistent with previous laboratory studies (Tokimatsu et al. 1986), is that the CRR_{tx} – V_s correlations are independent of stress history and sample preparation methods, but highly dependent on soil types.

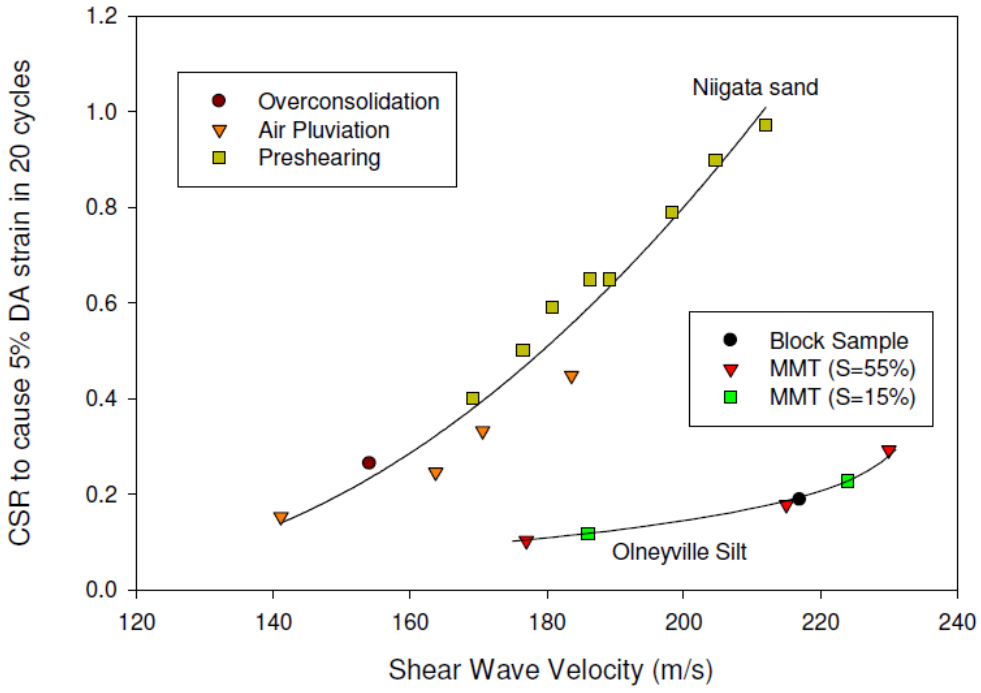

Figure 2-3: Soil specific CSR – V_S relationship independent of sample preparation methods (Baxter et al. 2008)

2.3 Cyclic Behavior of Calcareous Sands

The current state of the practice for determining liquefaction potential of a site with high seismicity is based on research associated with silica sands. This can be problematic for geographic locations where calcareous sands are present because the unique characteristics of calcareous sands suggests their geotechnical engineering behavior can be substantially different compared to terrigenous sands, including their behavior under seismic loading (Sandoval and Pando 2012) .

Research on the cyclic resistance of calcareous sands in the laboratory dates back to 1980 when Frydman et al. (1980) carried out a series of cyclic triaxial tests on reconstituted samples of cemented calcareous sand. This initial study suggested that silica sands have higher resistance to liquefaction than cemented calcareous sands. Since then, many researchers (e.g. Ross and Nicholson, 1995; Cataño and Pando 2010; Pando and Sandoval 2012; and others) have investigated the engineering properties and cyclic resistance of calcareous soils.

Ross and Nicholson (1995) conducted cyclic triaxial tests on calcareous sand samples dredged from the ocean bottom to determine the liquefaction potential for the low-lying areas south of Oahu between the Honolulu Airport and Waikiki. They prepared uncemented samples using the moist tamping method and applied 1 Hz cyclic loading until failure (+/- 5% double amplitude strain) was reached. They concluded that the similarity between the cyclic strength curves for the different materials tested indicates that under ideal laboratory conditions un-aged specimens of different grades of

calcareous and silica sands tested will reach failure in approximately the same number of uniform load cycles. However, the authors suggested other factors such as aging, field conditions, and so forth, need to be investigated before application.

Flynn (1997) expanded on the research of Ross and Nicholson (1995) by comparing the cyclic resistance of two different calcareous sands from Hawaii and one local silica sand. Those results indicated that the calcareous sands tested were more resistant to liquefaction than the silica sand. These contradictory findings highlight the challenge in understanding the behavior of these unique soils.

Sandoval and Pando (2012) compared undrained cyclic triaxial tests on isotropically-consolidated reconstituted samples of uncemented Cabo Rojo calcareous sands and Ottawa terrigenous silica sands. Figure 2.2 demonstrates that a comparison of similarly prepared medium to dense state samples of Cabo Rojo and Ottawa sand, the Cabo Rojo sand is more resistant to liquefaction. This conclusion of the calcareous sand being more resistant to liquefaction is the same as Flynn (1997).

Sandoval and Pando (2012) also compared the cyclic resistance of the Cabo Rojo sand with results from other published studies on calcareous sands. Figure 2-5 demonstrates that even among sands with similar mineralogy, there is considerable variability in the measured cyclic resistance.

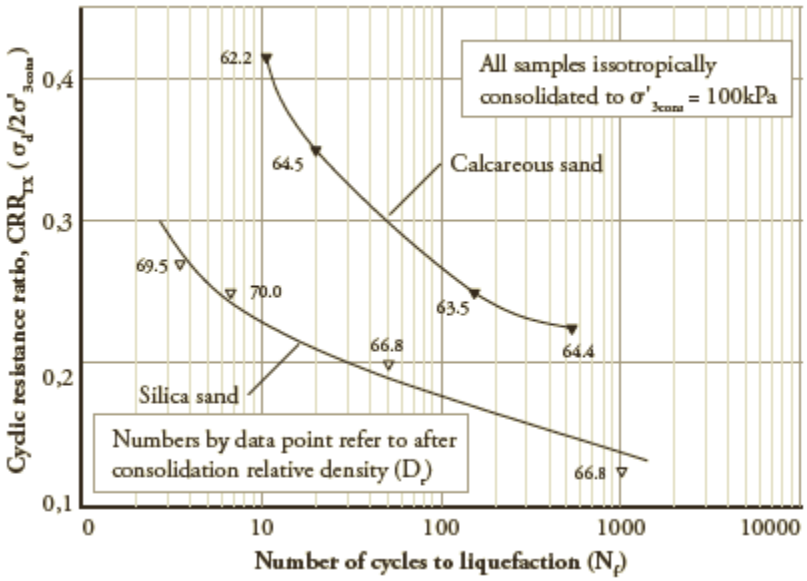

Figure 2-4: CRR curves for medium to dense relative density Cabo Rojo and Ottawa Sand (Sandoval and Pando 2012).

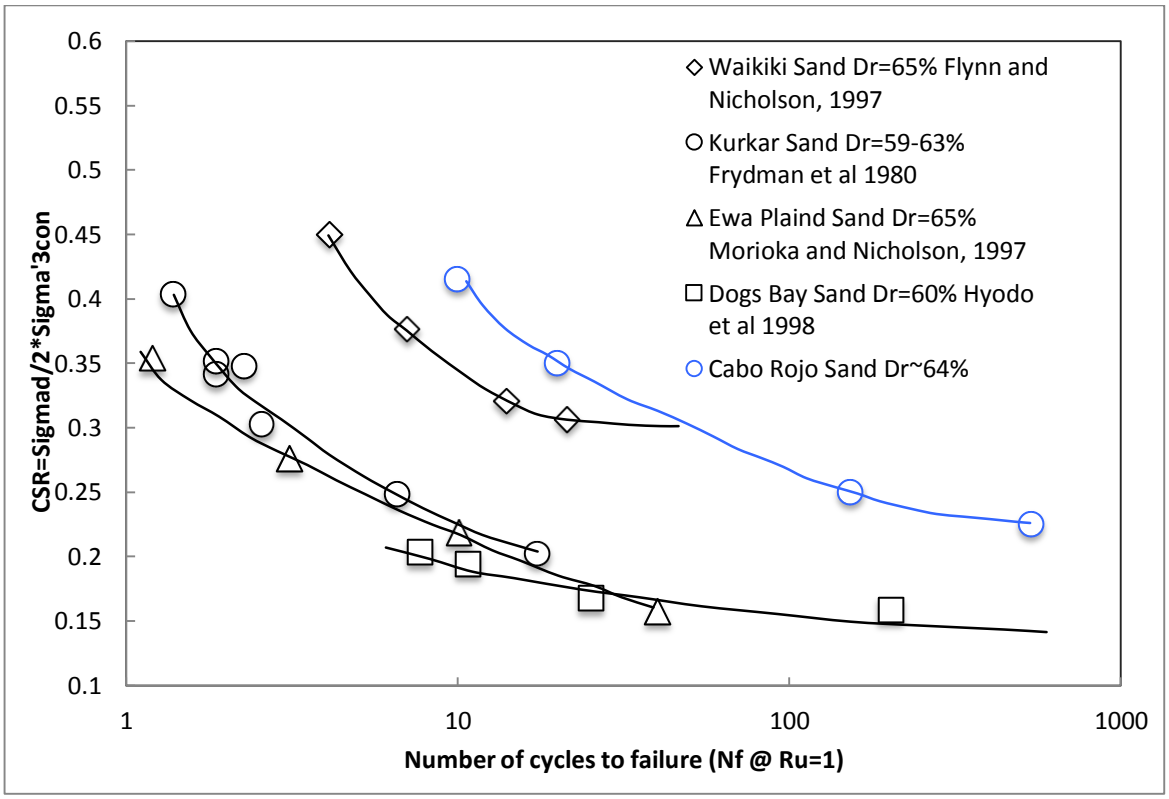

Figure 2-5: Comparison of cyclic resistance curves for calcareous sands (adapted from Pando and Sandoval et al. 2012)

2.4 Conversion of Laboratory Data to Field Conditions

In order to provide an effective comparison of laboratory data to field conditions due to differing stress and boundary conditions, the same approach used by Baxter et al. (2008) to convert laboratory shear wave measurements and laboratory cyclic resistance ratio measurements was used for this study.

This approach was similar to those used by Robertson et al. (1995) and Chillarige et al. (1977) where they demonstrated the comparable results between laboratory bender element and seismic cone shear wave velocity data when corrected for overburden stress and anisotropic conditions. This approach is highlighted in the following section.

2.4.1 Shear Wave Velocity

In order to determine an overburden stress corrected shear wave velocity (V_{s1}) for comparison to field data, the following formula was used (Robertson et al. 1992; Andrus and Stokoe 2000):

$$V_{s1} = V_s C_v = V_s \left(\frac{Pa}{\sigma`c}\right)^{0.25} \qquad 2.1$$

Where V_s = in situ shear-wave velocity; C_v = effective stress "correction factor" for shear wave velocity; P_a = reference stress (100 kPa); and $\sigma`_c$ = vertical effective stress at depth of the V_s measurement.

Cyclic triaxial testing is conducted using isotropic stress conditions and must be converted to anisotropic stress conditions to be compared with field data. In the field, normally consolidated sands are in at-rest conditions (K_0). Baxter et al. (2008) derived the following expression to account for this change.

$$V_{s1} = V_s K_o^n \left(\frac{P_a}{\sigma`_{c0}}\right)^{2n} \qquad 2.2$$

Where V_s = in situ shear wave velocity; K_0 = lateral earth pressure coefficient at rest; σ'_{c0}= principal stress acting normal to the plane defined by the direction of wave propagation and particle motion; P_a = reference stress (100kPa); n = exponent taken as 0.125 for most soils (Andrus and Stokoe 2000). Sands in the field will be assumed to be normally consolidated (K_o = 0.5) (Zhou and Chen 2007).

2.4.2 Conversion of Cyclic Resistance from a Triaxial Test to Field Conditions

Liquefaction is defined as the transformation of a granular material from a solid to a liquefied state as a consequence of increased pore-water pressure and reduced effective stress (Marcuson 1978). In this research, liquefaction refers to "cyclic liquefaction" involving cyclic softening of the soil due to cyclic loading (e.g. earthquake loading)

having sufficient intensity (i.e. cyclic stress levels and/or duration) to allow enough buildup of excess pore pressure to make the sandy soil reach a state of zero effective stress (Robertson 1994; Sandoval and Pando 2012). Cyclic liquefaction usually applies to level or gently sloping ground where shear stress reversal occurs during earthquake loading (Robertson and Wride 1998, and Sandoval and Pando 2012).

Often times the field based decision on whether the site liquefied or not is based on surface phenomena (sand boils, etc.) which is associated with 100% pore pressure, so using the failure criteria of 100% pore pressure in laboratory testing is most representative of field liquefaction determination. Cyclic liquefaction (failure) in this study was defined by when the ratio of the excess pore pressure divided by the initial effective confining stress equaled unity (r_u =1). At this point there is zero effective stress and the sample loses all strength.

Results for liquefaction testing are commonly presented in terms of the cyclic stress ratio (CSR) but the term cyclic resistance ratio can also be used because the same curve can also be called the cyclic resistance ratio (CRR) because it is where the soil resists liquefies (i.e. it's cyclic resistance is fully mobilized).

In cyclic triaxial testing, the cyclic resistance ratio (CRR) includes a subscript ($_{tx}$) to differentiate the difference between the laboratory testing and the field estimates. The triaxial cyclic resistance ratios (CRR_{tx}) gathered from this study will be converted to field values using the same expression as Baxter et al. (2008), which was originally developed by Seed (1979) and accounts for direct simple shear and multidirectional shaking.

$$CRR = 0.9 * c_r * CRR_{tx} \quad (2.3)$$

Where CRR = cyclic resistance ratio in the field; c_r = factor used to convert triaxial to direct simple shear conditions; and CRR_{tx} = CSR to cause failure in 15 cycles in a cyclic triaxial test. Seed (1979) initially proposed $c_r = 0.63$ for normally consolidated sands, which was also adapted for this research.

2.5 Comparison of Laboratory and Field Based Liquefaction curves

Kayen et al. (2013) combined a global catalog of 422 in situ case histories for V_s - liquefaction occurrence. The data was collected from China, Japan, Taiwan, Greece and the United States. They used Bayesian framework and structural reliability to estimate the probability of liquefaction and then compared their results to previously proposed models developed by Andrus and Stokoe (2000) and others.

Figure 2-6 is a comparison of the in situ based models with one laboratory model developed by Zhou and Chen (2007). Figure 2-7 shows the new data used for the Kayen et al. (2013) correlation, along with the proposed curves of Andrus and Stokoe (2000) and Zhou and Chen (2007).

Kayen et al. (2013) concluded that for a given soil, V_{s1} correlates directly with liquefaction resistance through the relationship between void ratio and relative density.

However, they also believe that for a soil type of unusual origin will correlate differently given the soil's specific void ratio-relative density relationship.

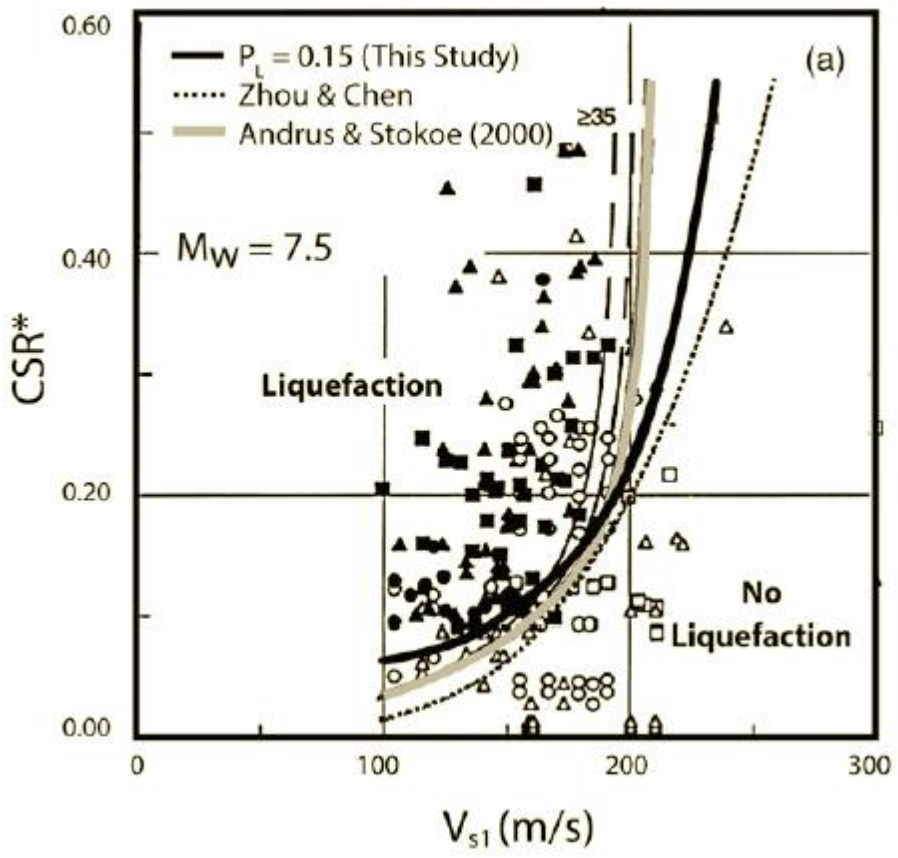

Figure 2-6: Comparison of in situ based Andrus and Stokoe (2000) data and correlation with laboratory based correlation from Zhou and Chen (2007) and in situ based correlation from Kayen et al. (2013)

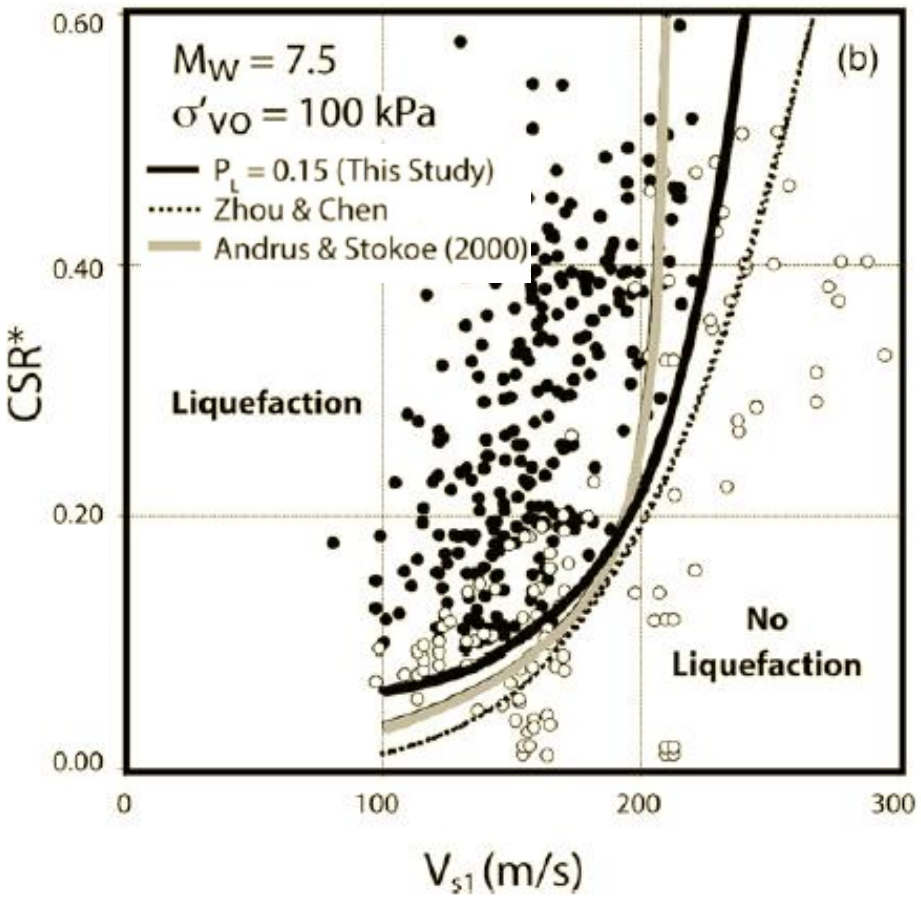

Figure 2-7: New data set with recently proposed correlation curves by Kayen et al. (2013)

Baxter et al. (2008) conducted triaxial tests on Providence silts and gathered testing data from Tokimatsu et al. (1986) for Niigata sand and Toyoura sands and from Huang et al. (2004) for Mai Liao sand. The authors then compared this data with the field based correlation presented by Andrus and Stokoe (2000), and concluded that there is significant underestimation of the liquefaction resistance of the Mail Liao and Niigata sands, while there is overestimation the resistance of the Toyoura sand and Olyneville

Silt. The authors recommended that soil-specific correlations should be developed through laboratory testing.

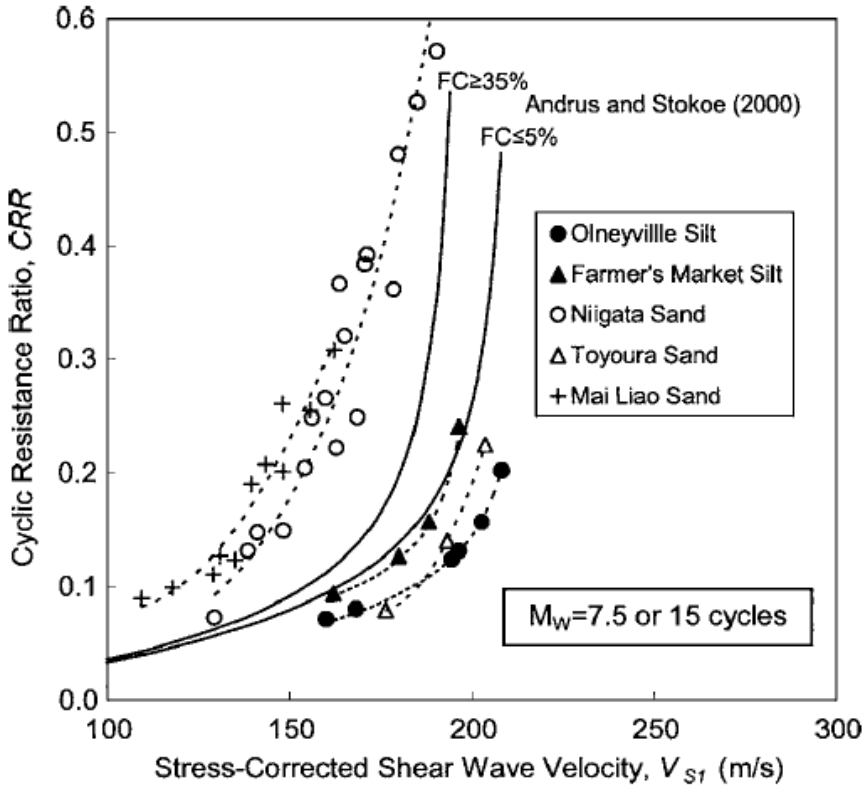

Figure 2-8: Comparison between existing field-based correlations of Andrus and Stokoe (2000) and laboratory-based correlations from two silts and three clean sands (Baxter et al. 2008).

More recently, Paydar and Ahmadi (2013) conducted undrained cyclic triaxial testing on sands with various fine contents and measured shear wave velocities using bender elements. Their objective was to demonstrate that not only did the percentage of fines change the liquefaction resistance, but the type of fines made an impact as well. This is in direct support that the CRR – V_s relationship is soil specific. Comparing their data with that of Andrus and Stokoe (2000), they concluded that the correlation between

CRR and V_{s1} is fines and soil specific, and there is a need for development of soil specific CRR and V_{s1} relationships in the laboratory.

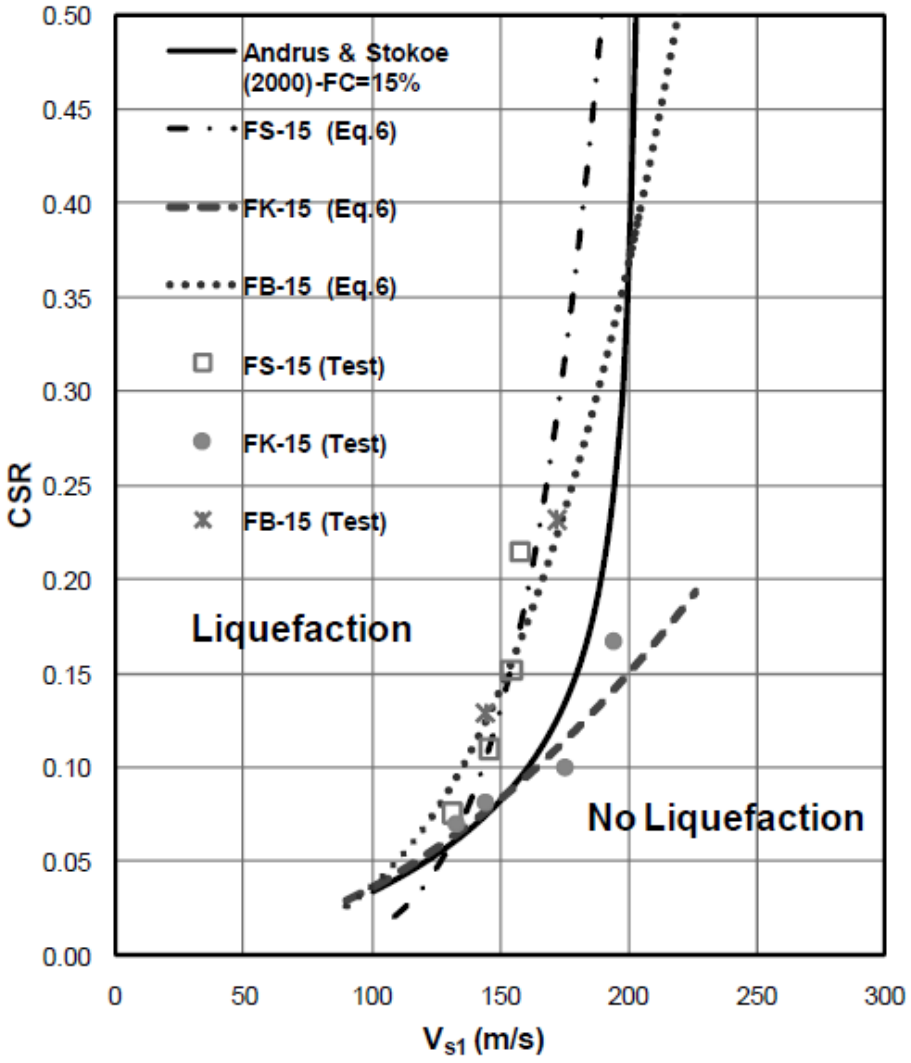

Figure 2-9: Correlation between CRR – V_s for sands with FC = 15% (Paydar and Ahmadi (2013)

2.6 Summary and Conclusions

This chapter has provided an overview of the past and current ongoing research into the liquefaction resistance of soils using shear wave velocity. Shear wave velocity measurements are a potentially good measure of liquefaction potential over others because they are not dependent on soil preparation method, instead only the soil type (Baxter et al. 2008 and Tokimatsu et al. 1986). Shear waves measurements made in the field can be directly compared to measurements in the laboratory when corrected for overburden stress and anisotropic conditions (Robertson et al. 1995 and Chillarige et al. 1977).

The current database used to determine the liquefaction potential of soils is growing, but needs to be expanded further, specifically in the field of calcareous soils. Using the current generalized CRR – V_s relationships can result in an underestimation of the liquefaction potential of soils that have not yet been studied. This research will help expand that database through undrained cyclic triaxial testing of different types of soils.

3. Laboratory Testing Program

3.1 Soil Properties

This chapter presents details of the laboratory testing program performed to evaluate the relationship between cyclic resistance and shear wave velocity for two types of sands. Properties of the soils tested are presented first, followed by a description of the sample preparation methodology. The rest of the chapter deals with equipment and testing details, including operation of the Instron load frame, shear wave velocity measurement system, and estimation of piston friction. A testing matrix is provided at the end of chapter.

Two types of sands were chosen for this study, a silica sand called Monterey #0/30 sand and a calcareous sand from Puerto Real, Cabo Rojo, southwestern Puerto Rico. Monterey sand is commercially available from Kleen Blast Abrasives, Danville, CA. Monterey sand has been widely used in laboratory liquefaction studies (e.g. Silver 1976, Mulilis 1977, De Alba et al. 1984, Lin 2007)

Cabo Rojo sand is a calcareous beach sand obtained as part of a project on the liquefaction behavior of calcareous sands (Morales-Velez, 2014). The sand used in this research is the same sand used by Sandoval and Pando (2012) and was gathered from the near surface beach using shovels and buckets. The sand tested was uncemented and classified as being white to yellow, fine to medium grained, poorly graded, having sub angular to angular grains and high internal porosity.

Calcareous sand is composed of calcium carbonate from the decayed bodies of marine organisms. This is shown in Figure 3-1, which shows a scanning electron micrograph of the Cabo Rojo sand. It, along with other calcareous sands found in tropical and subtropical regions, have higher void ratios, higher specific gravities and higher compressibility when compared to silica sands (Sandoval and Pando 2012).

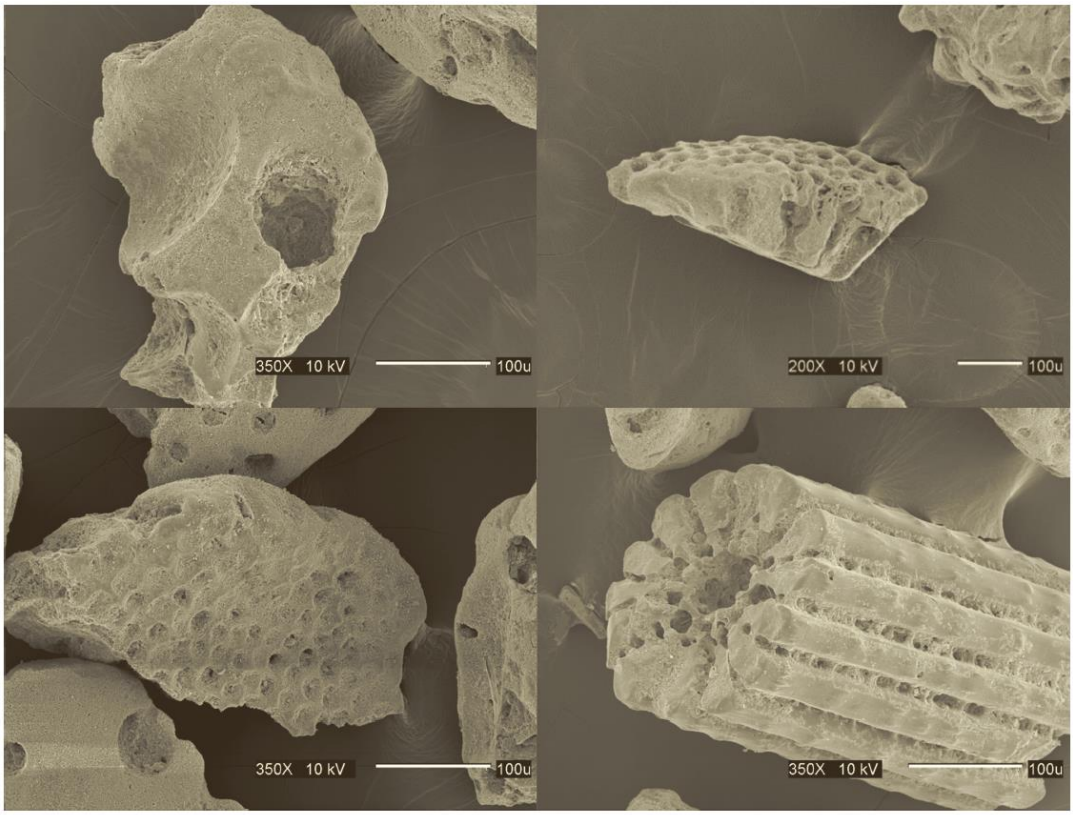

Figure 3-1: Micrographs of Cabo Rojo uncemented calcareous sand (Sandoval and Pando 2012)

Individual calcareous grains tend to be relatively soft, very angular, and can crush under relatively low pressures, particularly at grain to grain contact points (Ross and Nicholson 1995). Semple (1988) showed soil crushing can be a principal part of yield

for calcareous materials and to verify crushing, all tests on calcareous sands in this study will be sieved before and after testing.

Table 3-1 is a summary of index properties for the Monterey and Calcareous sand, and Figure 3-2 shows the grain size distribution for both sands. According to the Unified Soil Classification System (USCS), both-sands are a poorly graded sand (SP). The Cabo Rojo sand has a much higher e_{min} and e_{max}, possibly due to angularity of the grains.

Parameter	Monterey silica sand	Cabo Rojo calcareous sand	ASTM standard
D_{10} (mm)	0.33	0.24	ASTM D 422-63 (98)
D_{30} (mm)	0.45	0.30	
D_{50} (mm)	0.55	0.37	
D_{60} (mm)	0.58	0.42	
C_u	1.76	1.75	
C_c	1.06	0.89	
G_s	2.66	2.87	ASTM D 854-06
γ_{min} (kN/m3)	14.4	10.2	ASTM D 4254-00
e_{max}	0.808	1.755	
γ_{max} (kN/m3)	16.4	12.39	ASTM D 4253-00
e_{min}	0.589	1.273	

Table 3-1: Properties of Monterey #0/30 and Cabo Rojo sand used in this study

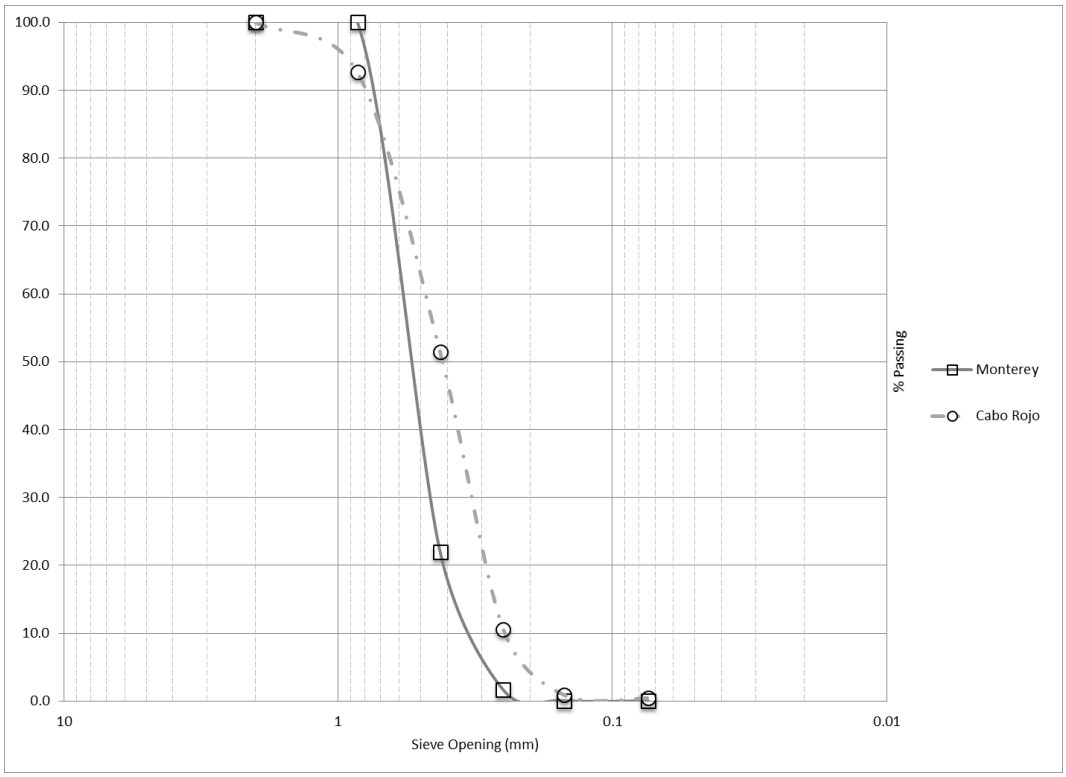

Figure 3-2: Grain size distribution for sands used in this study.

3.2 Sample Preparation

Because it is practically impossible to obtain undisturbed samples of sand from in situ, almost all laboratory studies of liquefaction are performed on reconstituted samples. Samples can be reconstituted in a variety of ways, including pluviating sand through air into a sample mold (dry pluviation), pluviation through water (slurry deposition or wet pluviation), and tamping of the soil to a known density (moist tamping).

Mulilis et al. (1977) demonstrated that the method of sample preparation can have a significant impact on the cyclic strength, as shown in Figure 3-3. Further research has

shown that the wet pluviation method most closely represents the in situ fabric of fluvial soils (Vaid and Sivathayalan 2001, Bradshaw 2006). However, wet pluviation it is difficult to test a range of densities and there can be segregation of particles during pluviation for well graded soils.

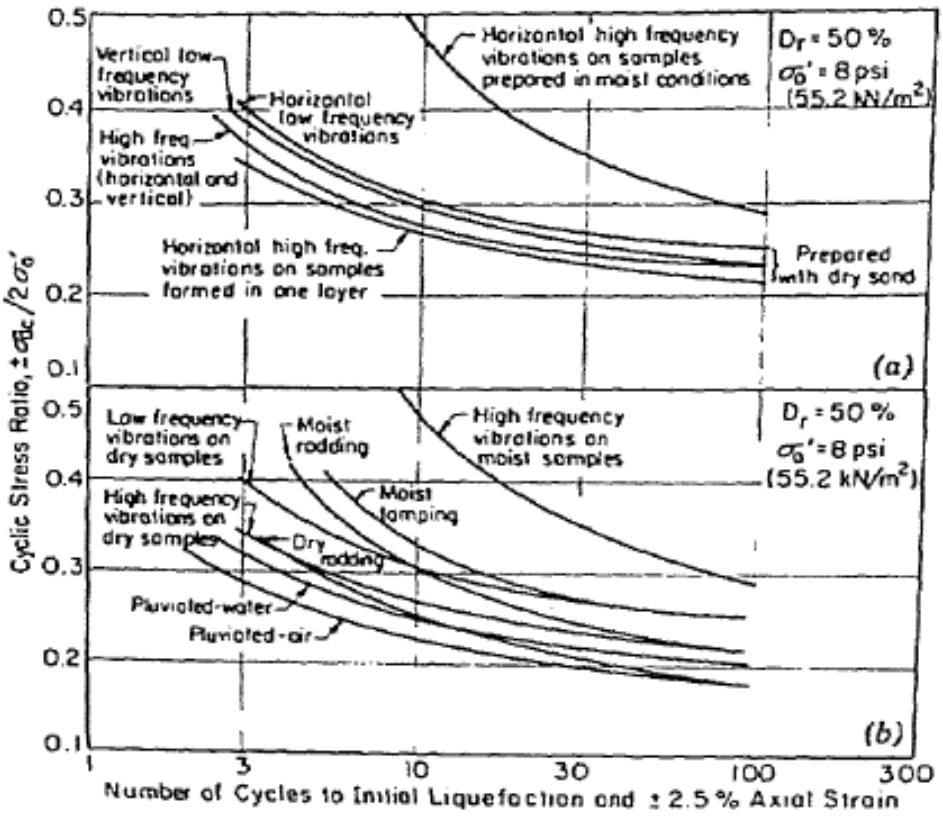

Figure 3-3: Cyclic stress ratio versus number of cycles for different; (a) vibratory compaction procedures, (b) compaction procedures (Mulilis 1977)

Moist tamping is used in many studies because it is relatively straight forward to produce replicate samples and a wide range of densities can be achieved. A potential drawback of moist tamping is that it is not always clear whether the behavior will be comparable to naturally deposited samples.

The work of Mulilis (1977) clearly shows the effect of sample preparation on the cyclic resistance of samples prepared to the same relative density. However, several researchers have shown that samples prepared to the same shear wave velocity will have the same cyclic resistance independent of sample preparation (Tokimatsu and Uchida 1986).

For example, Baxter et al. (2008) conducted cyclic triaxial tests on reconstituted samples of non-plastic silt using a modified moist tamping method (MMT) which resulted in similar shear-wave velocities as undisturbed block samples. The cyclic strength and shear wave velocity for samples reconstituted using MMT at 15% saturation and 55% saturation (i.e. different water contents) was compared with results from undisturbed samples trimmed from a block sample. This work demonstrated that silts prepared with a molding water content corresponding to a degree of saturation of 55% more closely represent the samples trimmed from the undisturbed block sample (see Figure 3-4). Because of this demonstrated independence of sample preparation method, all samples in this research will use the modified moist tamping (MMT) method developed by Bradshaw (2006).

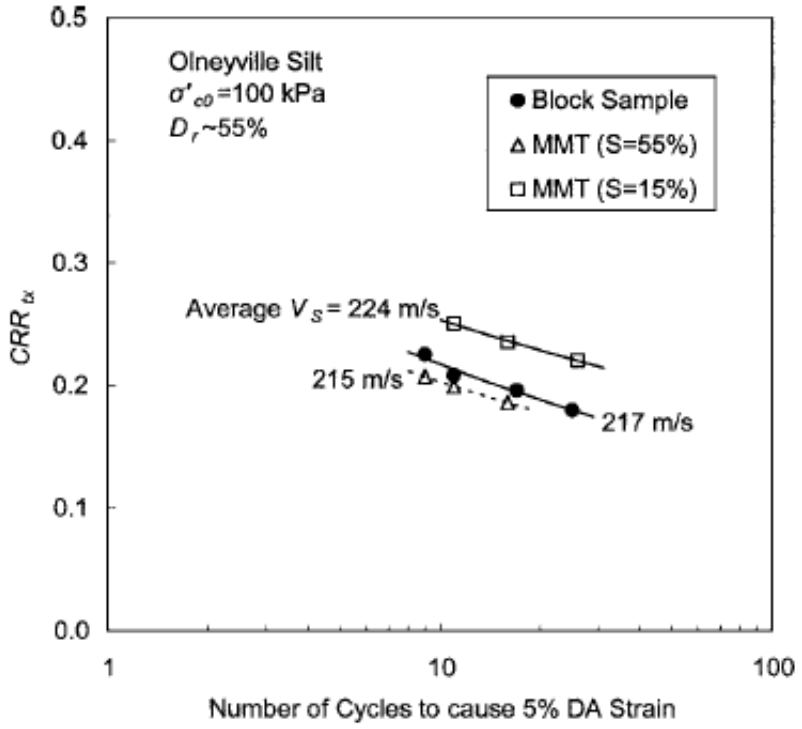

Figure 3-4: Cyclic Resistance of the Olneyville silt as determined from specimens trimmed from the block sample and prepared by modified moist tamping at different saturation percentages (Baxter et al. 2008)

The MMT method is based off of Ladd's (1978) undercompaction procedure using a tamping method to compact moist, coarse grained sand in layers, where each layer of equal mass is compacted to a uniform height to ensure uniform density of the sample.

The key modification of Ladd's moist tamping approach used in this study is that instead of compacting samples in layers with fixed layer thickness, layers are compacted with a given compactive energy.

The equipment used for preparing the samples is shown in Figure 3-5. The first step in the modified moist tamping method is to determine a relationship between the dry

density of the soil and the hammer drop height used to compact the sample (Bradshaw 2006). This was accomplished by preparing samples at a constant molding water content and compacting several different samples, each with its own constant hammer drop height.

The molding water content was based on the target relative density of the sample and the soil properties. The author adjusted the water content of the air dried specimen by mixing the water and sand in a plastic bucket, covering the bucket, and then letting it sit for 30 minutes.

Figure 3-5: MMT Sample Preparation Tools (mixing bucket, tamping rod with heavy hammer, split mold used for testing)

The author placed the soil into the split mold in eight layers keeping the layer height constant and the hammer drop height constant for each layer (see Figure 3-6). Once the eighth layer was complete, the split mold and sample were then weighed and the sample mass could be calculated.

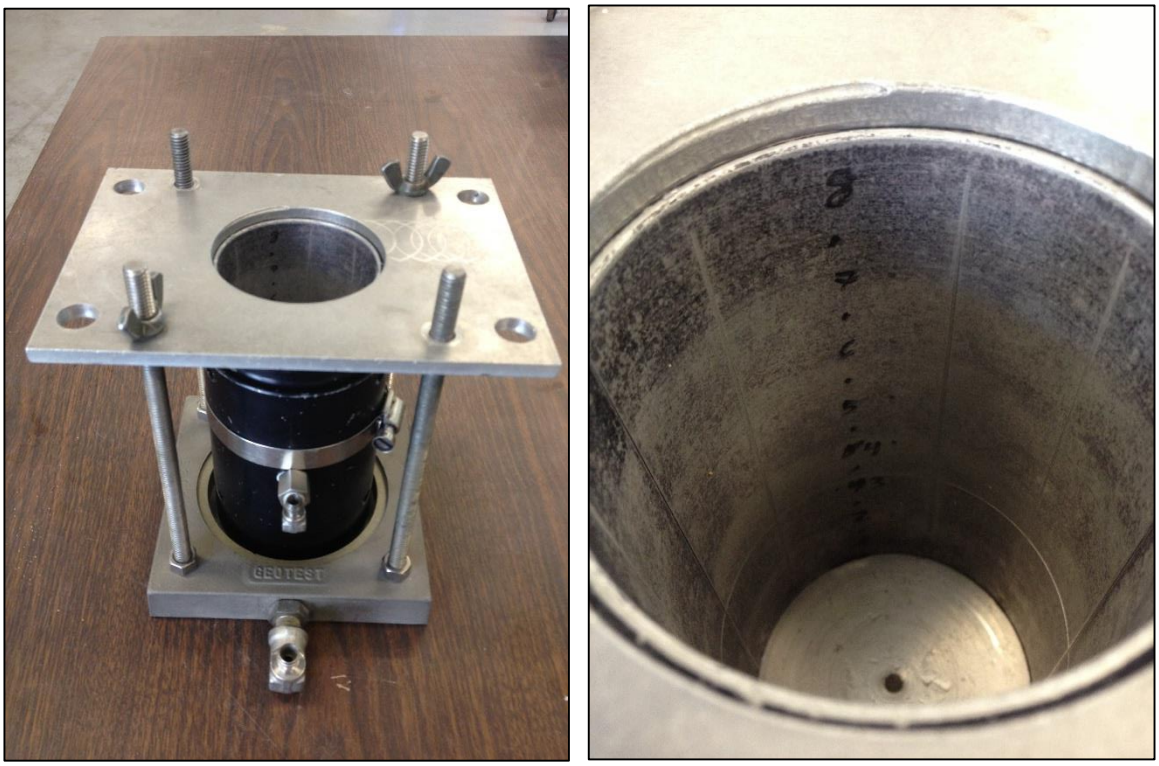

Figure 3-6: Split mold used for testing and a close up of the layer numbering used to keep the layer height constant

A water content sample then was taken from the top, middle, and bottom of the specimen (see Figure 3-7). The average water content for the sample could then be calculated and the saturation level was verified to be nearly 55%.

Figure 3-7: Setup for water content determination

This entire process was repeated a minimum of three times, adjusting the drop height of the tamping rod (i.e. the compactive energy) for each sample. The drop height of the hammer was adjusted using the hose clamp on the top of the tamping rod. Two different tamping rod hammers were used depending on the target density of the sample. For denser samples an 896 g brass hammer was used and for looser samples a 187 g plastic hammer was used.

The drop height and resulting dry density were plotted and a function was fit to the data as follows:

$$\rho_d = C_1 \ln H + C_2 \qquad 3.1$$

where ρ_d = average dry density; H = average drop height; and C_1, C_2 = constants (Bradshaw 2006). From equation 3.1 it is assumed that the initial density of the *n*th-layer (ρ_{dn}) is a function of the hammer drop height for the *n*th=layer by the following:

$$H_n = \exp\left(\frac{\rho_{dn} - C_2}{C_1}\right) \qquad 3.2$$

This is consistent with Ladd's undercompaction approach, the initial dry density of the nth-layer was assumed to increase from the bottom of the sample to the top in a linear fashion by the following:

$$\rho_{dn} = \rho_{dt}\,(1-\mu) + (n-1)\frac{2\rho_{dt}\mu}{N-1} \qquad 3.3$$

Where, ρ_{dt} = target dry density; μ = percent undercompaction (decimal); and N = total number of layers (Bradshaw 2006). Once C_1 and C_2 were determined, equations 3.2 and 3.3 were used to determine the drop height required for each layer. Figure 3-8 shows the variation of average dry density vs. drop height for nine samples of Monterey sand.

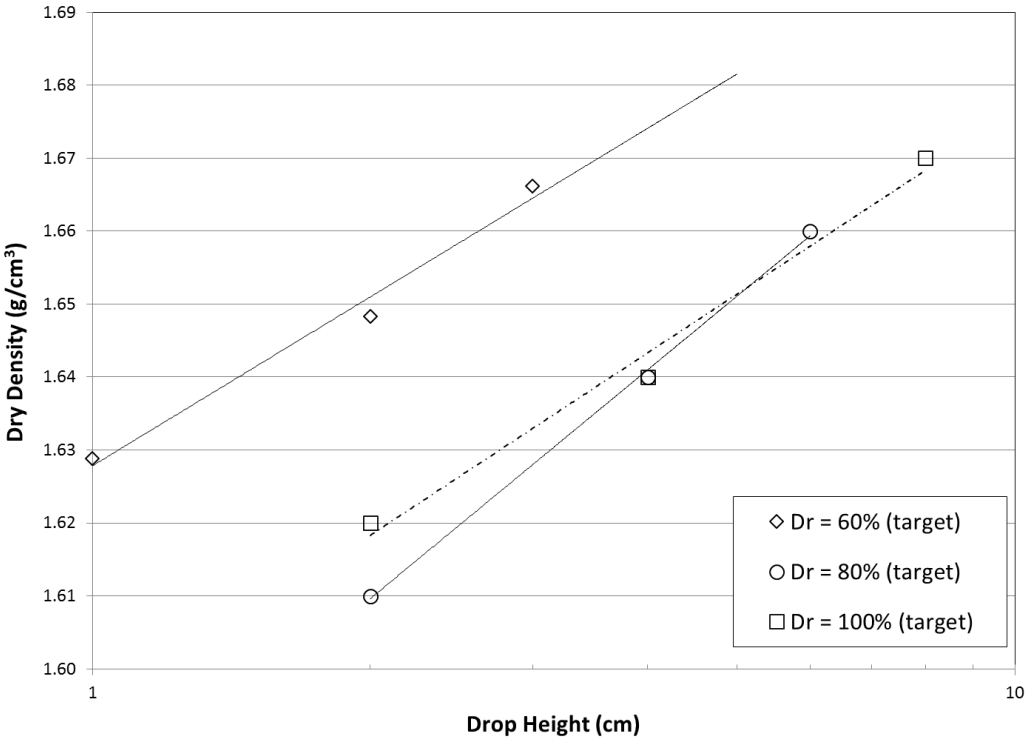

Figure 3-8: Undercompaction coefficient determination for samples of Monterey sand prepared to target densities corresponding to approximate relative densities of 60%, 80%, and 100%.

Table 3-2 summarizes the target density, molding water content, mass of each layer, undercompaction coefficients and the target dry density of each sample.

Sand type	Target relative density	Molding water content	Mass of each layer (g)	C_1	C_2	Target ρ_d (g/cm^3)
Monterey	60%	14%	124.7	0.0356	1.5896	1.59
Monterey	80%	13%	128.6	0.0453	1.5782	1.63
Monterey	100%	12%	131.7	0.0361	1.5933	1.67
Cabo Rojo	0%	34%	97.3	0.0408	0.9801	1.044
Cabo Rojo	30%	31%	100.0	0.0477	1.0665	1.093
Cabo Rojo	60%	29%	103.0	0.0460	1.0554	1.146

Table 3-2: Undercompaction variables developed for the sands in this study

Samples were then prepared by using the target water content percentage and mixing air dried soil with a de-aired water in a plastic bucket, covering the bucket, and setting it aside for 30 minutes. Table 3-3 is a summary of the sample target relative density, mass of sand and water used to prepare sample, target water content and the undercompaction (UC) percentage used to prepare the samples.

Sand Type	Target Density	Air Dried Mass of Sand (g)	Mass of water (g)	Water Content	UC
Monterey	60%	1200	168.0	14%	2%
Monterey	80%	1200	157.2	13%	2%
Monterey	100%	1200	146.4	12%	1%
Cabo Rojo	0%	900	291.6	34%	3%
Cabo Rojo	30%	900	280.8	31%	2%
Cabo Rojo	60%	900	259.2	29%	2%

Table 3-3: Sample preparation values

The undercompaction percentage (UC) was determined through a series of tests at one, two, and three percent. The author determined the optimal undercompaction percentage based on watching the sample as it liquefied to observe where it fails (i.e. top, middle or bottom). The denser samplers were hard to prepare because the hammer drop height created so much energy that it displaced the soil at the top layer making the samples looser than expected at the top. In order to compensate for this, the author used an additional plastic ring placed on top of the sample to keep the sand from displacing with each blow.

To prepare a sample for testing, the author prepared the triaxial cell with a split mold and a 0.3048 mm thick rubber membrane. The membrane was placed over the bottom cap and rubber o-ring was used to seal the membrane and bottom cap. A twelve millimeter PVC ring was placed around the base of the bottom cap because the bender element bottom cap was taller than most bottom caps and the ratio of height to diameter was less than two without the PVC ring. Vacuum grease was applied to both sides to ensure a good seal for the split mold. The split mold was then assembled on top of the PVC ring. A second rubber o-ring was placed on the external side of the top of the split mold for use with the top cap when the sample was finished. The rubber membrane was then pulled over the top edge of the split mold and a 30 kPa vacuum was applied to the split mold. A plastic collar was placed around the top of the split mold to easily collect any overflow of the sample mass during tamping. The assembled split mold is shown in Figure 3-9.

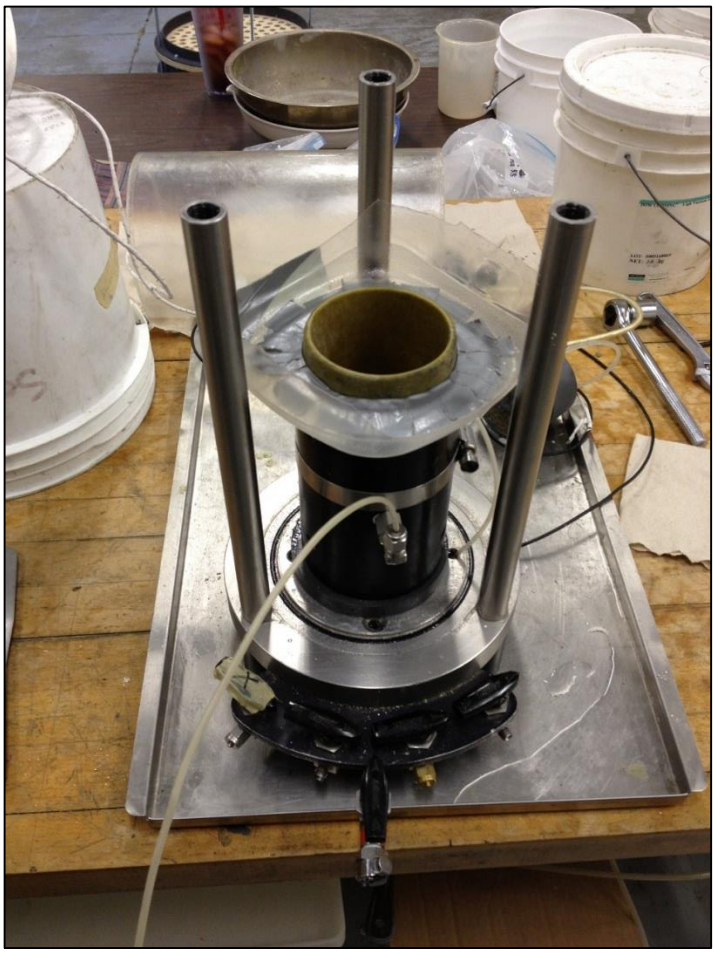

Figure 3-9: Spit mold assembled for sample preparation with vacuum connected

After thirty minutes had elapsed, the author began weighing and tamping the sample in layers, keeping the mass of moist soil constant with each layer, but adjusting the drop height of the tamping rod hammer. The drop height was done by adjusting the hose clamp along the tamping rod. An example of the drop heights for Sample 51 are shown in Table 3-4.

Layer	Layer Mass (g)	Drop Height (cm)
1	128.64	1.5
2	128.64	1.9
3	128.64	2.3
4	128.64	2.8
5	128.64	3.5
6	128.64	4.3
7	128.64	5.2
8	128.64	6.4

Table 3-4: Example of moist tamping mass layer and drop height

As seen in the table above, the samples were prepared in eight layers, keeping the mass uniform for each layer and adjusting the hammer drop height. The initial layers were undercompacted, but with each consecutive layer, the density increased, resulting in a uniform density for the entire sample.

Great care was taken to keep the sample water content the same throughout the sample preparation. This was achieved by re-covering the sand bucket after each layer and placing a saturated paper towel over the split mold between layer tamping. After each layer was placed, the layer was scarified with the putty knife to a depth of one tenth the layer height and the moist paper towel was placed back on top of the split mold.

For the samples prepared using the 896g brass tamping rod, the author had to take extra care when compacting the last layer so to not drop the tamping foot on the split mold and puncture the rubber membrane stretched along the top of the split mold during tamping.

Figure 3-10: Specimen top leveling before placement of top cap

Once the eighth layer was placed, the sample was levelled off with a putty knife and the top cap was placed in a direction so the bender element in the top cap was aligned with the bender element in the bottom cap (Figure 3-10).

The rubber membrane was then pulled over the top cap and the rubber o-ring pulled into place to seal the sample. The 30 kPa vacuum was then adjust to 20 kPa, removed

from the split mold and applied to the sample. The split mold was removed and the sample diameter and height were each recorded in three locations. A completed sample with an effective stress of 20 kPa from vacuum is shown in Figure 3-11.

Figure 3-11: Specimen ready for testing

Vacuum grease was applied to the top and bottom of the cell to ensure a good seal and no leakage during testing. The external cell was carefully placed around the specimen and the shear wave cable secured to the top of the cell (Figure 3-12). A bucket was used to raise up the triaxial cell top so not to break the shear wave cable because of over extension.

Figure 3-12: Assembling triaxial cell around sample

The top of the cell was then put into location and the piston was screwed into the top cap. The three bolts connecting the top of the cell were tightened first and the piston was locked into place. The bolts were tightened first to avoid any sample disturbance if the piston was locked in place and the tightening of the bolts would compress the piston and thus the sample.

The cell was then transferred to the Instron load frame. A quick connect was placed onto the top of the cell and the cell was filled with water by connecting the pressure panel to the bottom of the triaxial cell.

The pressure panel in Kirk Hall is tapped directly into the water supply, so the cell could be filled with water by applying a 30 kPa pressure to the cell section of the pressure panel and using the switch at the bottom of the pressure panel to re-fill the storage tube.

Once water began flowing out of the top quick connect on the triaxial cell, the line connected to the bottom of the cell was turned off, the storage filled to the top and the pressure source switched from storage to burette. The quick connect on top of the cell was then removed and the cell pressure line connected in its place. The pressure was then reapplied with the burette pressure. If the burette level did not stabilize, that meant there was a leak somewhere in the cell or the sample membrane.

Once the burette level stabilized, the burette level was recorded so volume change during CO_2 flushing and sample inundation could be measured. The sample vacuum was then removed and the sample was flushed with CO_2 for ten minutes. The CO_2 was flushed through the sample by connecting the CO_2 supply to the bottom of the sample and leaving the switch for the top of the sample open. The sample was then inundated with de-aired water by creating a syphon from a burette filled with de-aired water placed next to the pressure panel and leaving the top cap connection open (Figure 3-13).

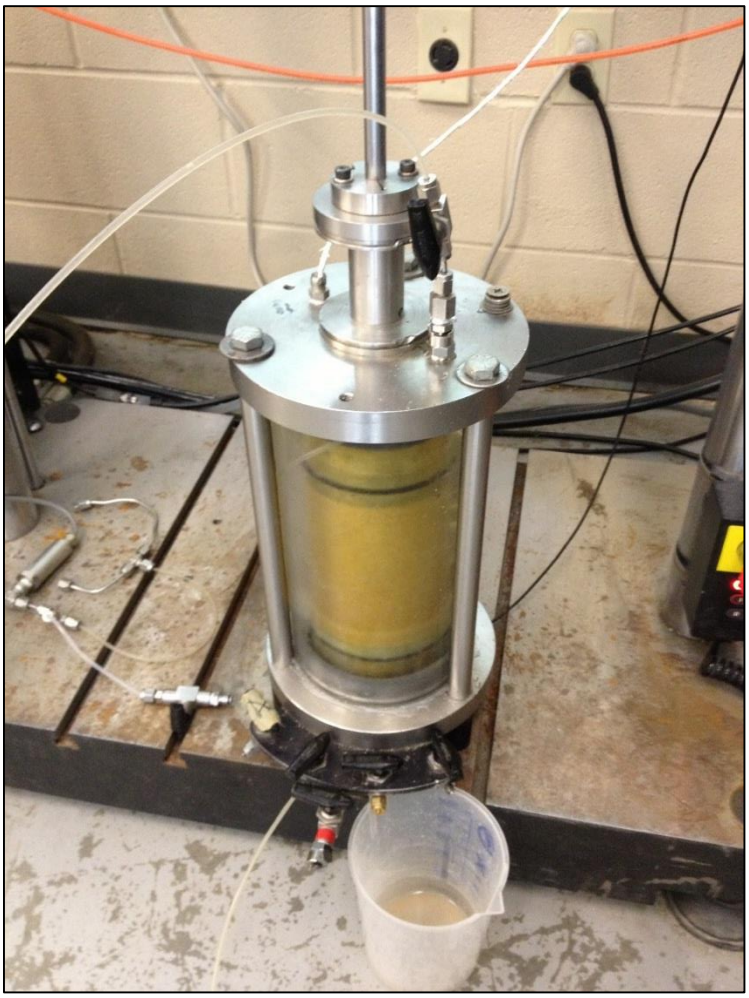

Figure 3-13: Set up for sample flushing with CO_2 and inundation

After inundation was complete, the pore pressure transducer was then connected to the bottom of the triaxial cell by first flushing the lines to remove any air bubbles and then connecting the lines to the cell with a wet connection. The final set up of the triaxial cell in the Instron load frame and connected to the pore pressure panel is shown in Figure 3-14.

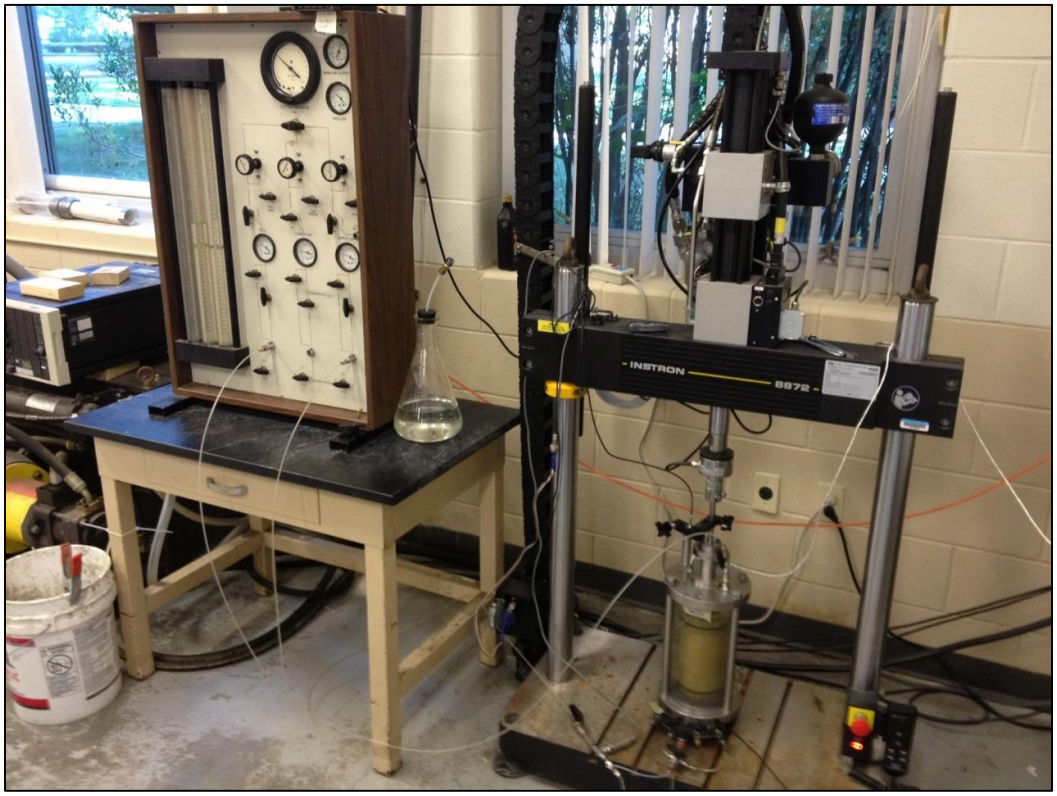

Figure 3-14: Triaxial cell in Instron Load Frame connected to the pressure panel

3.3 Instron Machine PID settings

The Instron load frame was controlled using the Instron software package called the Instron Wavematrix.

The Instron Wavematrix software has an auto tuning wizard function that is used to determine the correct Proportional Integral Derivative (PID) settings for sample testing. This function works very well when tracking the applied load, except for the last few cycles of the testing when the pore pressure ratio reaches about 0.8. At this point, the

software overcompensates due to the decreased strength and increases the deviator stress. This overcompensation causes the samples to pre-maturely fail (Figure 3-15).

In an effort to eliminate this increased deviator stress, and knowing the deviator stress started to increase at a pore pressure ratio of approximately 0.8, the auto tuning wizard was run on samples with an effective confining pressure of 20 kPa, 30 kPa and 50 kPa. The confining stress was then increased to 100 kPa during consolidation and the test was conducted.

The hypothesis was that a sample with an effective confining stress of 20kPa had the same strength as the sample with a pore pressure ratio of 0.8 when being tested at 100 kPa. By auto tuning at this effective confining stress, the author attempted to eliminate the increased deviator stress at the end of testing.

Table 3-5 shows the resulting auto tuning PID settings for various effective confining pressures.

σ'_c (kPa)	Proportional (dB)	Integral (I/sec)	Derivative (mSec)
20	-12	0.1	0.5
30	-16.8	9.2	0.37
50	-18	8.6	0.34
100	-19.5	11.2	0.38

Table 3-5: PID setting calibration

The sample auto tuned at 30 kPa still had an increase in the deviator stress, while the sample auto tuned at 20 kPa had a decrease in the deviator stress as the sample failed (Figure 3-16).

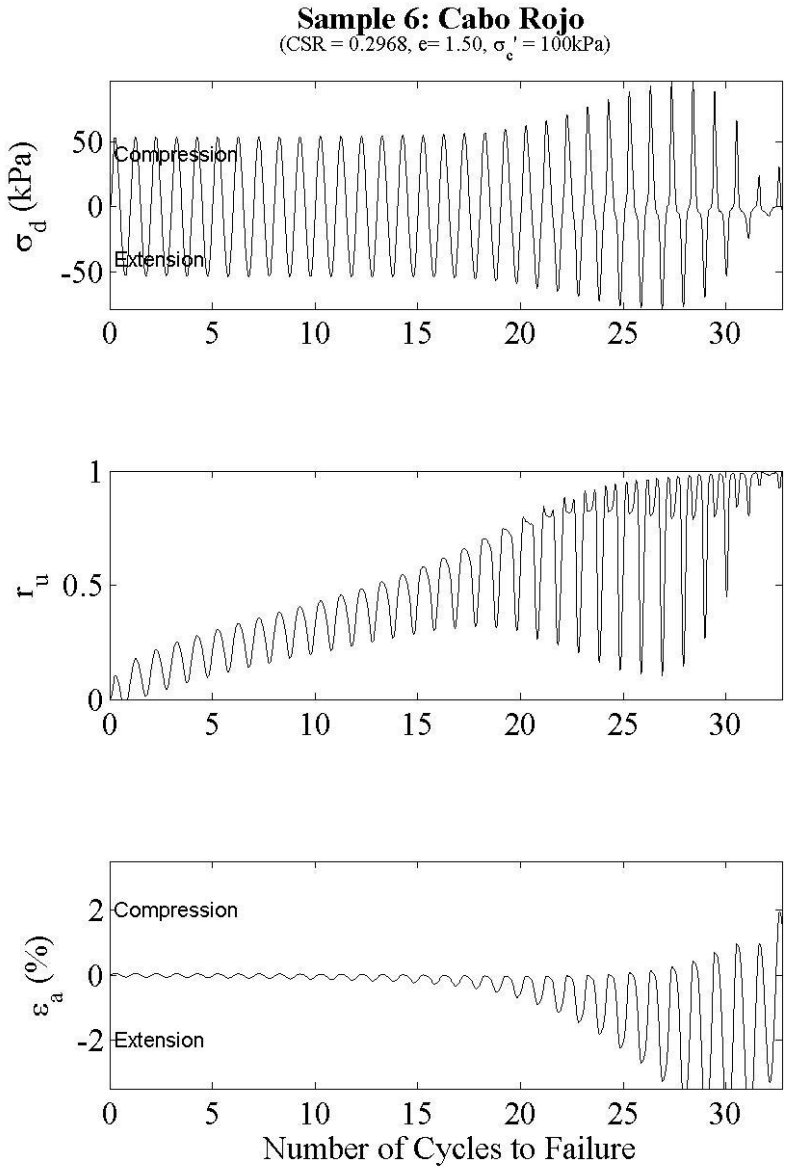

Figure 3-15: Results of sample auto-tuned at 50 kPa showing increase of the deviator stress at sample softening.

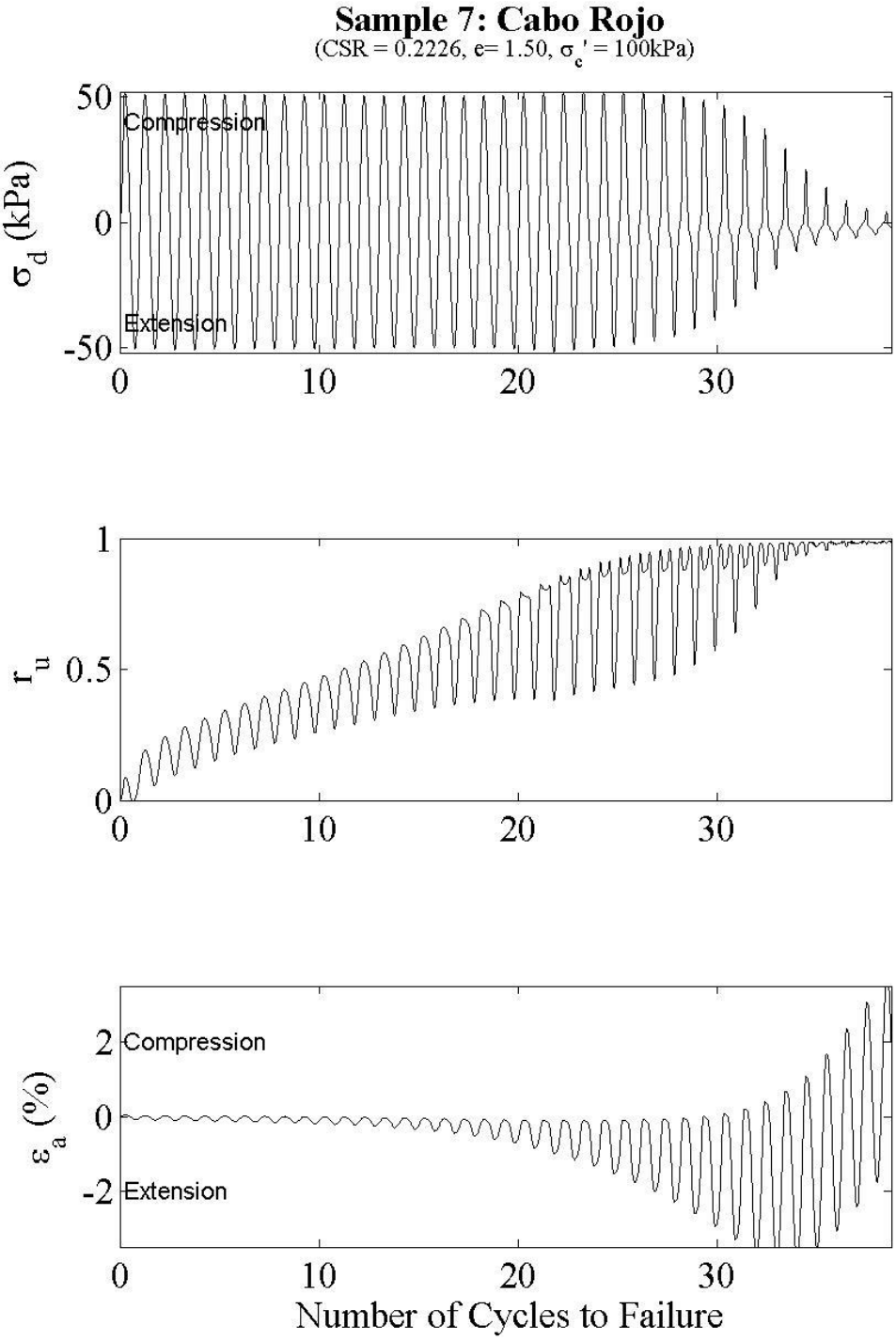

Figure 3-16: Results of sample auto-tuned at 20 kPa showing decrease in deviator stress at sample softening.

After discussions with the Instron technical staff, the author learned the most important PID parameter was the proportional (P) setting. The deviator stress decreased toward failure for the test auto tuned at 20 kPa and the deviator stress increased for the test auto tuned at 30, so the author chose a PID setting in between. As a result, the author used a PID setting of P= -14, I = 0.1 and D = 0.5 for all tests conducted in this research.

Figure 3-17 shows the first test conducted using the new PID settings. The sample reaches liquefaction in 42 cycles and the deviator stress tracks very well up until the last 4 cycles.

The Instron staff also recommended trying the "tri-modal" testing option. This was not used in this study, but should be explored by future studies using this same equipment.

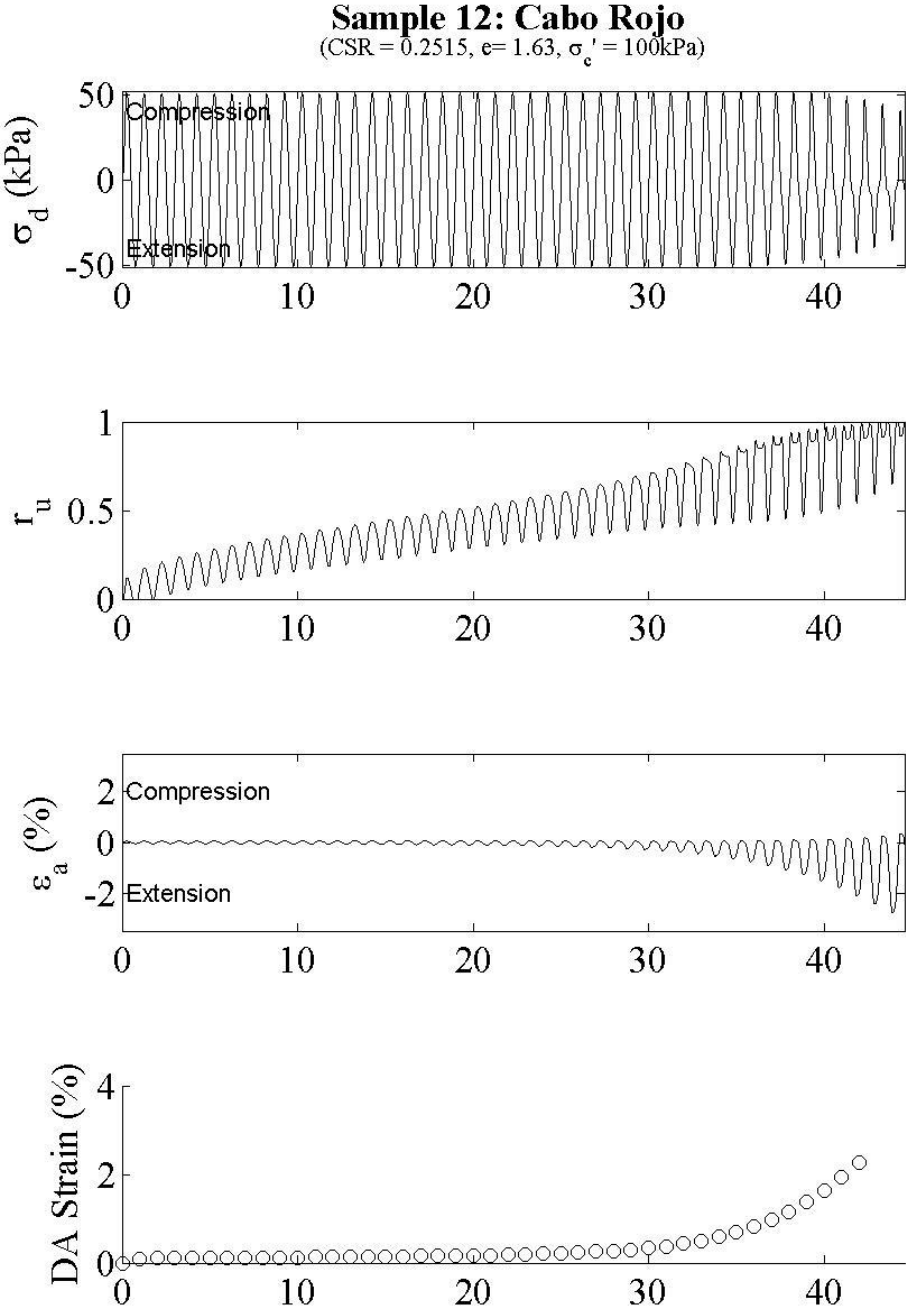

Figure 3-17: Sample 12 comparison plot for PID settings

3.4 Instron Machine Operation

The Instron machine is turned on by a switch located on the backside of the large Instron Processor. The Instron Console program was selected from the start menu of the desktop computer. Once the program is opened, an "R" will appear above the pore pressure transducer and the LVDT icons. Click on each icon and then click "restore calibration" option for each one.

Next, turn on the hydraulic pump (Figure 3-18) next to the pressure panel by selecting "low" and then "high". Return to the Instron load frame and press the "I" button followed by the II button.

Figure 3-18: Hydraulic pump in operation

The load cell was then zeroed by clicking on the load frame icon inside the Instron Console program, “control” and then selecting “balance” (Figure 3-19). Note that the load cell cannot be zeroed if there are limits selected for the load cell, so they need to be unselected first.

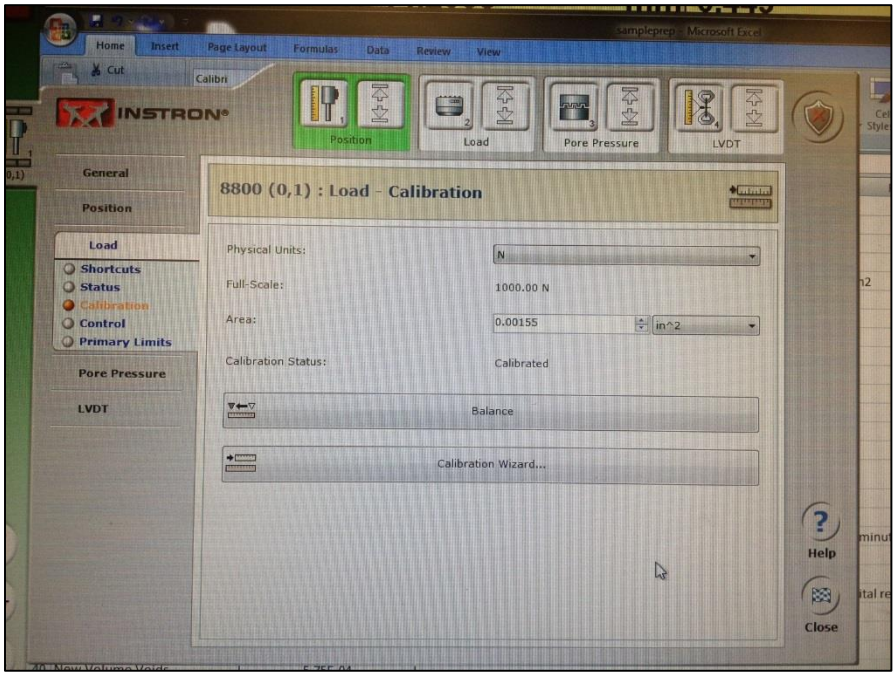

Figure 3-19: Zero-ing the load frame

The LVDT was connected to the piston and the sample was centered in the load frame. A small load (4N) was applied to the piston to ensure 100% contact between the load frame and the piston. This was done by clicking on the blue arrow icon, selecting “load” from the drop down menu and inputting a value of -4 N. The time for the load to be applied was set at 20 seconds to avoid the crushing of the sample.

All loads that are entered into the Instron Machine are negative because that is the downward (compression) direction. If the negative sign is not included, the machine will apply an upward (extension) load.

While the load was being applied, the LVDT was adjusted so the reading on the Instron console was close to 0.000 mm. This allows for maximum extension and compression of the LVDT during testing.

The piston coupling was then securely fastened by tightening the two bolts and the triaxial cell piston was un-locked from the top of the triaxial cell. The author then connected the bottom of the triaxial cell to the load frame with two bolts and washers to keep the cell in place during cyclic loading.

The sample was then subjected to isotropic 30kPa increases in pressure using the pressure panel (Figure 3-20), while maintaining an effective consolidation pressure of 30kPa, until the cell pressure was 240 kPa and the sample pressure was 210 kPa. Samples were left at this pressure from five minutes to twenty-four hours based on testing schedule and then a B parameter saturation check was performed to ensure the samples were fully saturated.

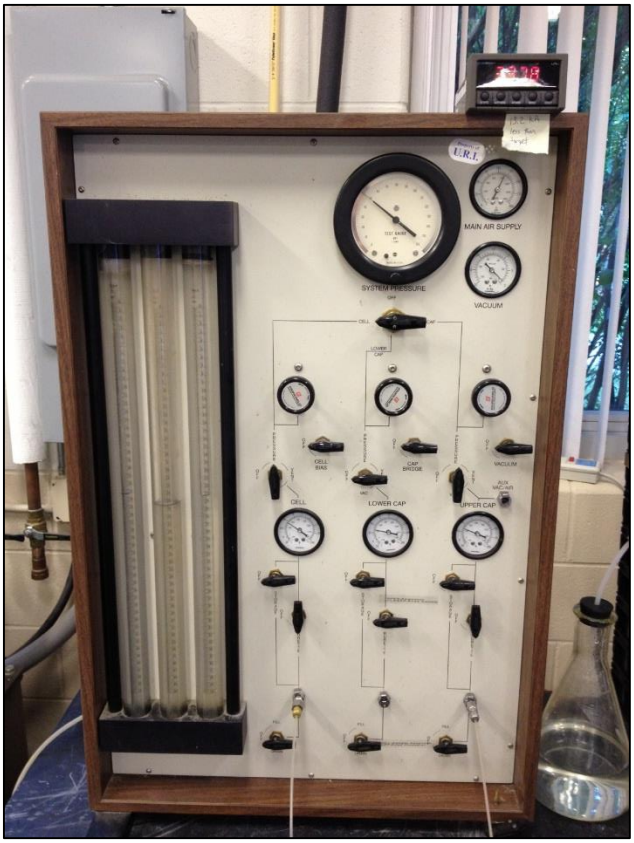

Figure 3-20: Pressure panel setup during saturation

The sample and the cell pressures were read from the sample pore pressure transducer connected to the Instron Console Software (Figure 3-21). This removed any error associated with calibration discrepancies of two separate pore pressure transducers.

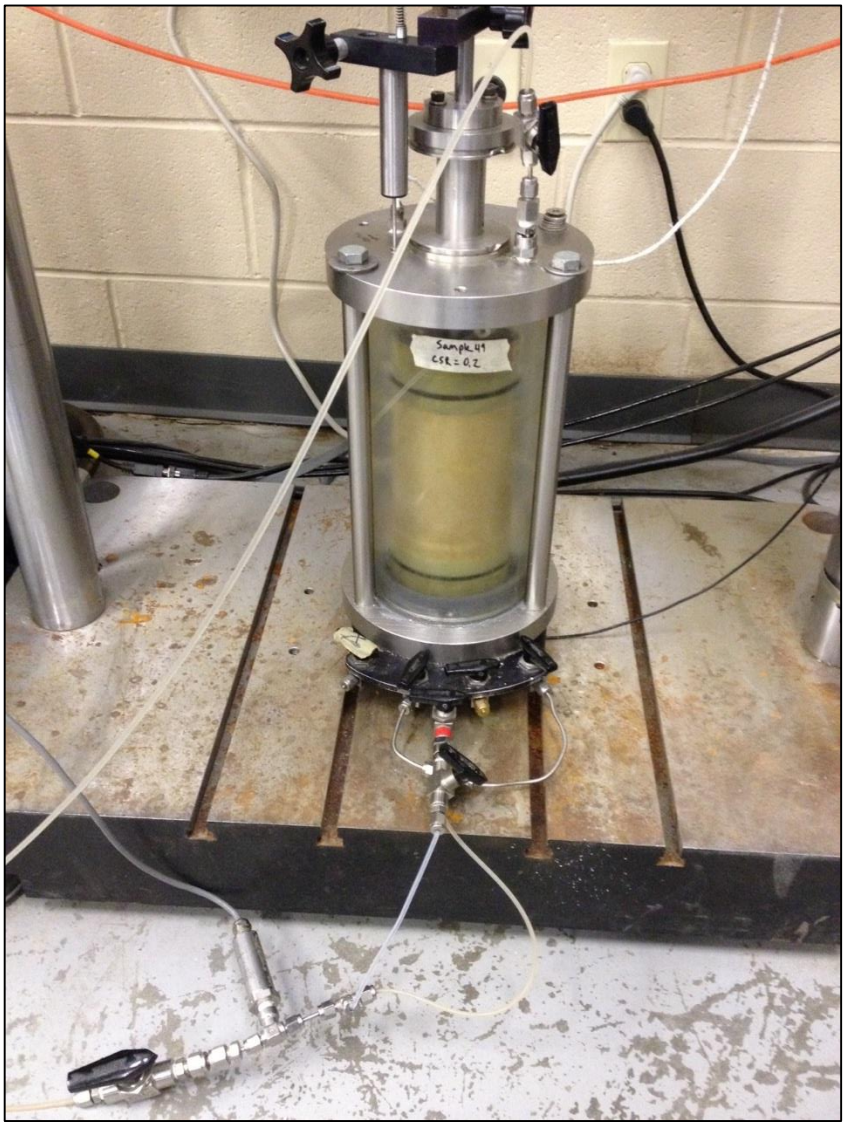

Figure 3-21: Pore Pressure transducer connection for reading the cell and sample pressures

Saturation was verified using Skempton's pore pressure ratio, B. If the sample was fully saturated ($B \geq 0.95$), the next step was to create an air gap necessary for cyclic testing. The pressure applied to the top of the cell was slightly increased while a separate line was connected to the bottom of the cell with a slightly lower pressure so the water could be drained into the "storage" section of the pressure panel. Great care was taken to

make sure the cell pressure did not decrease to the point where the cell pressure equaled the sample pressure. The water in the cell was drained until it reached the top of the sample top cap.

The next step was consolidation of the sample. For tests conducted at an effective consolidation pressure of 100 kPa, an isotropic effective consolidation stress was applied by increasing the applied load over sixty seconds to -42.78 N and the pressure panel was turned up to 340 kPa during the same time period. The sample pressure was maintained at 240 kPa. LVDT and burette readings were taken before and after consolidation to record the change in sample volume. All samples underwent fifteen minutes of consolidation.

At the end of consolidation, the cell pressure and sample pressure were accurately measured to calculate the necessary cyclic loading amplitude for testing. The amplitude is calculated by:

$$\text{Amplitude (N)} = 2 \times CSR \times \sigma`_c \times A_s \times 1000 \qquad 3.4$$

Where the amplitude is in Newtons, CSR is the cyclic stress ratio chosen for a given test, $\sigma`_c$ is the effective confining pressure (kPa) at the end of consolidation and A_s is the cross sectional area (m^2) of the sample. The cross sectional area was corrected for the 0.3408 mm thick rubber membrane on the exterior of the sample.

The Instron Wavematrix was then opened and a new test was selected. The amplitude calculated from equation 3.4 was inputted for each test. A sinusoidal cyclic load applied

at 1 Hz was used and data sampling was done every 0.2 seconds. The waveform was chosen to start in 180 degrees because this would start the test in compression (Figure 3-22).

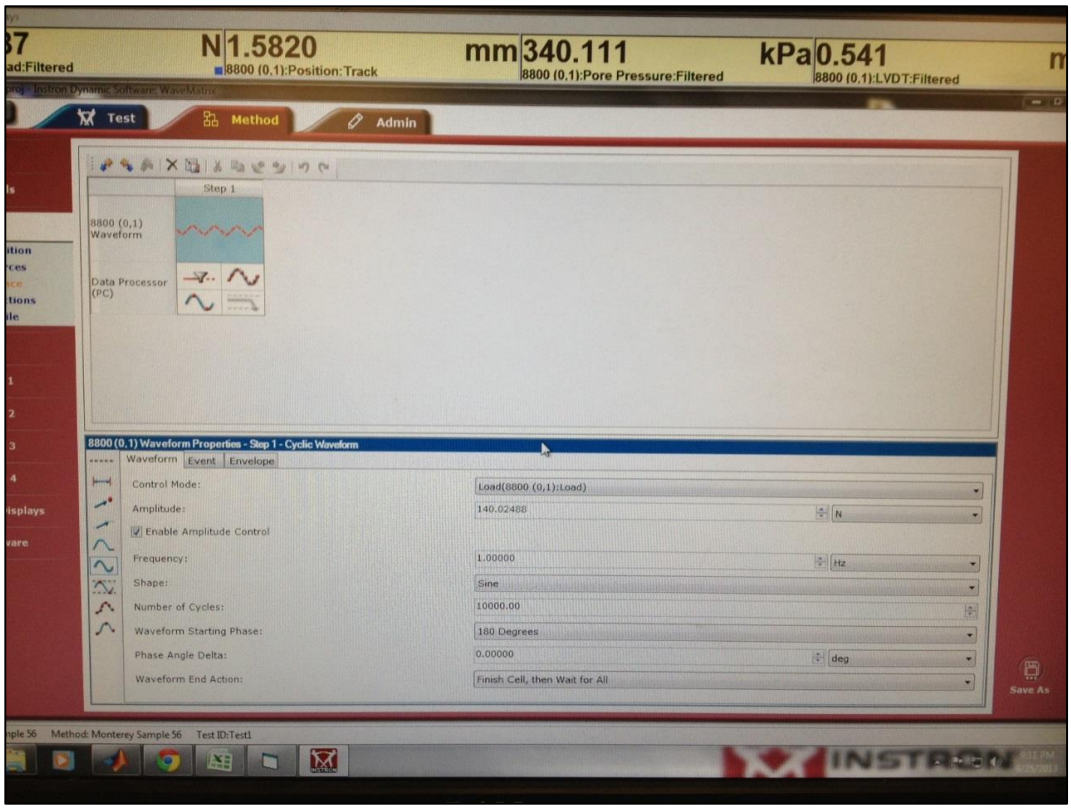

Figure 3-22: Testing parameter input screen

Before a test was run, the author made sure the limits were set for the load and the LVDT in the Instron Console window (Figure 3-23). This ensured if something went wrong, the Instron Load Frame would stop the test if for some reason the limits were tripped.

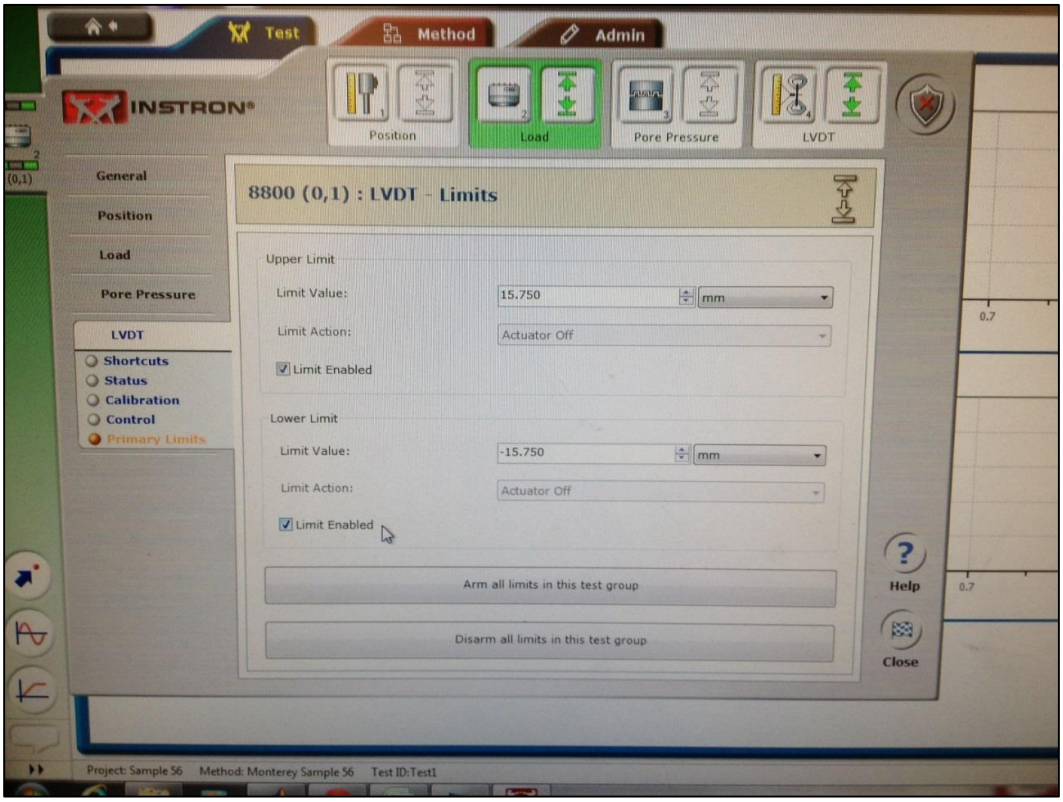

Figure 3-23: Setting Instron testing limits

Finally to run the test, the "start" button was selected and a screen appeared confirming that a test will be performed. At this point, the valve between the pressure panel and the sample pressure was closed so that excess pore pressures could be measured by the external pressure transducer during cyclic loading.

The author double checked to make sure the triaxial cell was unlocked from the cell and that it was securely fastened to the load frame. The test was then run by selecting the "ok" button.

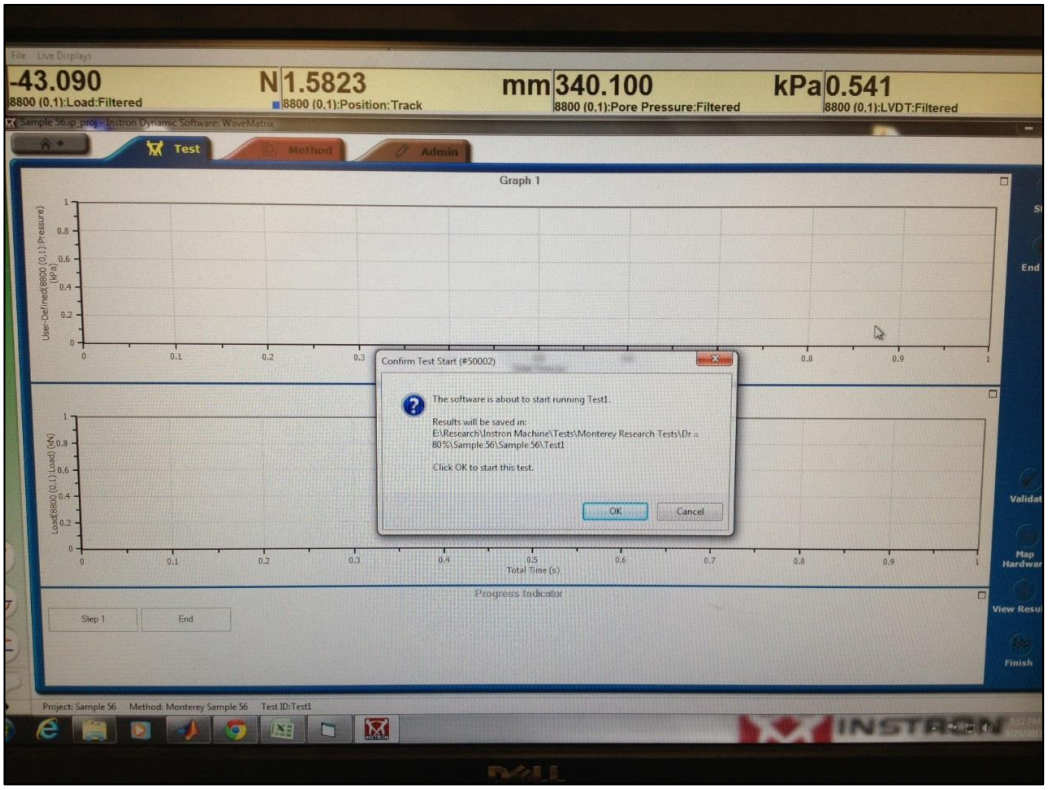

Figure 3-24: Start of cyclic testing

3.5 Shear wave velocity measurements

A triaxial cell with bender elements in the top and bottom cap was used to measure the shear wave velocity. This bender element system was first developed at the University of Rhode Island (Hanchar 2006) and was successfully used by Bradshaw (2006). The system used in this study was built by Yaurel Guadalupe-Torres (Guadalupe-Torres 2013) and the Ocean Engineering Laboratory Technician, Mr. Fred Pease. These bender elements are constructed of a piezeoceramic material capable of converting a voltage to mechanical bending and vice versa. A shear wave was generated within the bender element mounted in the bottom cap and received in the bender element located in the top cap.

Shear wave velocity was determined by "peak to peak" as the arrival time of the shear wave (Lee and Santamarina 2005; Kumar and Madhusudhan 2010) as shown in Figure 3-25. The system delay was removed by touching the bender elements and measuring the signal (Baxter et al. 2008).

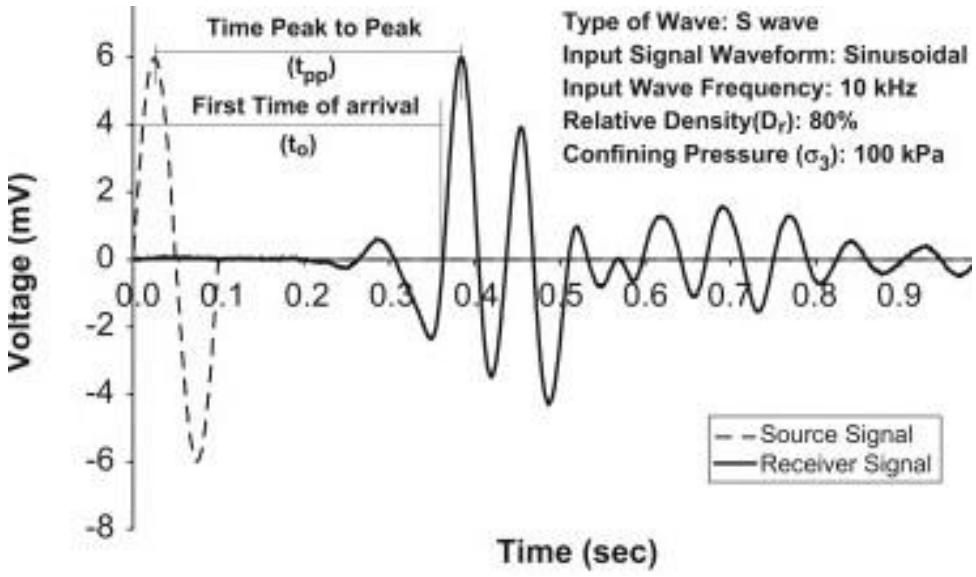

Figure 3-25: Typical peak to peak measurement (Khumar and Madhusudhan 2010)

The shear wave velocity was measured at the end of consolidation using a Tektronix TDS 2014B four channel digital storage oscilloscope (Figure 3-26). The shear wave is measured by using the cursor function on the oscilloscope and measuring the travel time from the peak of the input signal to the peak of the arrival signal. A signal of five kHz was used for the testing because of the clarity of the peak to peak, but the author also tried other frequencies from one to fifteen kHz and the travel time was always the same.

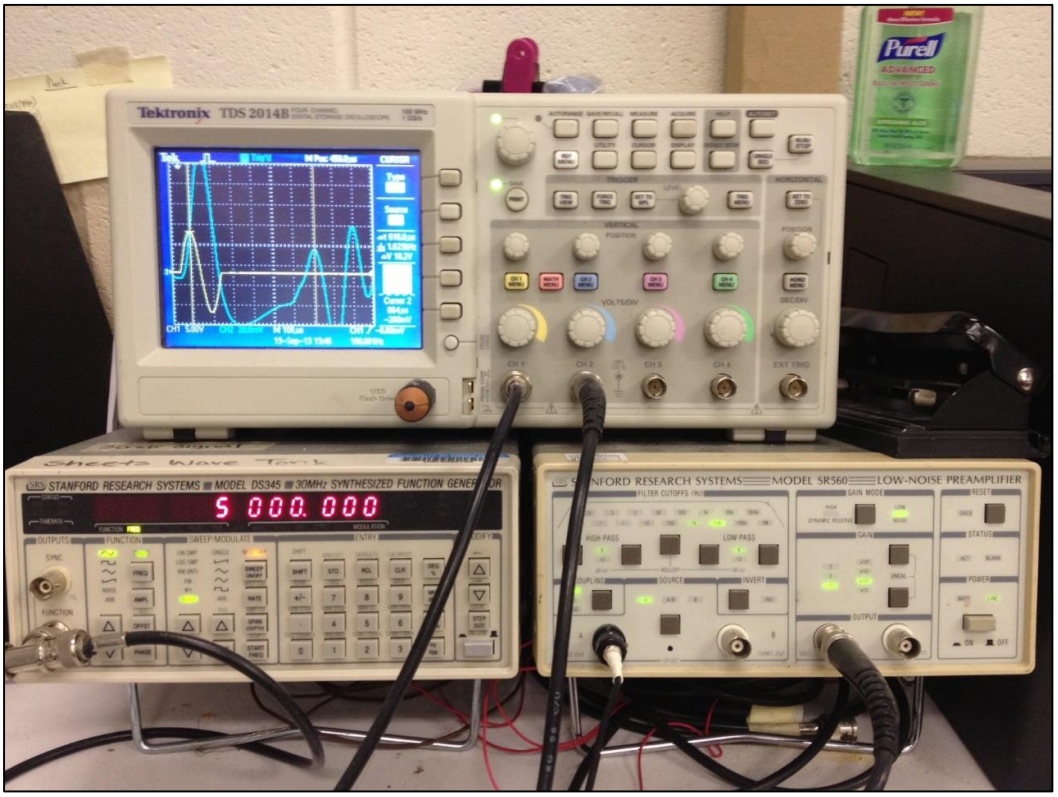

Figure 3-26: Shear Wave Measuring Setup

Figure 3-27 shows a typical shear wave measurement where the shear wave velocity was calculated using the tip-to-tip measurement by the following

$$V_s = \frac{\Delta t}{H} \qquad 3.5$$

Where Δt = travel time, H = distance between bender elements. The delay in travel time was determined by touching the bender elements together and measuring the signal. This delay, 12 µs, was subtracted from the travel time measured during each test. The height of each bender element was five millimeters and this was subtracted from the sample height at the end of consolidation to get the final distance between bender elements.

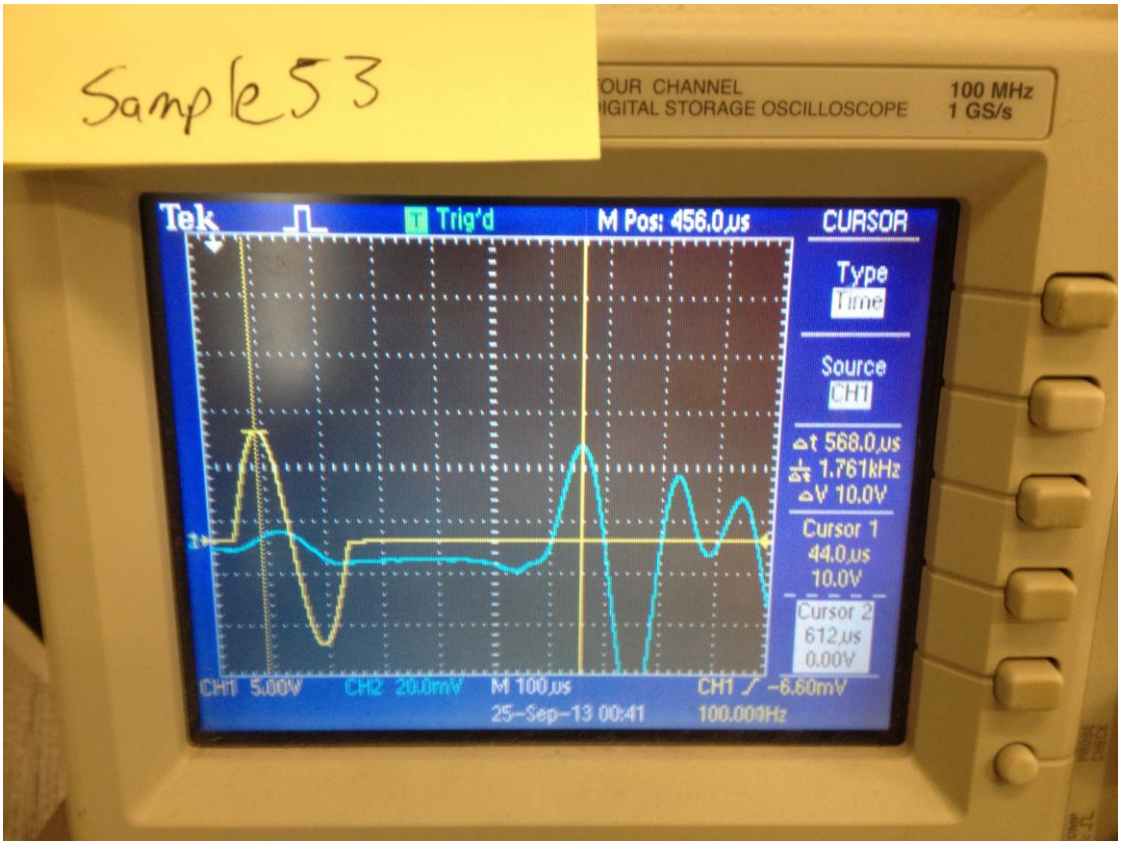

Figure 3-27: Typical screenshot from the oscilloscope showing a transmitted and received signal, in this case the travel time is 568 µs

Once the test was complete, the triaxial cell was disconnected and removed from the load frame. The cell was disassembled and the sample sand was careful rinsed from the rubber membrane to ensure an accurate sample mass could be obtained. The sample was then placed into the drying oven for 24 hours and then weighed to obtain the sample mass. In the case of the calcareous sand, the sample mass was then combined with the dried excess mass and sieved to check for grain crushing.

3.6 Evaluation of Piston Friction

A strain controlled test was conducted to determine the effect of piston friction. The test was conducted by applying a 240 kPa pressure to the cell and conducting a strain controlled test for one centimeter to determine the necessary load application to overcome friction.

This test was corrected for the additional load due to the mass of the Piston, 2.8 N. Figure 3-28 shows is a plot of ten cycles and shows the Instron setup is very good in tracking strain controlled tests.

Figure 3-29 demonstrates the piston friction is less than 5 N in the compression direction, but is closer to 7 N in the extension direction. This could be due to the rolling effect of the rubber membrane used to create the seal around the piston.

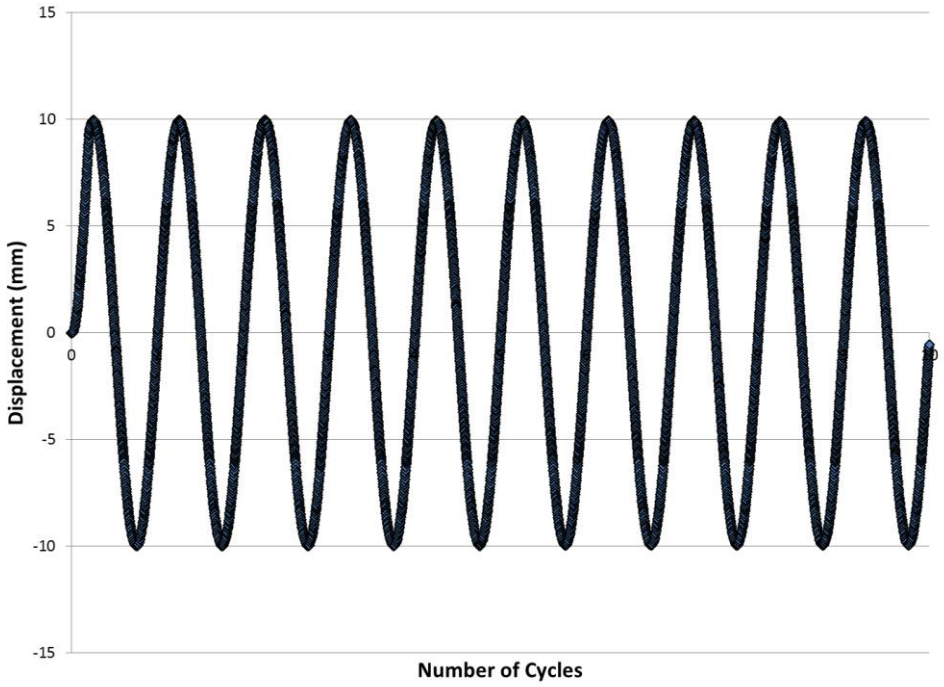

Figure 3-28: Piston friction displacement vs. number of cycles

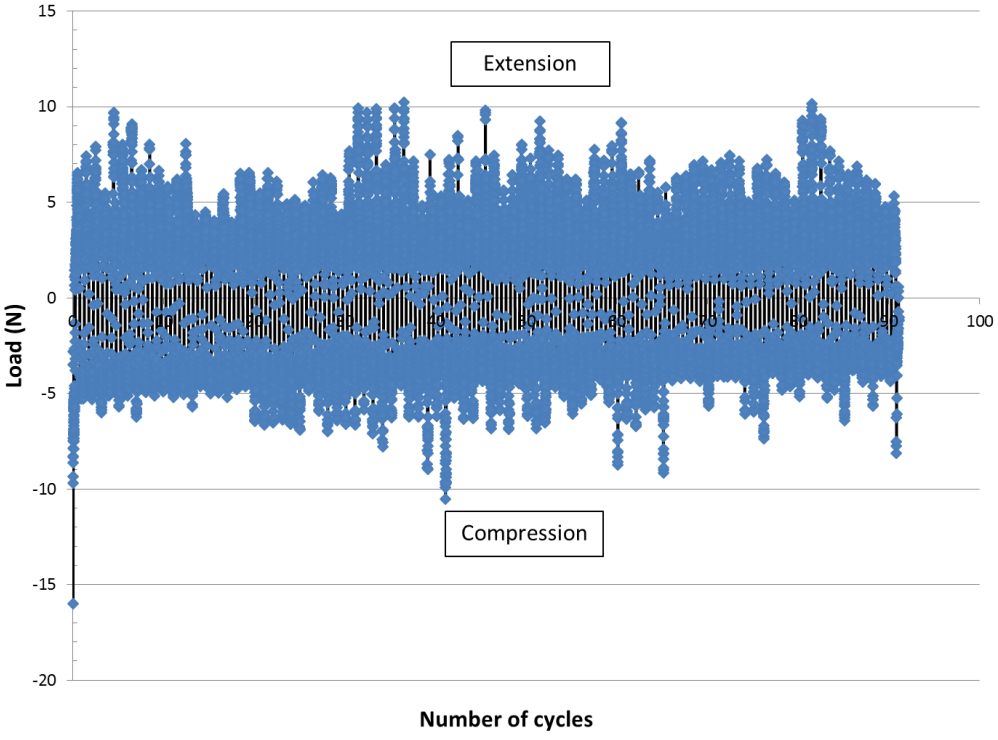

Figure 3-29: Piston friction load vs. number of cycles

The weight of the LVDT and bracket was also taken into consideration. The weight of the LVDT and bracket was 0.324 kg's (3.2 N). In compression, the mass of the LVDT nearly balances out the effect of the friction. In extension, this is not the case, so a more in depth look was taken.

Sample 26 had the lowest amplitude of all the tests at 121.78 N. To calculate the loss in the extension force, the following

$$DF_{ext} = LCL_{ext} - L_p - L_{LVDT} - L_{friction} \quad 3.6$$

Where LCL_{ext} is the force applied by the Instron Load Frame (121.78 N), L_p is the force applied due to the friction mass (2.8 N), L_{LVDT} is the force applied due to the mass of the LVDT (3.2 N) and $L_{friction}$ is the force applied due to the piston friction (7 N). By inputting these numbers into Equation 3.5, the result is 108.78 N. This is a reduction of nearly 11% in extension amplitude.

However, if you are to combine the deviator stress in extension with the deviator stress in compression and take the average, the resultant is a cyclic amplitude equal to 116 N. To calculate the effect on the CSR we use the following

$$CSR = \frac{Amplitude}{2 \times \sigma`_c \times A_s} \quad 3.7$$

where Amplitude = 115.28 N, $\sigma`_c$ = 100 kPa (kN/m^2), and A_s = 0.0004 m^2. The resultant is a CSR = 0.1441. The actual CSR used for the testing was 0.1494, resulting in a

difference in CSR = 0.0053. The author deems this insignificant and will not be including any corrections for piston friction, mass of the LVDT, or mass of the piston in the calculations for this study.

3.7 Equipment Maintenance

The large air compressor operates between 90-120 psi. If something happens to the motor, the portable compressor can be connected via the air line and it will operate between 90-125 psi. Regardless of the pressure source, the compressor holding tank needs to be drained weekly to remove moisture build up and prevent rusting of the tank.

The hydraulic pump needs to have the oil changed and this process should be performed every two years, or every 2000 motor hours.

4. Results and Discussion

A total of twenty nine cyclic triaxial tests were performed in this study, eleven for Monterey sand and eighteen on Cabo Rojo Calcareous sand.

All samples were prepared using the modified moist tamping method as described in Chapter three and had an initial height of 14.2 cm and diameter of 7.14 cm. This diameter measurement included a correction for the 0.3048 mm thick rubber membranes used to contain the sample. Samples were inundated and backpressure saturated up to 240 kPa, using an effective stress of 30 kPa.

All samples were subjected to a 100 kPa isotropic consolidation stress for fifteen minutes and the volume change was recorded. The shear wave velocity was measured using a frequency of five kHz prior to shearing.

A one Hz sinusoidal cyclic loading was applied until failure, which was when the pore pressure ratio reached unity ($r_u = 1$).

4.1 Results of Cyclic Triaxial Tests on Monterey Sand

The results of a single test Monterey sand test (Sample 45) are shown in Figure 4-1. Figure 4-1a shows the applied deviator stress, Figure 4-1b shows the pore pressure ratio, Figure 4-1c shows the axial strain, and Figure 4-1d shows the double amplitude strain, all as a function of the number of cycles of loading. Double amplitude strain is calculated by the summation of the axial strain in compression and extension for each cycle. Failure (or liquefaction) was defined as when the pore pressure equals the confining stress and the resulting effective stress becomes zero. Figure 4-1b shows that liquefaction occurs after 107 cycles of loading when $r_u = 1$ ($r_u = \Delta\mu/\sigma`$).

The stress path shows the reduction in effective stress (p') with cycling. As the effective stress approaches zero, the stress path hits a failure envelope in both compression and extension. The slope of these envelopes is analogous to the Mohr-Coulomb failure envelope. It is interesting to note that the slope of the envelope is steeper in compression than in extension, which suggests that the sample is weaker in extension. This is supported by the stress-strain relationship in Figure 4-2b and Figure 4-1c. The sample clearly underwent more strain in extension than in compression and this was true all the samples tested in this study. Detailed plots of the other tests shown in Table 4-1 are included in Appendix A.

Figure 4-2 shows the stress path and stress vs. strain during the test until failure.

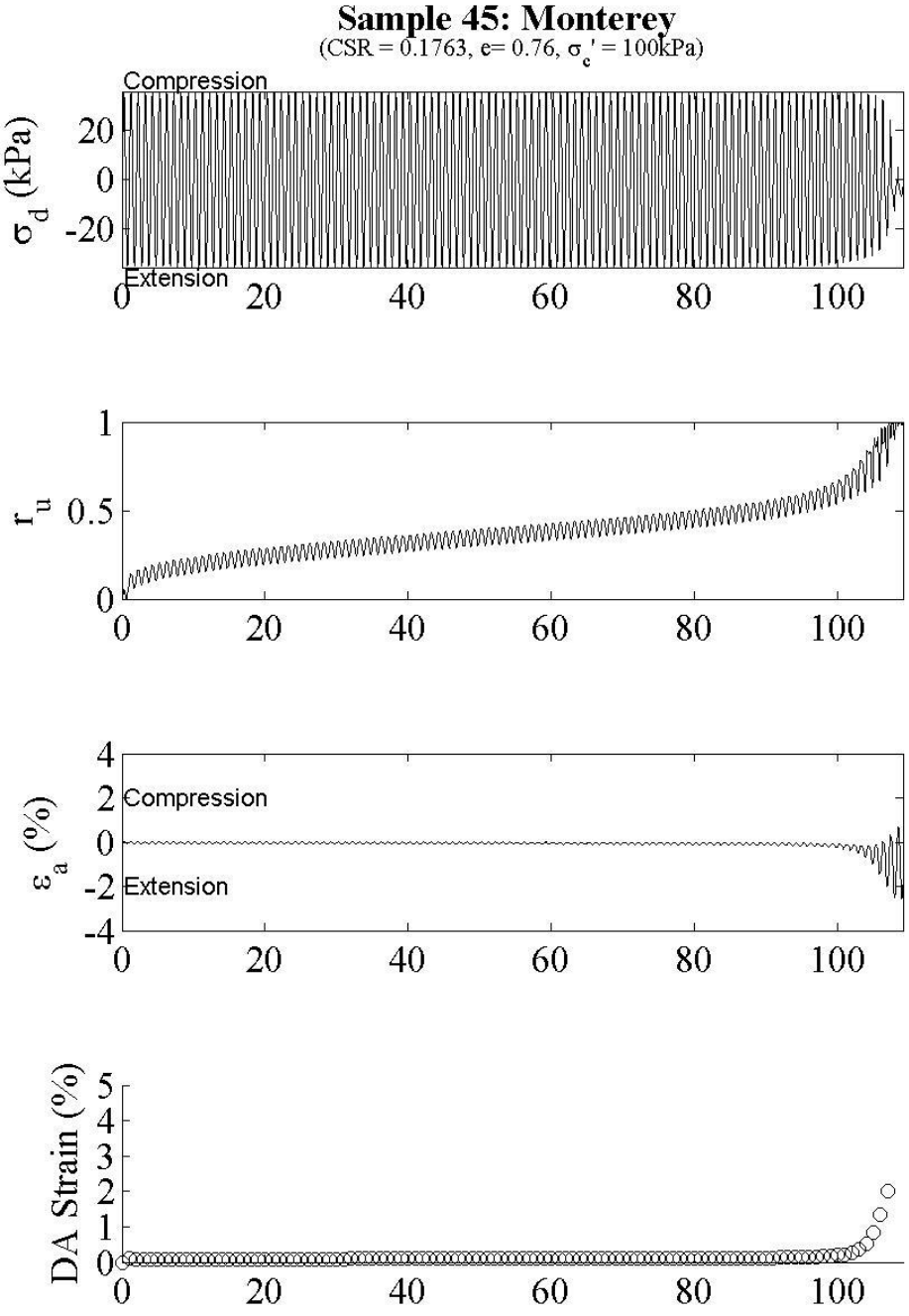

Figure 4-1: Typical results from cyclic testing on Monterey sand showing; a) deviator stress, b) pore pressure ratio, c) axial strain, and d) double amplitude strain as a function of cycles.

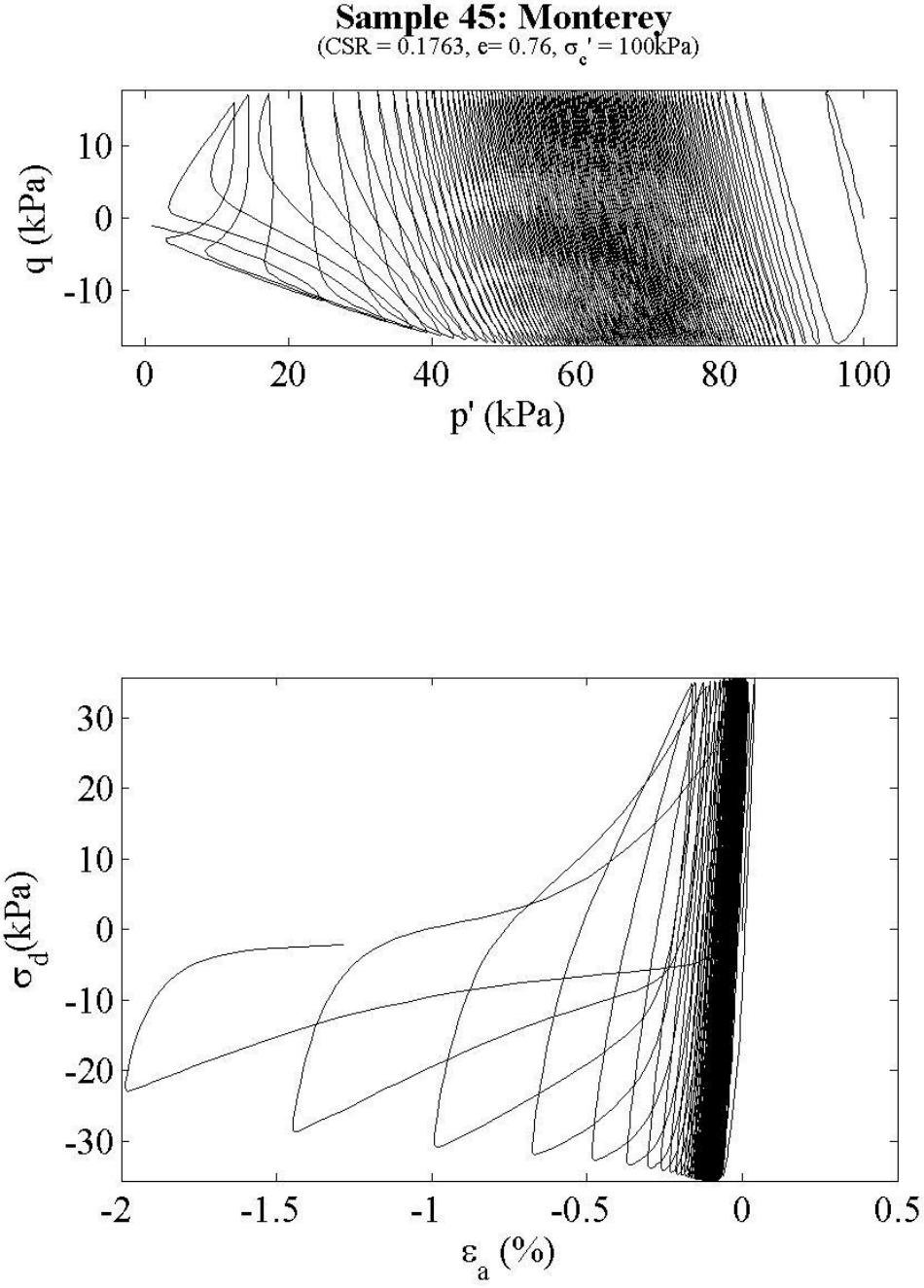

Figure 4-2: Sample 45 stress path and stress vs. strain plots

The results of eleven cyclic triaxial tests are summarized in Table 4.1. Included in the table is the void ratio before and after consolidation, the shear wave velocity (V_s), the applied cyclic stress ratio (CSR), and the number of cycles to liquefaction (N_l).

Sample #	e_o	e_c	V_s (m/s)	CSR	N_l
43	0.76	0.76	226	0.2233	32
45	0.77	0.76	220	0.1763	107
46	0.77	0.76	220	0.2466	6
47	0.77	0.76	227	0.2296	18
51	0.69	0.69	239	0.2641	13
53	0.68	0.68	237	0.2225	62
54	0.69	0.68	242	0.1978	83
56	0.69	0.69	232	0.1737	125
57	0.66	0.66	262	0.2472	49
58	0.65	0.64	258	0.3092	14
60	0.66	0.65	248	0.1983	119

Table 4-1: Results of Monterey sand testing

Figure 4-3 is a plot of the data from Table 4-1. A dashed line is drawn to indicate the location of 15 cycles, which represents an earthquake magnitude of 7.5. Figure 4-4 shows the CRR – V_s data representing an earthquake magnitude 7.5.

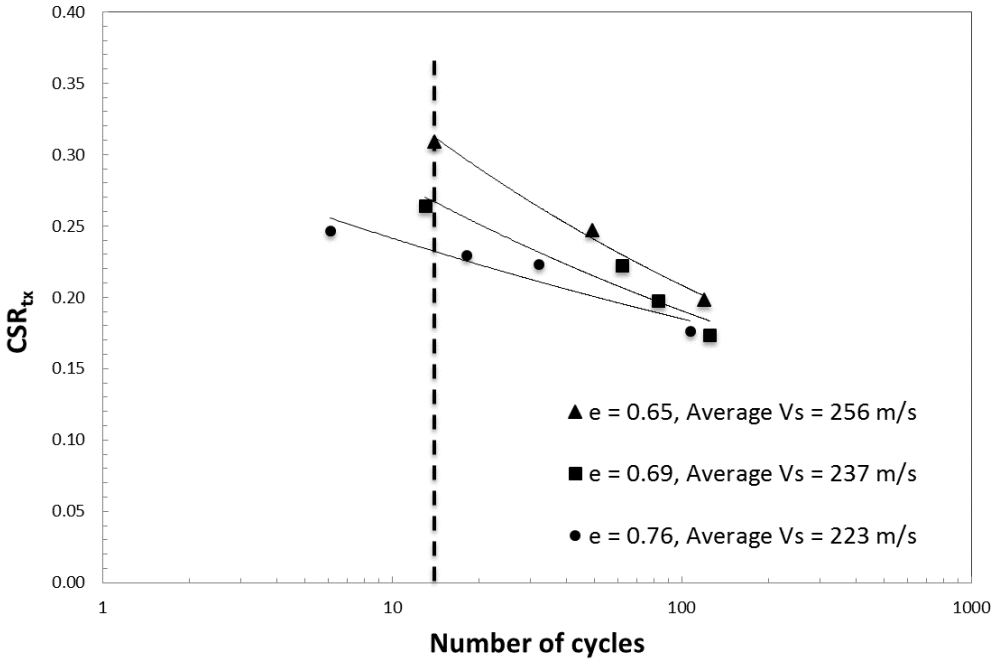

Figure 4-3: CSR_{tx} vs. Number of cycles to failure Monterey results with a dashed line indicating a Magnitude 7.5 earthquake (15 cycles)

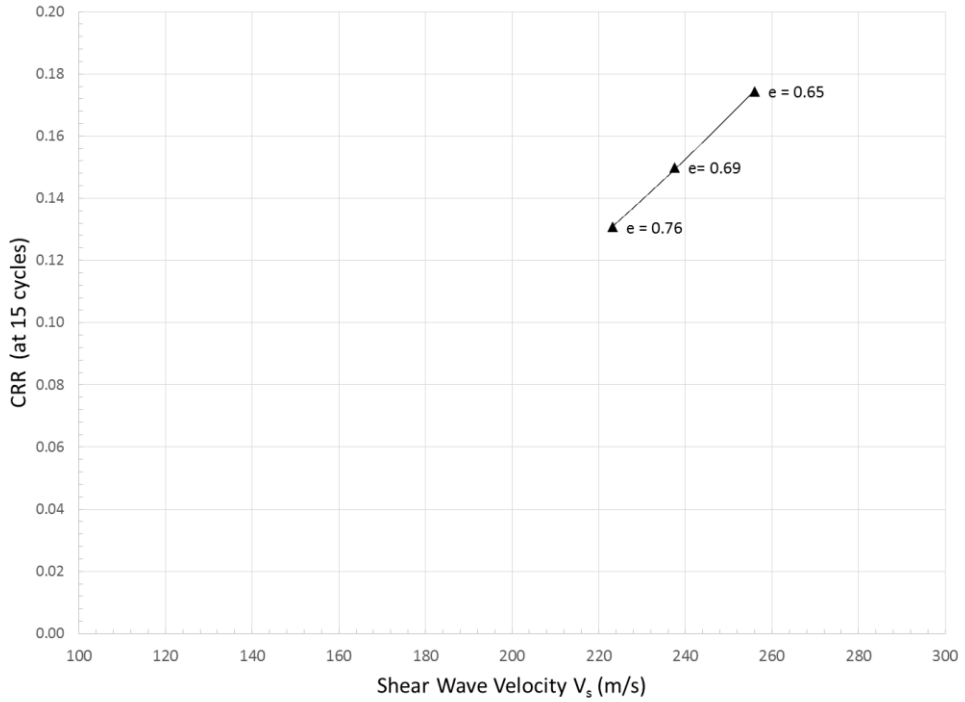

Figure 4-4: CRR vs. V_s for Monterey sand

4.1.1 Comparison with Published Data

In this section the Monterey sand test results are compared to results published in the literature.

The cyclic triaxial tests are complicated geotechnical tests and it is important to try to validate these results with the work of others. This can be difficult because the results can be influenced by many factors, including the equipment used, sand type, sample preparation, and experience of the tester.

Monterey sand was chosen specifically for this study because it has been used widely in the U.S. for laboratory liquefaction studies. Two five-gallon buckets of Monterey sand were purchased from Kleen Blast Abrasives, Danville, CA. One of the buckets was shipped to Virginia Tech and one to URI. Index tests (grain size, specific gravity, and minimum and maximum void ratio) were obtained on samples from both buckets and showed the contents were the same (see Table 4-2). Cyclic triaxial tests were performed at Virginia Tech by Ph.D. candidate Sam Lasley (personal communication 2013) using a cyclic triaxial apparatus manufactured by GCTS Testing Systems. Samples at Virginia Tech were prepared using wet pluviation and 60 Hz horizontal vibration to achieve a desired void ratio.

Figure 4-5 shows a comparison of test results on samples of Monterey sand with void ratios of 0.75 and 0.76 tested at Virginia Tech and at URI.

The agreement is very good considering the differences in equipment and sample preparation methods. The latter is surprising considering the long-standing understanding that sample preparation can greatly affect cyclic resistance (Mulilis et al. 1977).

Figure 4-5 is a comparison plot of data received through personal correspondence from Ph. D candidate Sam Lasley from Virginia Tech. Lasley tested Monterey sand purchased from the same supplier as Monterey sand used for this study. Lasley prepared samples using wet pluviation and 60 Hz shear vibration to densify the samples.

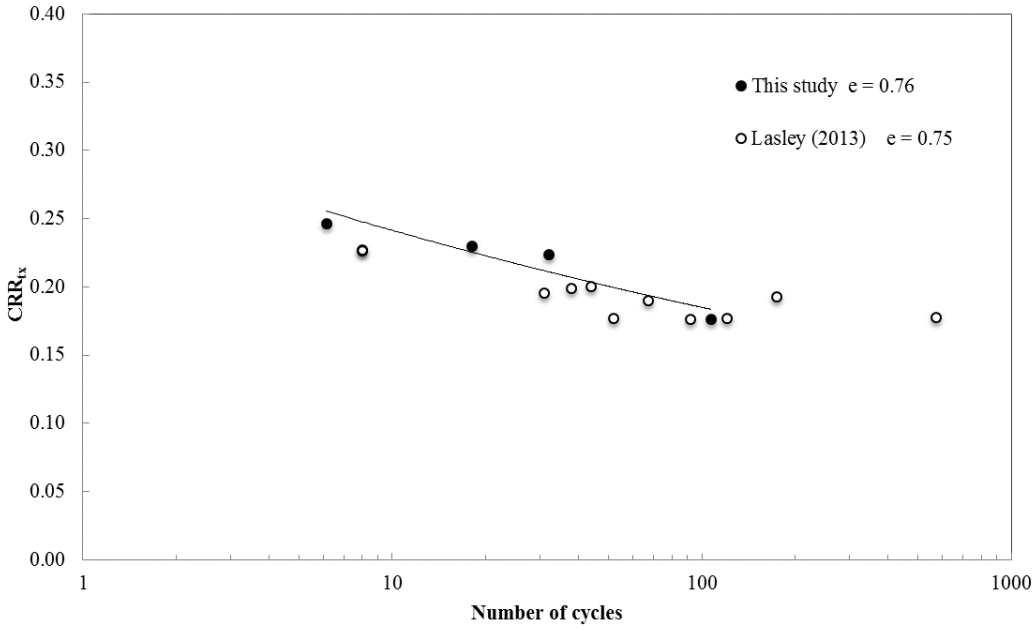

Figure 4-5: Comparison between cyclic triaxial test results on samples of Monterey sand performed at Virginia Tech and at URI for this study

Additional cyclic triaxial test data for Monterey sand and has been published by Silver (1976) and Mulilis (1977). Silver and Mulilis prepared samples using moist tamping and tested them with cyclic triaxial testing equipment. Table 4-2 shows details of their testing program, including the void ratio (e) used for testing, e_{min}, e_{max}, relative density (D_r) and the effective confining stress. Data from this study is included for comparison.

Figure 4-6 shows a comparison of cyclic triaxial tests results from this study with those from Mulilis (1977) and Silver (1976). It is expected that the data from Mulilis had a lower cyclic stress resistance than the Silver (1976) data tested at 100 kPa because of the K_σ effect.

In general, the cyclic resistances obtained in this study are consistently lower than the data from Silver (1976) and Mulilis (1977). The trend of increasing CRR with decreasing void ratio is consistent, however the curves appear to be "flatter", particularly at low cycles to failure.

Author	e	e_{min}	e_{max}	D_r (%)	$\sigma`_c$ (kPa)
Silver (1976)	0.73	0.560	0.850	50	100
Mulilis (1977)	0.71	0.564	0.852	50	55
Lasley (2013)	0.75	0.530	0.845	30	100
This Study	0.76	0.589	0.808	22	100
This Study	0.69	0.589	0.808	57	100
This Study	0.65	0.589	0.808	73	100

Table 4-2: Details of cyclic triaxial tests on Monterey sand from Silver (1976), Mulilis (1977), Lasley (2013), and this study.

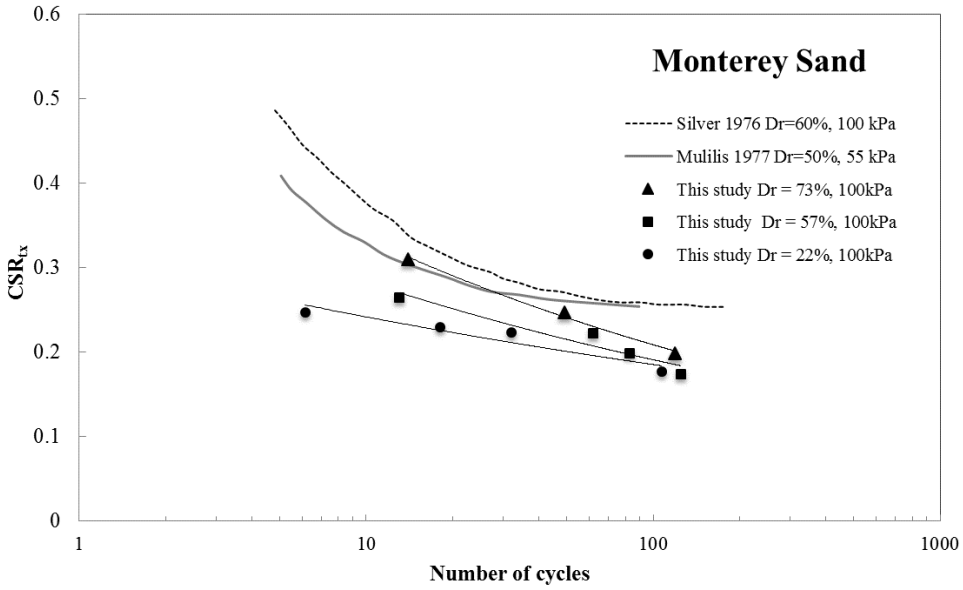

Figure 4-6: Comparison of Monterey Sand Cyclic Triaxial Testing with Published data from Silver (1976) and Mulilis (1977)

The comparison of the results from this study and published data shows reasonable agreement for the loose and medium dense samples. The CRR of the dense samples (e = 0.60; D_r = 73%) is lower than expected when compared to Silver (1976) and Mulilis (1977). For these samples, the undercompaction was two percent, meaning that the density of each layer was varied slightly to achieve an overall uniform density of the sample. A subjective way of assessing whether the level of undercompaction is appropriate is to observe where failure occurs along the length of the sample during cyclic loading. Ideally failure should occur in the middle of the sample away from the end caps. For the loose and medium samples, failure always occurred in the middle of the samples. For the dense samples, however, failure consistently occurred in the upper

portion of the samples. This may have been caused by inadvertent loosening of the last layer during tamping, which was discussed in section 3.2. Possible changes to the sample preparation methodology are discussed in the next chapter.

Another possible explanation for the differences between the results of this study and the results of Mulilis (1977) and Silver (1976) is that the sands were prepared to different void ratios because different values of e_{min} and e_{max} were obtained by Silver (1976), Mulilis (1977), Lasley (2013), and this study. There is considerable uncertainty in the determination of e_{min} and e_{max}, and because of this, the results are more accurately displayed in terms of void ratio instead of relative density.

4.2 Cabo Rojo Calcareous Sand

The results of eighteen undrained cyclic triaxial tests on Cabo Rojo Calcareous sand are summarized in Table 4.3. Included in the table is the void ratio before and after consolidation, the shear wave velocity at the end of consolidation (V_s), the applied cyclic stress ratio (CSR), and the number of cycles to failure (N_l).

Three sets of tests were conducted in this study: loose (e=1.89), medium dense (e = 1.79), and dense (1.62).

Sample #	e_o	e_c	V_s (m/s)	CSR	N_l
12	1.64	1.63	258	0.2515	42
13	1.62	1.60	263	0.2735	30
14	1.61	1.59	266	0.2984	26
16	1.62	1.61	268	0.3225	20
17	1.62	1.59	257	0.3425	10
18	1.61	1.60	193	0.2026	155
19	1.61	1.60	262	0.3243	12
34	1.61	1.59	252	0.2314	44
20	1.77	1.75	217	0.1980	37
22	1.80	1.78	217	0.2392	13
23	1.79	1.77	221	0.2221	24
24	1.79	1.77	222	0.1758	112
25	1.80	1.79	219	0.2513	8
26	1.79	1.77	223	0.1519	400
38	1.89	1.85	205	0.1930	14
39	1.89	1.86	210	0.1507	80
40	1.87	1.85	201	0.2009	12
41	1.88	1.86	208	0.1312	185

Table 4-3: Results of cyclic triaxial testing on Cabo Rojo calcareous sand

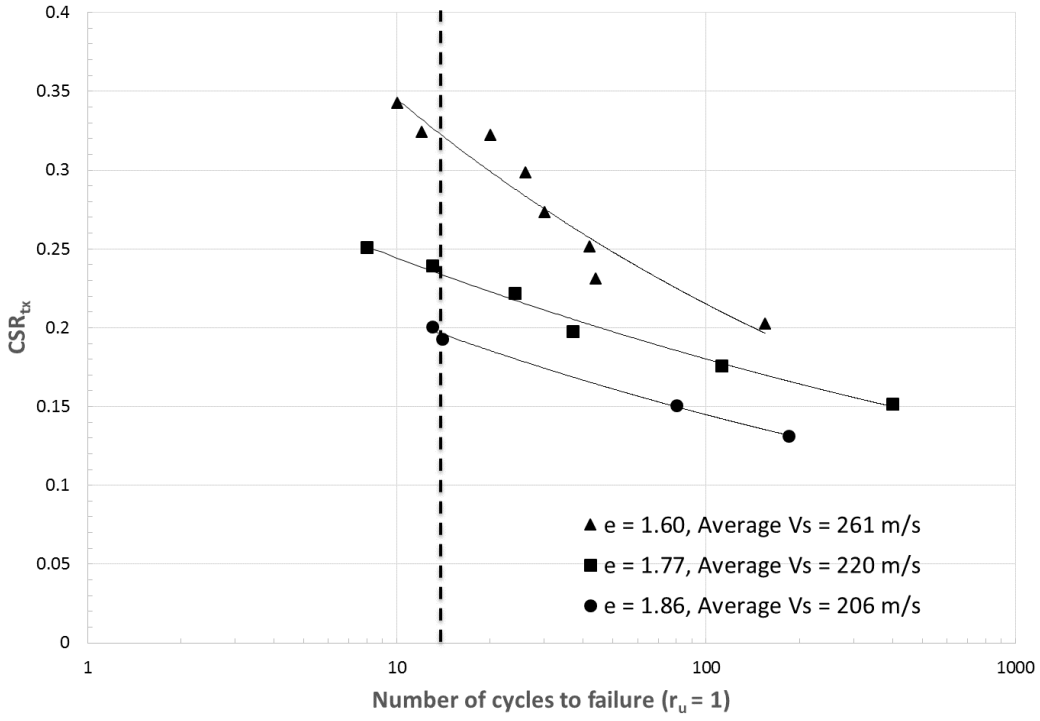

Figure 4-7: CSR_{tx} vs. Number of cycles to failure for Cabo Rojo sand in this study

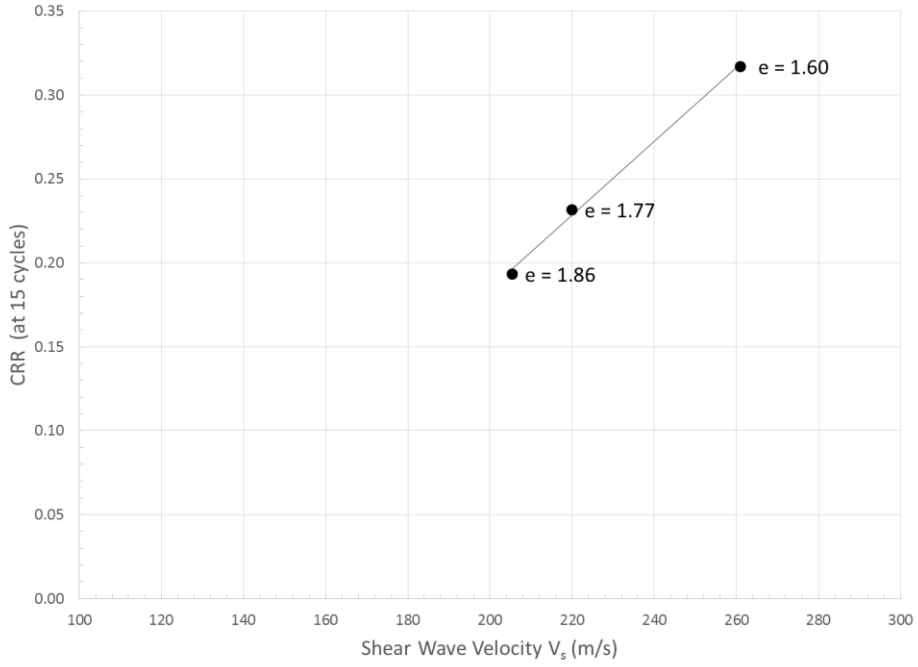

Figure 4-8: CRR vs. V_s for Cabo Rojo sand in this study

The results of a single test (Sample 12) are shown in Figure 4-9. Figure 4-9a shows the applied deviator stress, Figure 4-9b shows the axial strain, Figure 4-9c shows the development of excess pore pressure, and Figure 4-9d shows the double amplitude strain, all as a function of the number of cycles to loading.

Figure 4-10 is a typical plot of the stress path and stress vs. strain for the Cabo Rojo samples. As with the samples of Monterey sand, all the samples of Cabo Rojo sand failed in extension.

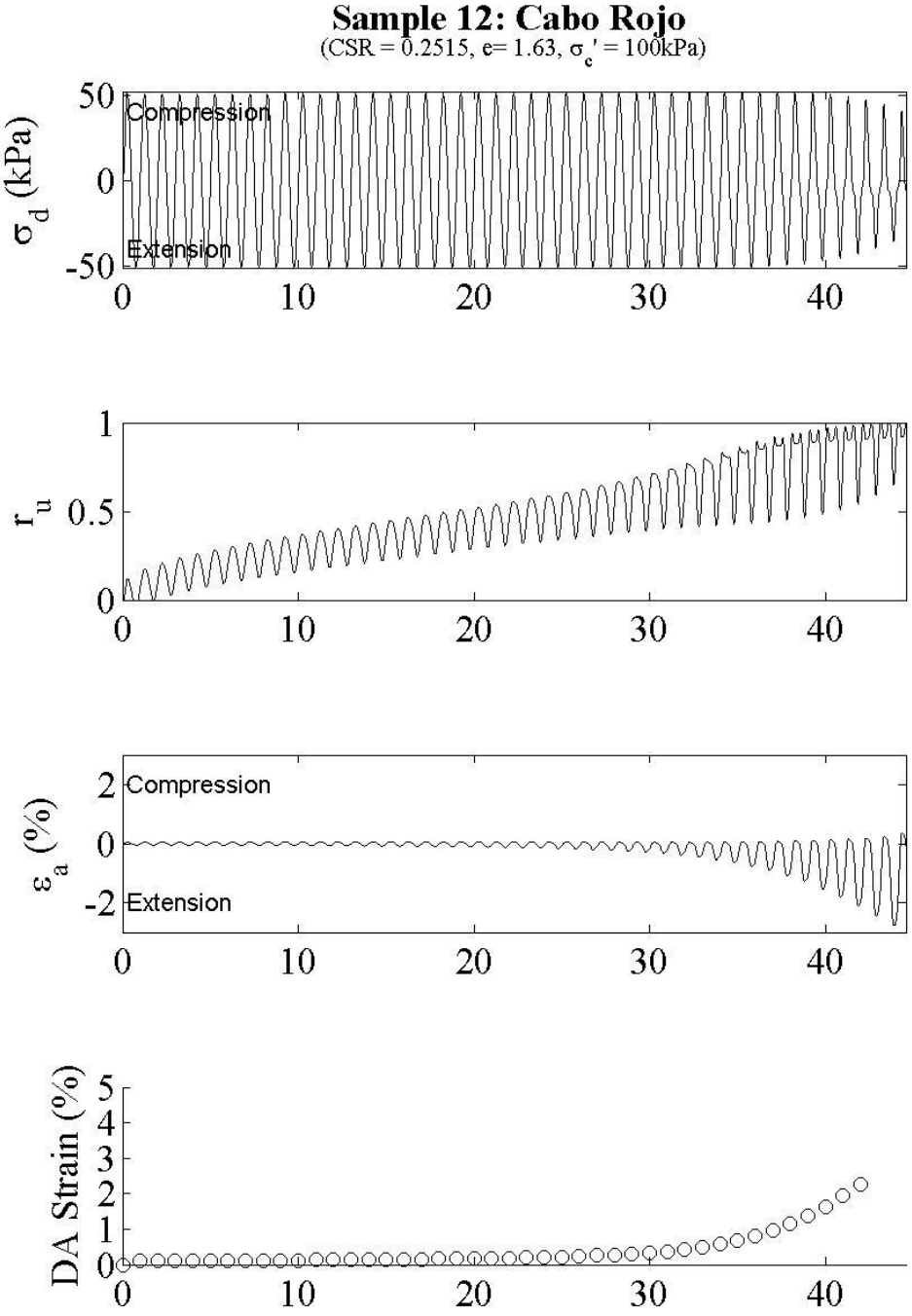

Figure 4-9: Typical Results from cyclic testing on Cabo Rojo sand; a) deviator stress, b) pore pressure ratio, c) axial strain d) double amplitude strain.

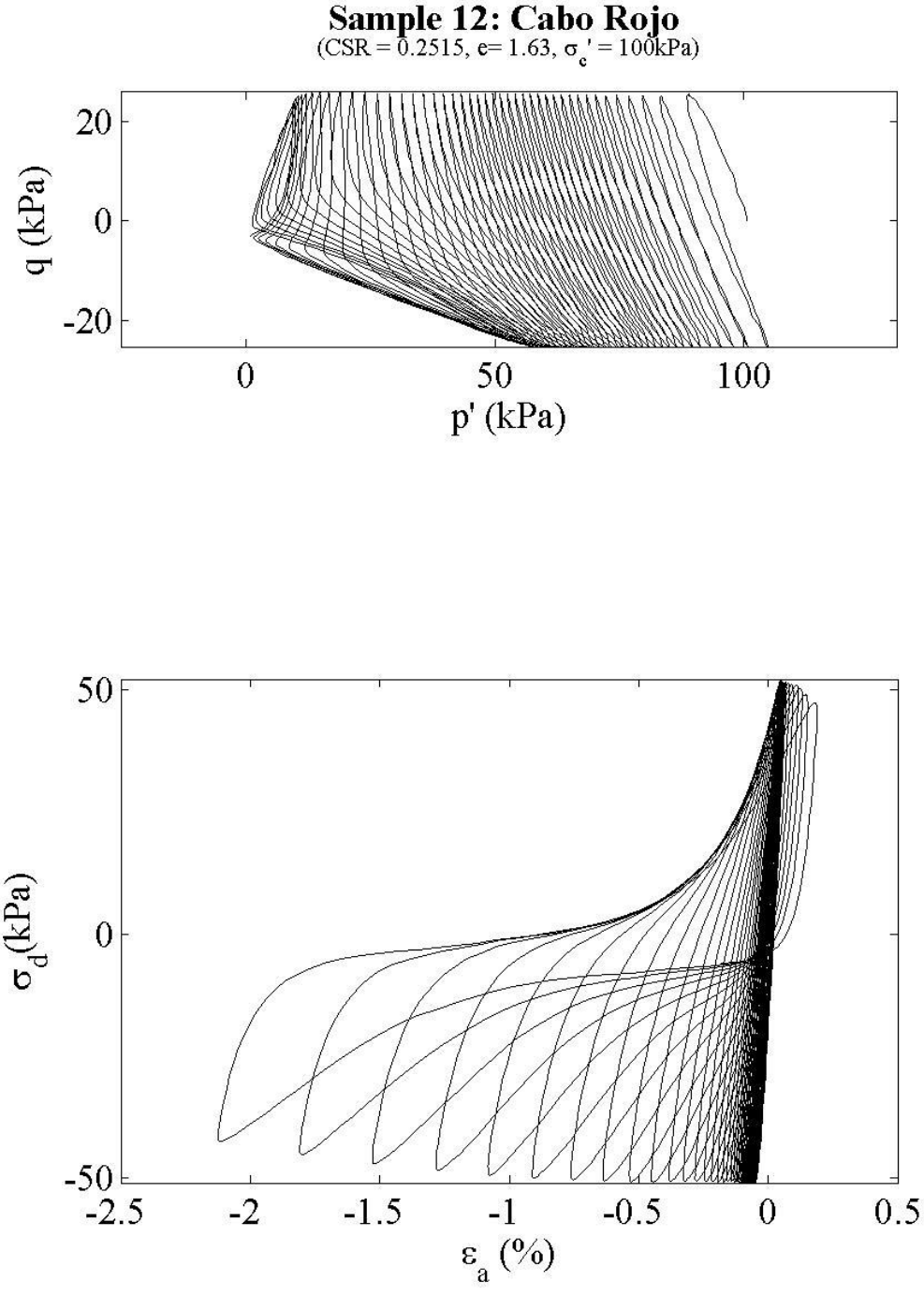

Figure 4-10: Cabo Rojo stress path and stress vs. strain plots

All samples were sieved before and after testing to verify if soil grain crushing was occurring or not. Figure 4-11 shows the sieving before and after all tests for the Cabo Rojo calcareous sand and indicates there was no crushing in this study.

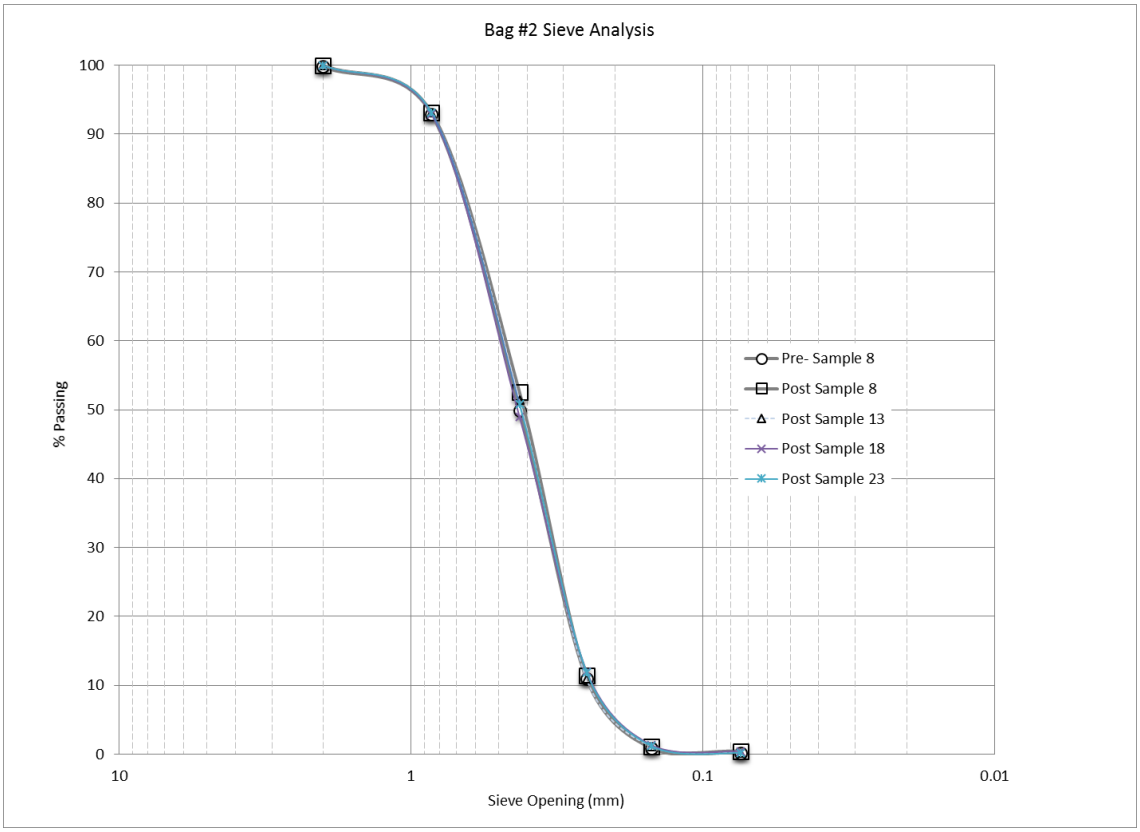

Figure 4-11: Typical sieve analysis for Cabo Rojo sand

4.2.1 Comparison with Published Data

Calcareous sands are difficult to study because of their chemical composition and variability in grain size distribution and grain shape. Their properties can vary greatly from samples taken from the same location.

Table 4-4 shows measured index properties of samples of Cabo Rojo sand obtained from the same location as part of two separate studies.

Index Property		Cabo Rojo Sand (Sandoval and Pando)	Cabo Rojo Sand (Dobling)	ASTM
D_{10}	mm	0.24	0.24	ASTM D 422-63 (98)
D_{30}	mm	0.30	0.30	
D_{50}	mm	0.37	0.37	
D_{60}	mm	0.41	0.42	
C_u		1.75	1.75	
C_c		0.94	0.89	
G_s		2.84	2.87	ASTM D 854-06
γ_{min}	kN/m^3	9.10	10.20	ASTM D 4254-00
e_{max}		2.07	1.76	
γ_{max}	kN/m^3	11.10	12.39	Dobling = ASTM D 4253-00 Sandoval and Pando = Alternative Method
e_{min}		1.51	1.27	

Table 4-4: Comparison of index properties of Cabo Rojo sand samples collected from the same beach in 2006 (Sandoval and Pando 2012) and in 2012 for this study.

The grain size distributions and values of Specific Gravity are almost identical, however there are significant differences between the minimum and maximum void ratios.

Although both studies followed ASTM standards in determining these values, it is believed that the differences in results are more due to variability in the tests rather than in the soil. For this reason, comparison of cyclic resistance between these two studies are done based on void ratio rather than relative density.

The results of the cyclic triaxial testing on Cabo Rojo sand from this study are shown in Figure 4-12 and compared to the cyclic triaxial testing results by Sandoval and Pando (2013). The results for the loose and medium dense samples are in good agreement between the two studies. Similar to the results of the Monterey sand, however, the cyclic resistance of the dense samples in this study was lower than the dense samples performed by Sandoval and Pando (2013).

Sandoval and Pando (2013) prepared samples using the Ladd (1976) moist tamping method with undercompaction. Their samples were prepared in five layers with a final height of 102 mm and diameter of 51 mm.

One difference in the sample preparation methods between this study and Sandoval and Pando (2013) is the molding water contents used in the moist tamping. The molding water contents (W_m) used in this study were calculated with the goal of keeping a saturation level of 55% to be consistent with Baxter et al. (2008). The molding water contents in this study ranged from 29% to 33.5%, while the molding water contents in Sandoval and Pando (2013) ranged from 4% to 25%. The molding water contents in this study decreased with increased density, while the molding water contents in Sandoval and Pando increased with increased density.

Ladd (1976) never specified if the water content should be increased or decreased with density, only that the initial sample saturation level should be between 20% to 70% and that samples with lower fines contents will need less saturation percentage levels.

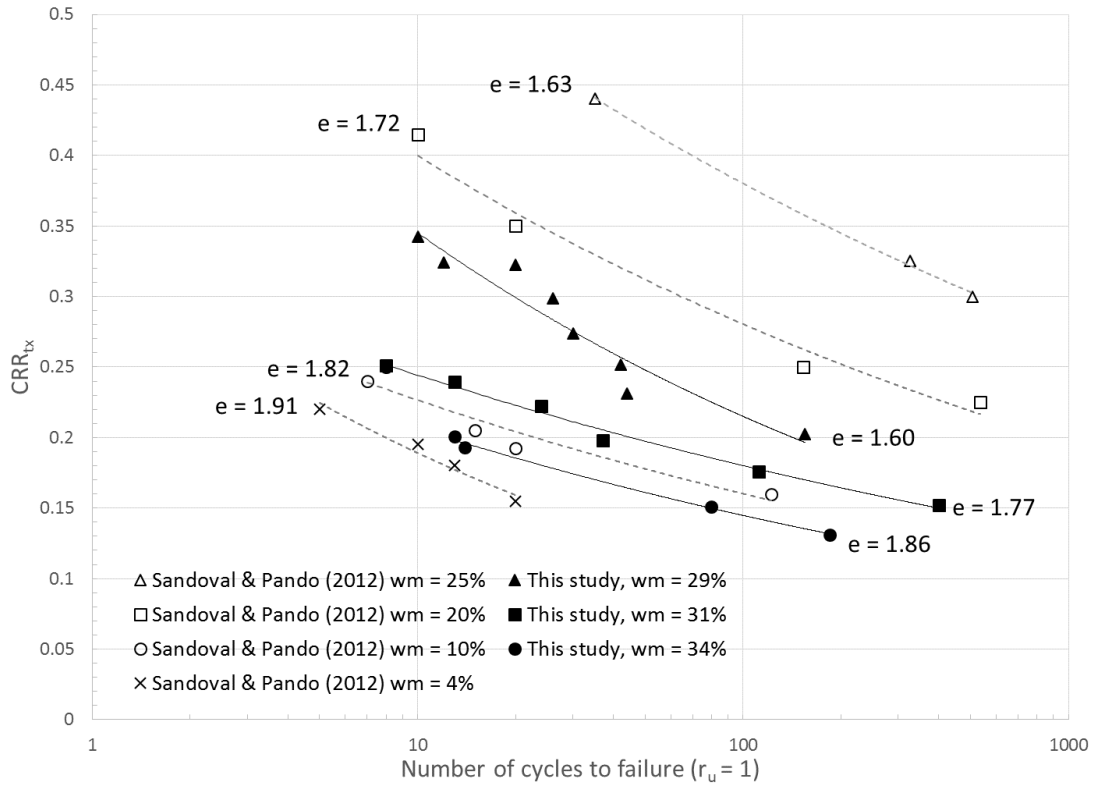

Figure 4-12: Comparison of Cabo Rojo calcareous sand with Sandoval and Pando (2012)

Figure 4-13 is a comparison of the results from the dense sample in this study (e = 0.60) with the results from published data on calcareous sands. This plot shows the wide range in cyclic resistance for calcareous sands at similar relative densities.

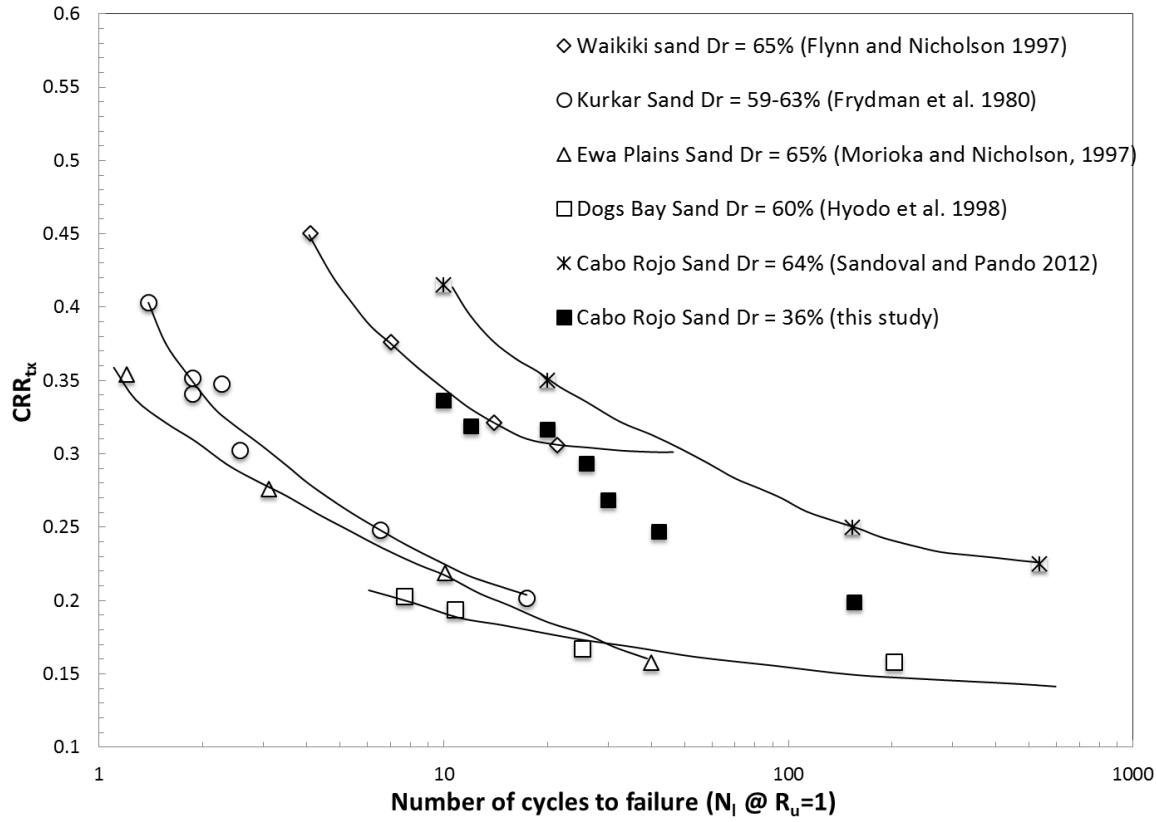

Figure 4-13: Comparison of Calcareous sands (adapted from Sandoval and Pando 2012)

4.3 Comparison of CRR - Shear Wave Velocity Relationships

The overall objective of this research was to evaluate the relationship between the cyclic resistance and shear wave velocity for Monterey and Cabo Rojo sand. In order to evaluate the cyclic resistance for different values of shear wave velocity, the cyclic resistance needs to be defined for a specific level of shaking (i.e. specific number of cycles to liquefaction). The state-of-the-practice is to use an equivalent number of cycles to failure to represent a given earthquake magnitude, and it is generally agreed that 15

cycles to failure corresponds to a magnitude 7.5 earthquake (Seed and Idriss 1971). The CRR values shown in Figure 4-4 and Figure 4-8 were obtained in this manner. The equivalent number of cycles to failure used for this study was fifteen and failure was achieved when the pore pressure ratio reached unity (r_u =1).

The CRR_{tx} and V_s from laboratory testing were converted to in situ conditions as discussed in chapter three so a direct correlation could be made between field based correlations by Kayen et al. (2013) and Andrus and Stokoe (2000).

The equations for developing an equivalent "field-based" CRR – V_s curve are detailed in Section 2.4 of this thesis and summarized here:

- CRR_{tx} corresponding to 15 cycles (CRR-N_l) was used to obtain values of $CRR_{MW = 7.5}$
- $CRR_{MW = 7.5}$ were converted to " field values by multiplication by 0.9 (for multidirectional effects) and 0.63 (for conversion from triaxial to simple shear conditions (Baxter et al. 2008))
- Values of V_s were normalized to 100 kPa vertical effective stress and correction to K_o conditions

First a comparison was made in Figure 4-15 for the Cabo Rojo calcareous results from this study with data adapted from Cataño (2006) and Sandoval and Pando (2013). Cataño (2006) measured the shear wave velocity of the same Cabo Rojo calcareous sand used by Sandoval and Pando (2012) prepared using air pluviation in resonant column

tests. Sandoval and Pando (2013) conducted cyclic triaxial testing but did not measure shear wave velocity.

The agreement between the CRR-Vs relationship in this study and the relationship inferred from Sandoval and Pando (2012) and Cataño (2006) is not good. This could be simply due to the way in which the data was combined in the previous studies. However it is a concern that the curve in this study is significantly less sensitive to the values of shear wave velocity (i.e. "flatter").

The final comparison is the field corrected soil specific relationships developed for Monterey sand and Cabo Rojo sand with the field-based approach proposed by Kayen et al. (2013). This is shown in Figure 4-16. Both curves developed in the laboratory fall to the right of the field-based curve. This suggests that for these soils, use of the field-based curve is unconservative (i.e. the liquefaction resistance of these soils is lower than suggested by the field-based approach). There is some concern that the slope of the laboratory curves are much flatter than the field-based curve, particularly at high values of shear wave velocity. This is a direct result of the dense samples discussed earlier and the cause for this discrepancy is not clear.

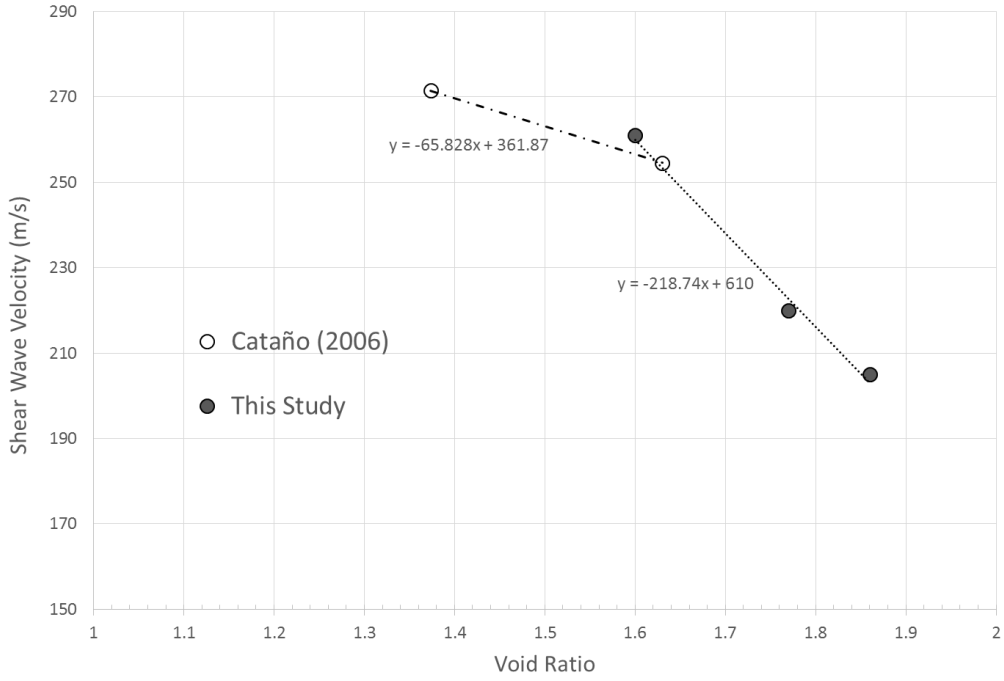

Figure 4-14: Correlation between shear wave velocity and void ratio for Cabo Rojo sand (adapted from Cataño (2006))

The author used Figure 4-14 to obtain a correlation between shear wave velocity and void ratio and then calculated the shear wave velocity for the void ratios used in Sandoval and Pando (2012). Table 4-5 is a summary of the values calculated.

Void Ratio (Sandoval and Pando 2012)	**Number of Cycles (r_u = 1)**	**CSR_{tx}**	**CRR**	**V_s (m/s)**	**V_{s1} (m/s)**
1.91	15	0.17	0.10	236.14	207.83
1.82	15	0.21	0.12	242.06	213.04
1.72	15	0.38	0.21	248.65	218.84
1.63	15	0.50	0.28	254.57	224.05

Table 4-5: CRR and V_{s1} adapted from Cataño (2006) and Sandoval and Pando (2012)

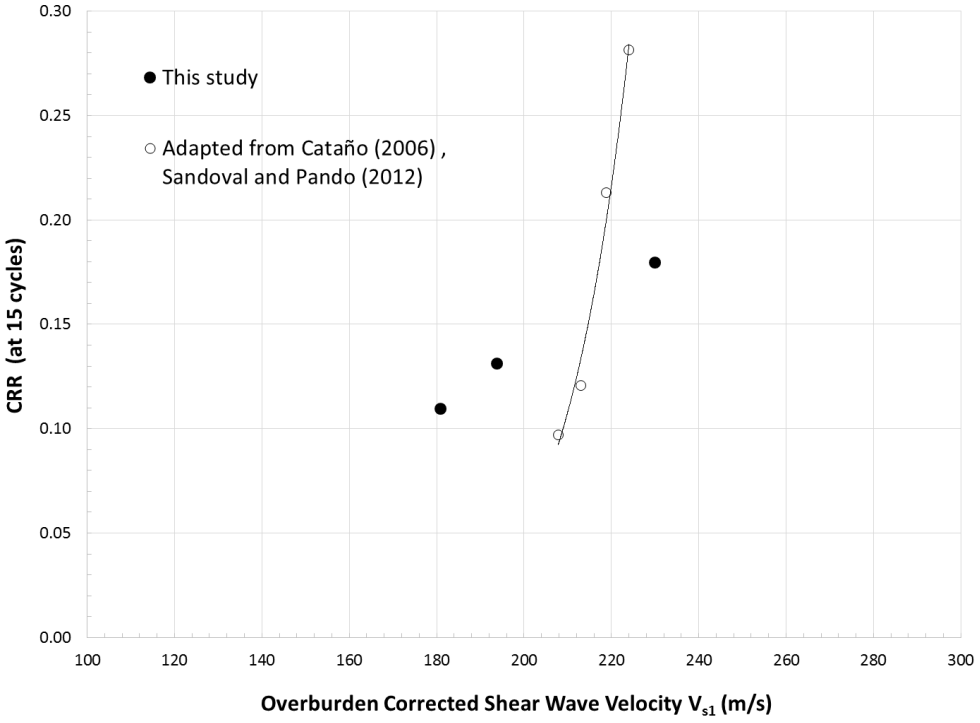

Figure 4-15: Comparison of CRR – V_{s1} with data adapted from Cataño (2006) and Sandoval and Pando (2013)

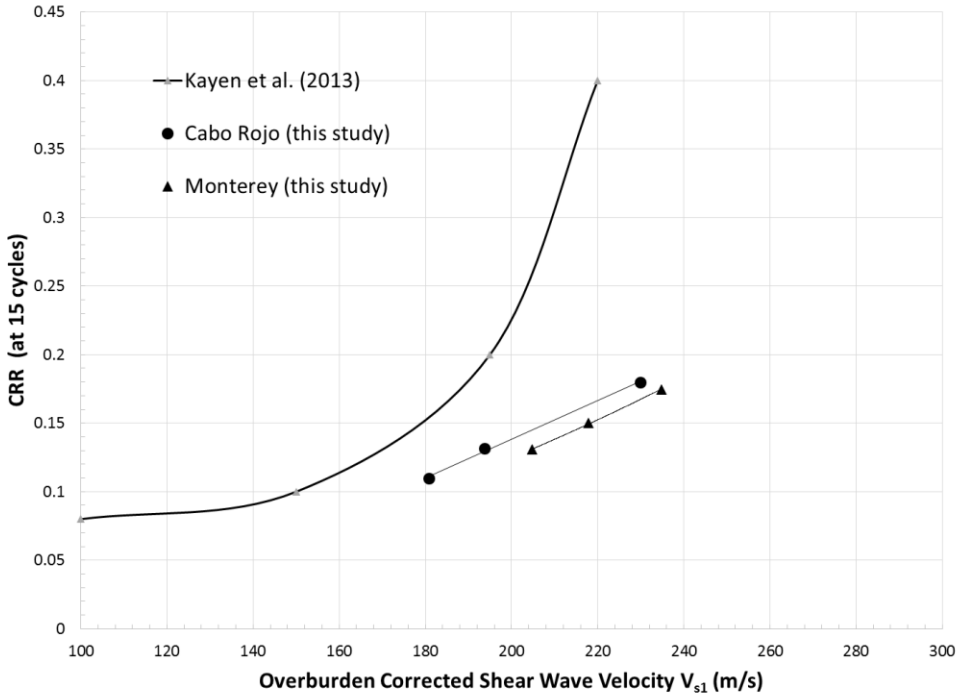

Figure 4-16: Comparison of data with field-based correlation of Kayen et al. (2013)

5. Conclusions

The objective of this study was to evaluate whether the relationship between Cyclic Resistance Ratio (CRR) - Shear Wave Velocity (V_{s1}) is soil specific for two soils.

To evaluate whether the relationship between CRR –V_{s1} was soil specific, a detailed laboratory testing program was established to compare the CRR – V_{s1} relationship for Monterey sand and a calcareous sand from Cabo Rojo, Puerto Rico. Twenty-nine undrained cyclic triaxial tests were conducted with shear wave velocity measurements taken using bender elements.

Eleven cyclic triaxial tests were conducted on Monterey sand and eighteen cyclic triaxial tests were conducted on a calcareous sand from Cabo Rojo, Puerto Rico. Three different void ratios were chosen for each sand and the data was compared against published data on comparable soils.

The significant results from the experimental study were as follows:

- There was very good agreement between the cyclic resistance (CRR_{tx} - N_l) of Monterey sand on samples prepared to a void ratio of 0.75 tested at URI and Virginia Tech. This is despite the fact that different sample preparation methods were used. The good agreement gives some confidence in the quality of the testing in this study and the reproducibility of the testing.

- The CRR – V_s relationships developed in this study were less sensitive to changes in shear wave velocity (i.e. the curves are flatter) than reported in previous studies.
- A comparison of test results from a similar calcareous sand from Cabo Rojo, Puerto Rico did not demonstrate a similar CRR – V_{s1} correlation. However, differences in e_{min} and e_{max} suggests that they may be two different soils. Another possible reason for the differences could be due to differences in laboratory testing programs.
- The CRR – V_{s1} correlation for the Monterey sand and Cabo Rojo Calcareous sand are in fact different.
- The comparison of test results for this study with field based correlations suggests that the Monterey sand and calcareous sand from Cabo Rojo lies outside the liquefaction resistance curves used in practice. Using the field-based correlation would significantly overestimate the liquefaction resistance of the Cabo Rojo and Monterey Sands.

This last significant finding is very important suggesting that the liquefaction resistance of both the Monterey and Cabo Rojo calcareous sand is lower than predicted by the field-based approaches of Andrus and Stokoe (2000) and Kayen et al. (2013). In this case, using the field-based shear wave velocity approach significantly overestimates the liquefaction resistance of the Monterey and Cabo Rojo sands. More research is needed, however, the results of this study support the hypothesis that the CRR-V_s relationship is soil specific.

5.1 Recommendations for future work

For further continuation of this project, the author recommends the following:

- First, more time should be taken with regards to the PID settings of the Instron equipment and the possible use of the tri-modal option for testing. A substantial amount of time on this study was dedicated to correct the PID settings so the deviator stress would remain constant throughout testing, but it can further be refined.
- More research needs to be done into achieving sample failure at the middle of the sample for the modified moist tamping method. For one set of Cabo Rojo testing, the author tested samples at 2%, 3% and 4% undercompaction to achieve sample failure in middle. The interesting outcome was the number of cycles of failure did not change regardless of the sample failure location.

6. Appendix A: Cabo Rojo Test Plots

A.1 Void ratio = 1.60

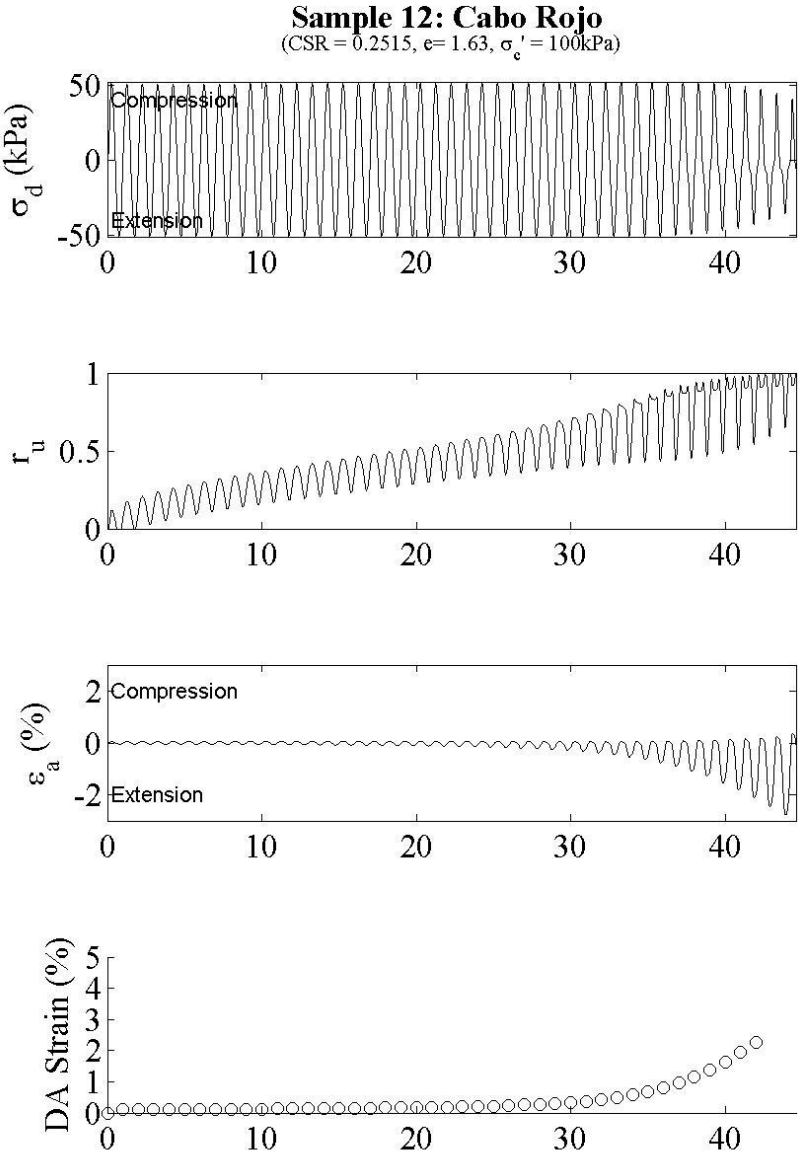

Figure 6-1: Sample 12 comparison plot

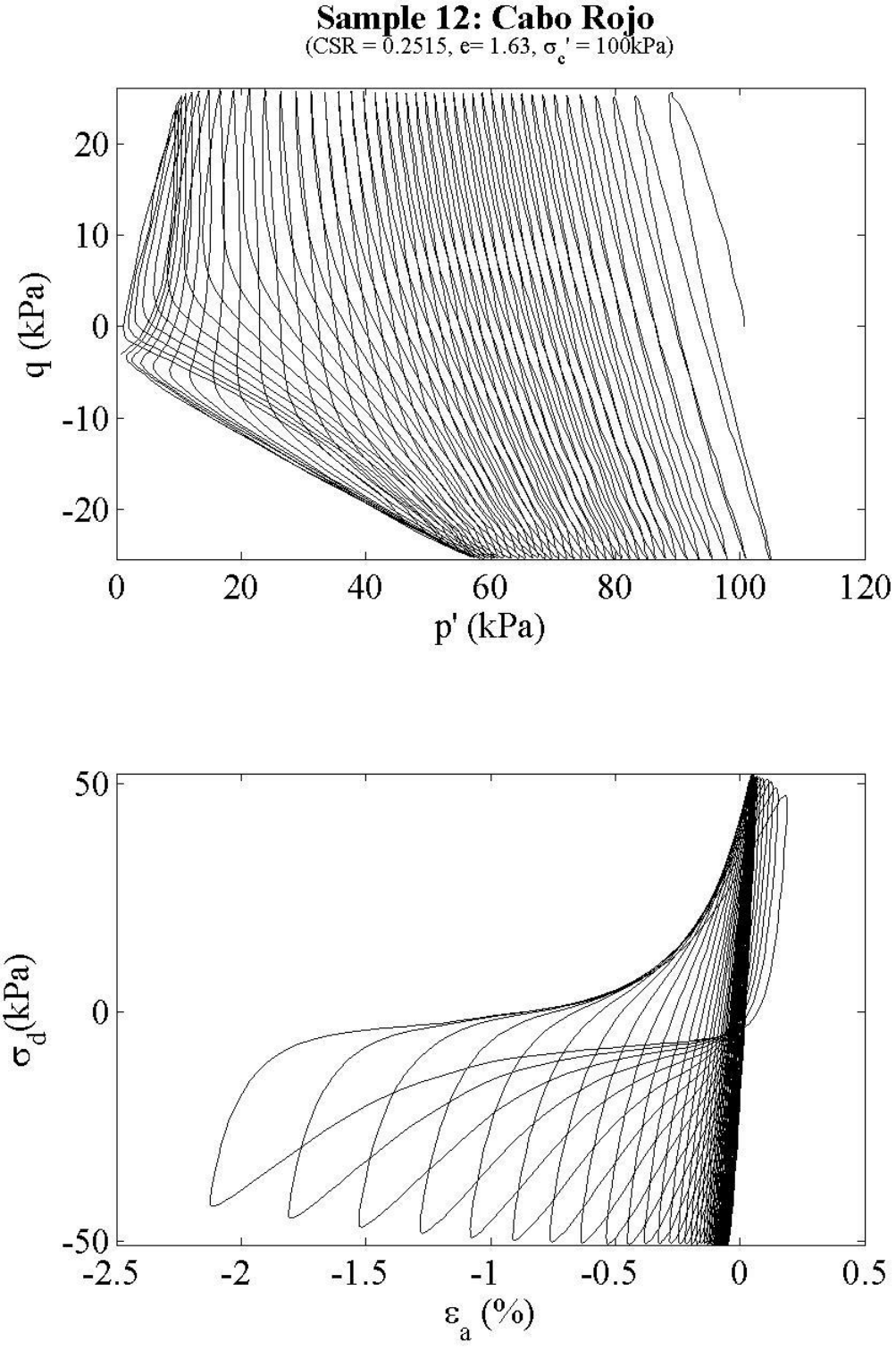

Figure 6-2: Sample 12 stress path and stress vs. strain

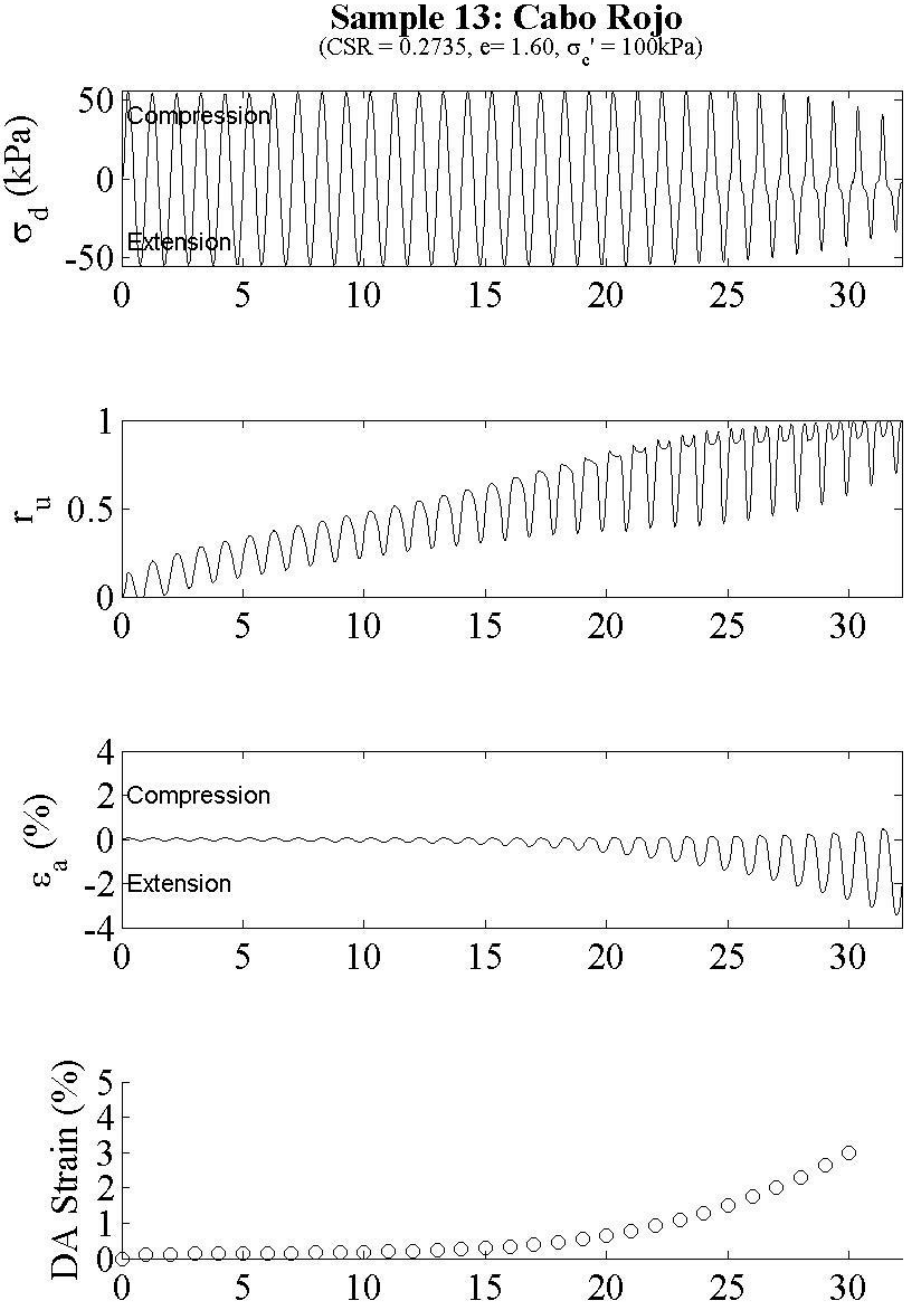

Figure 6-3: Sample 13 comparison plot

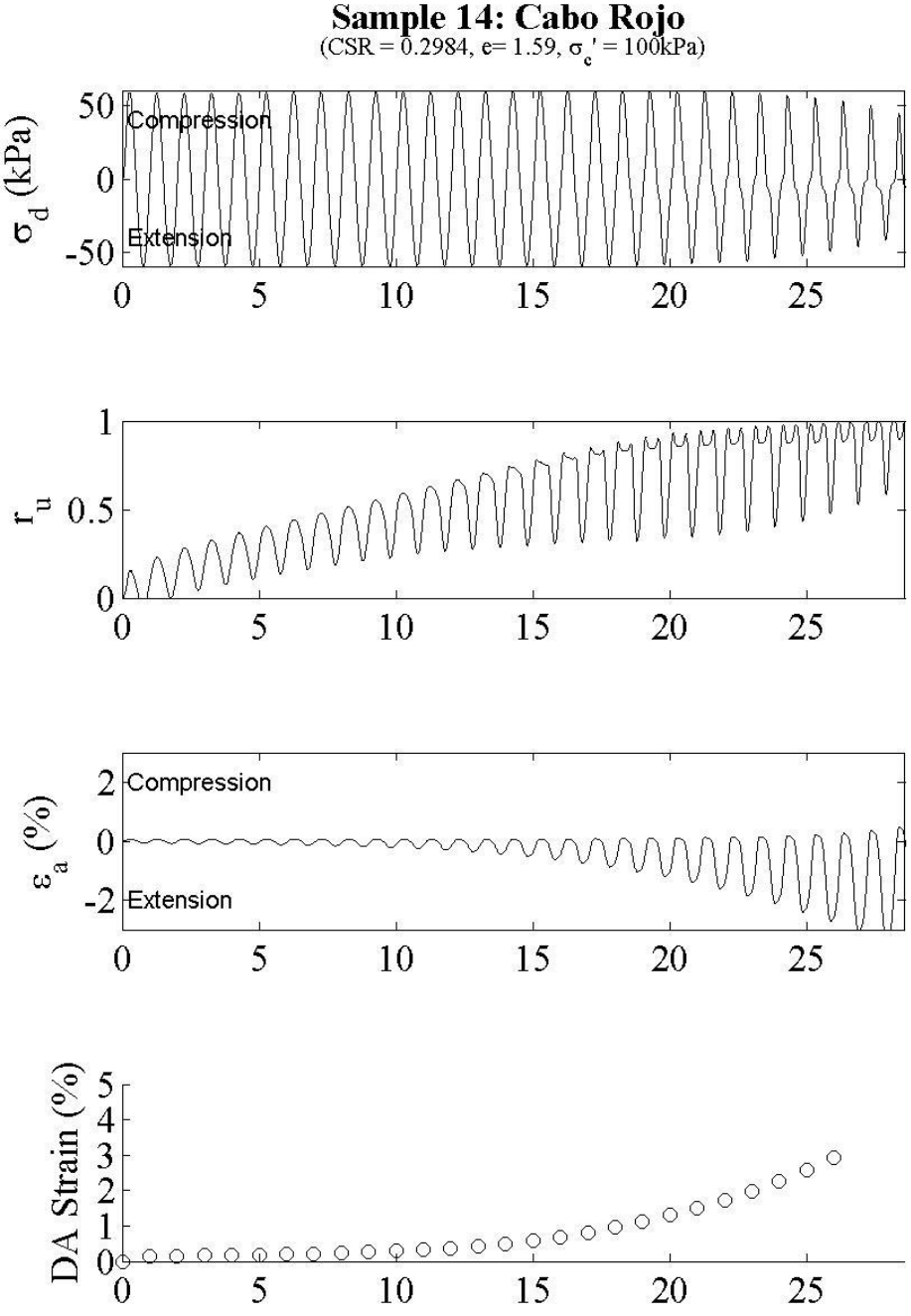

Figure 6-4: Sample 14 comparison plot

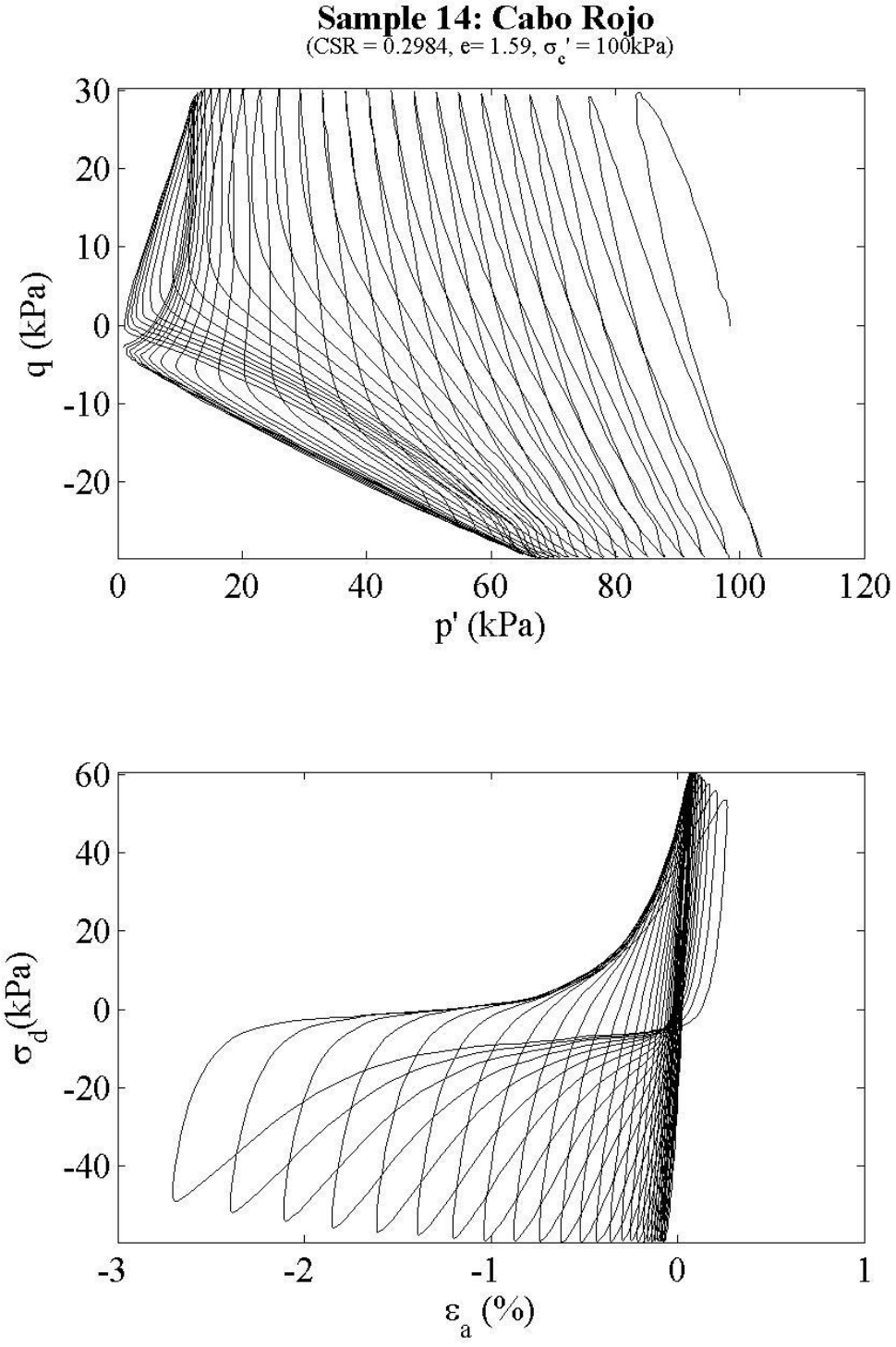

Figure 6-5: Sample 14 stress path and stress vs. strain plots

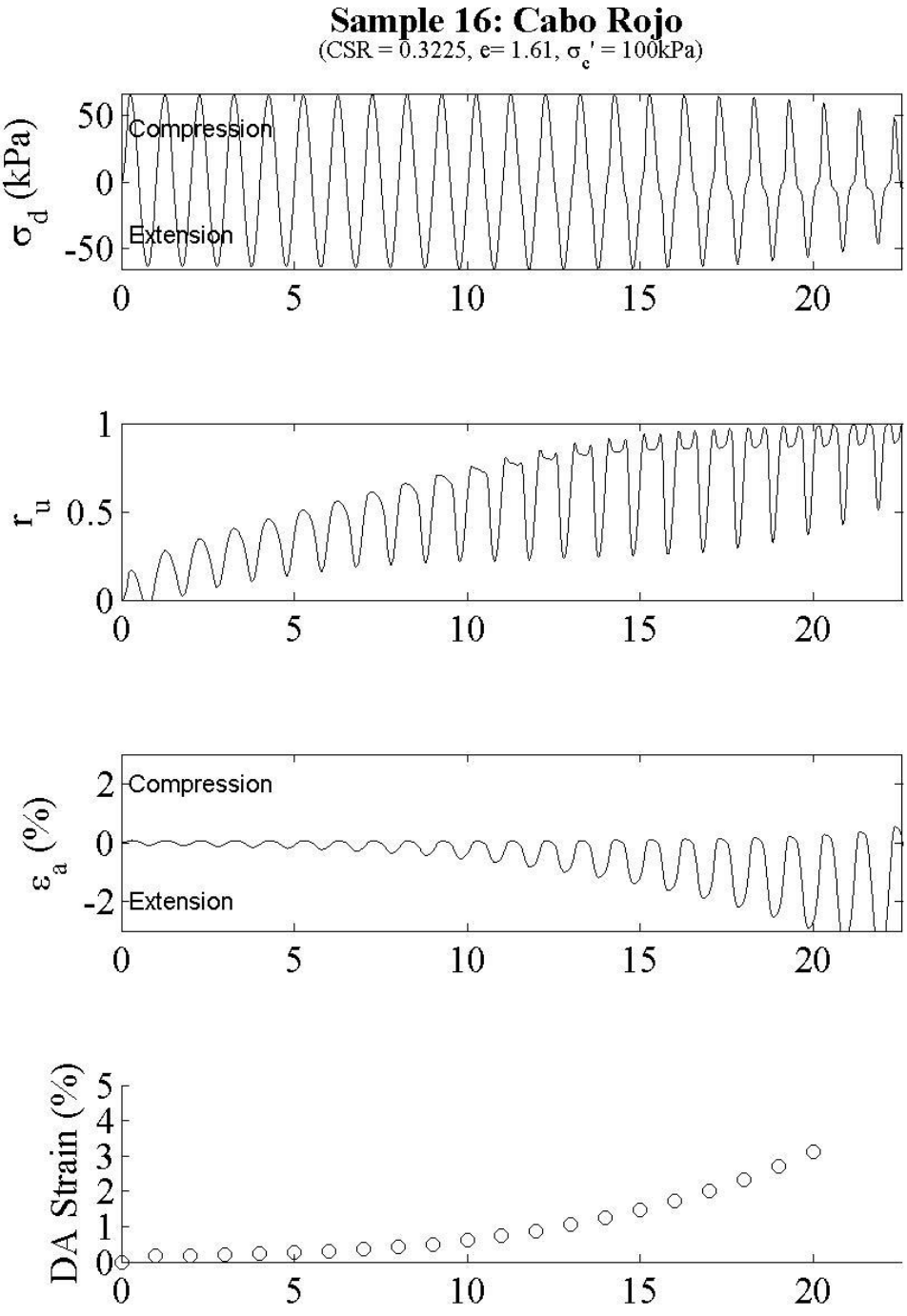

Figure 6-6: Sample 16 comparison plot

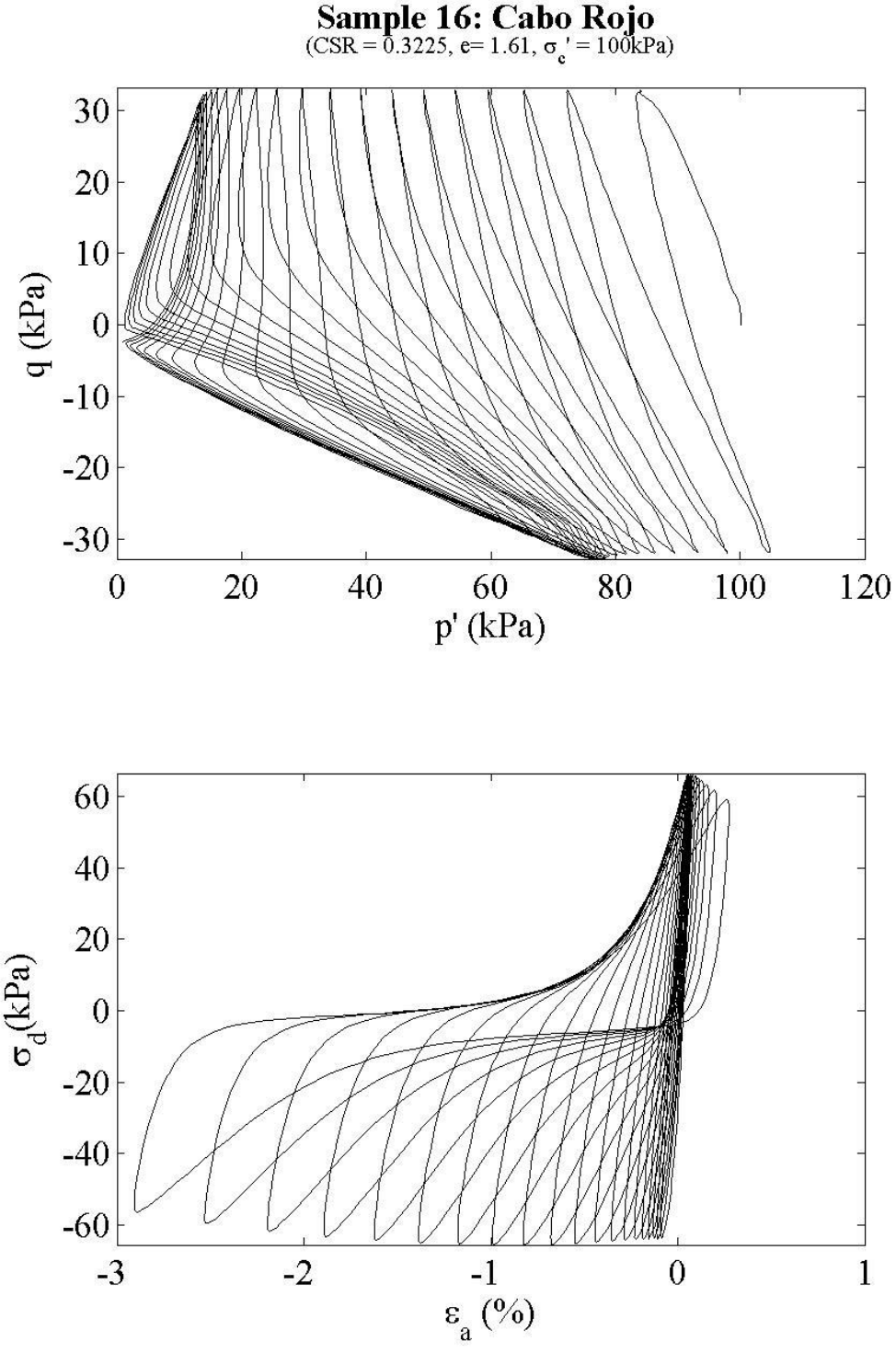

Figure 6-7: Sample 16 stress path and stress vs. stain plots

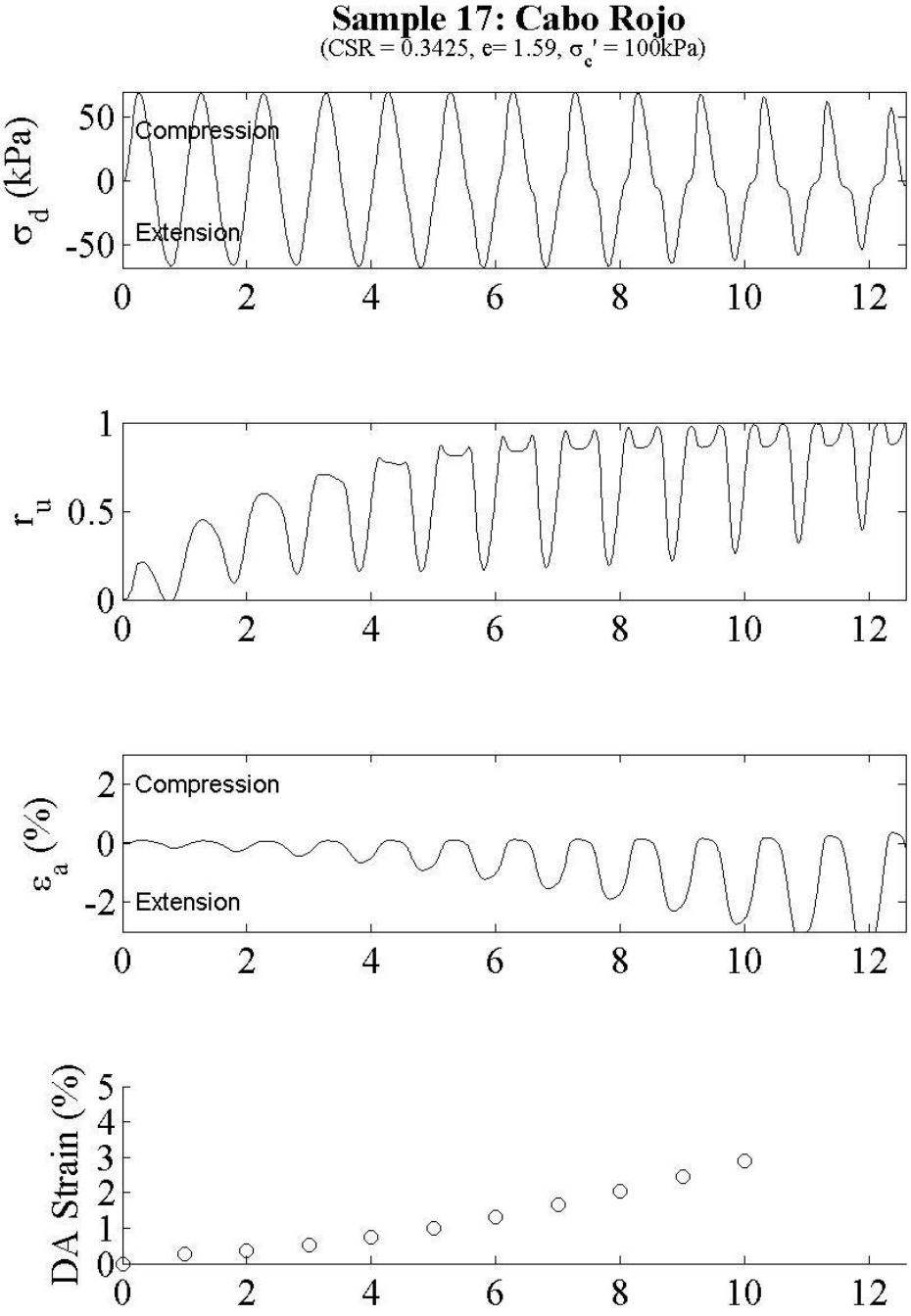

Figure 6-8: Sample 17 comparison plot

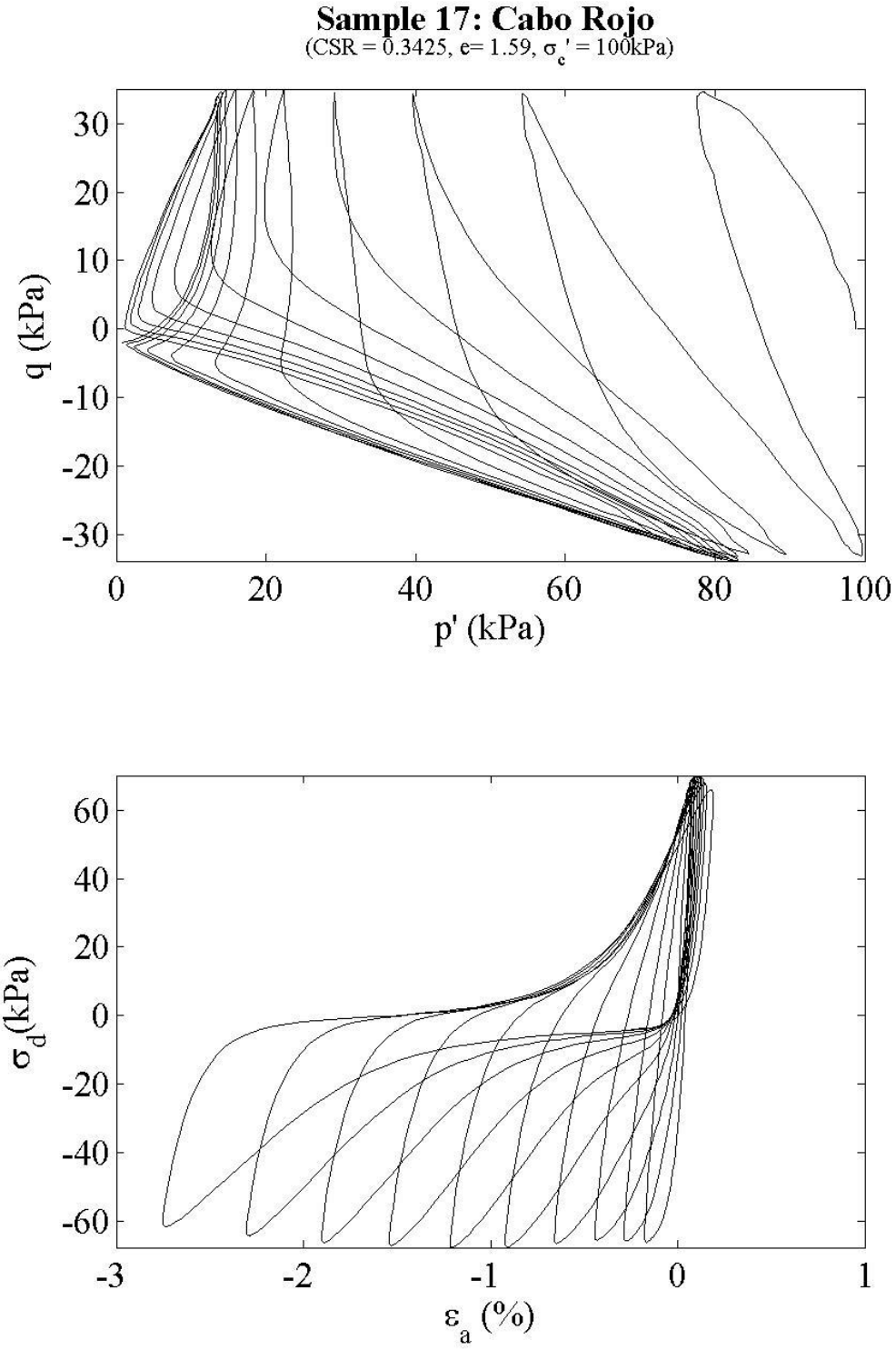

Figure 6-9: Sample 17 stress path and stress vs. strain plots

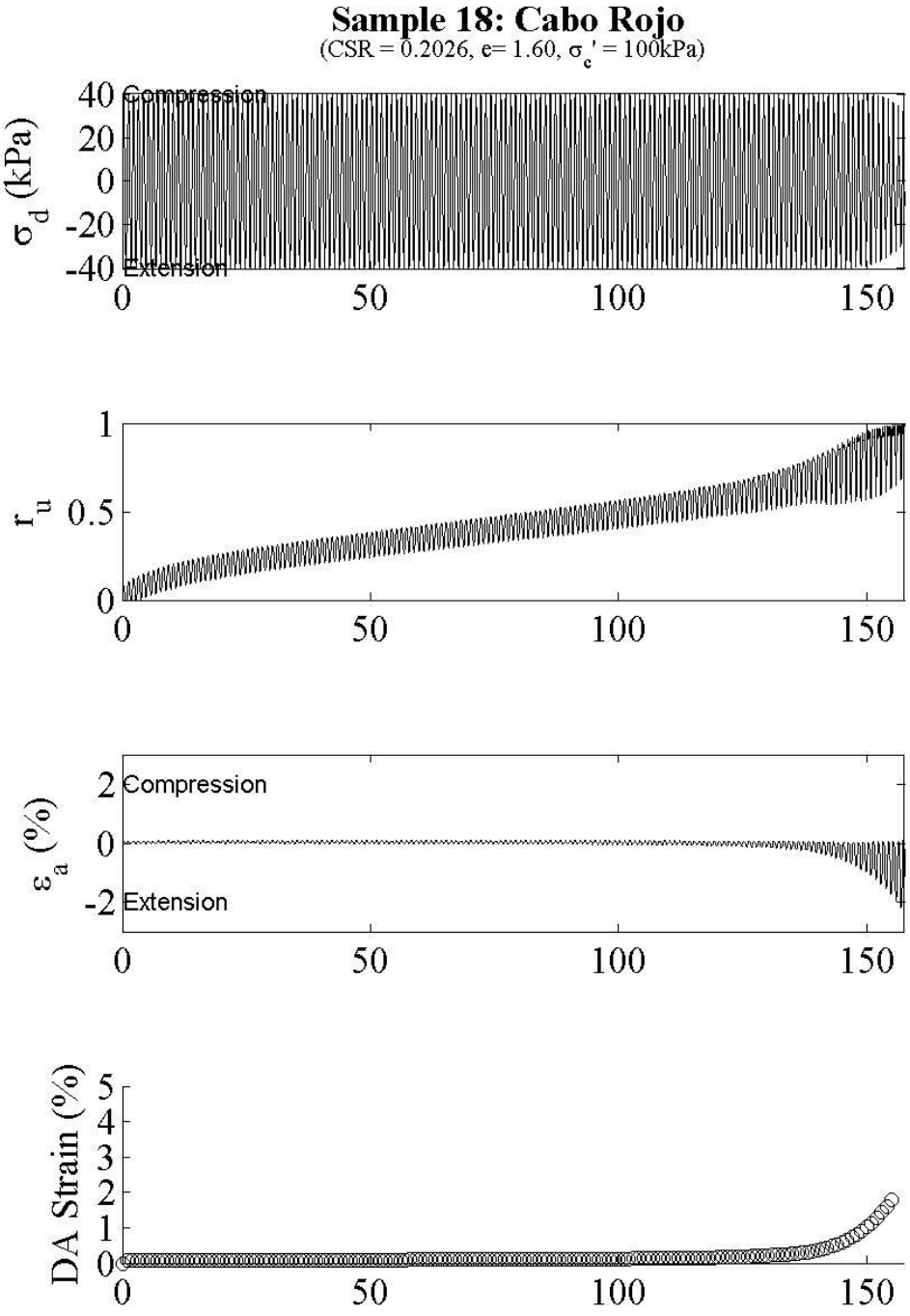

Figure 6-10: Sample 18 comparison plot

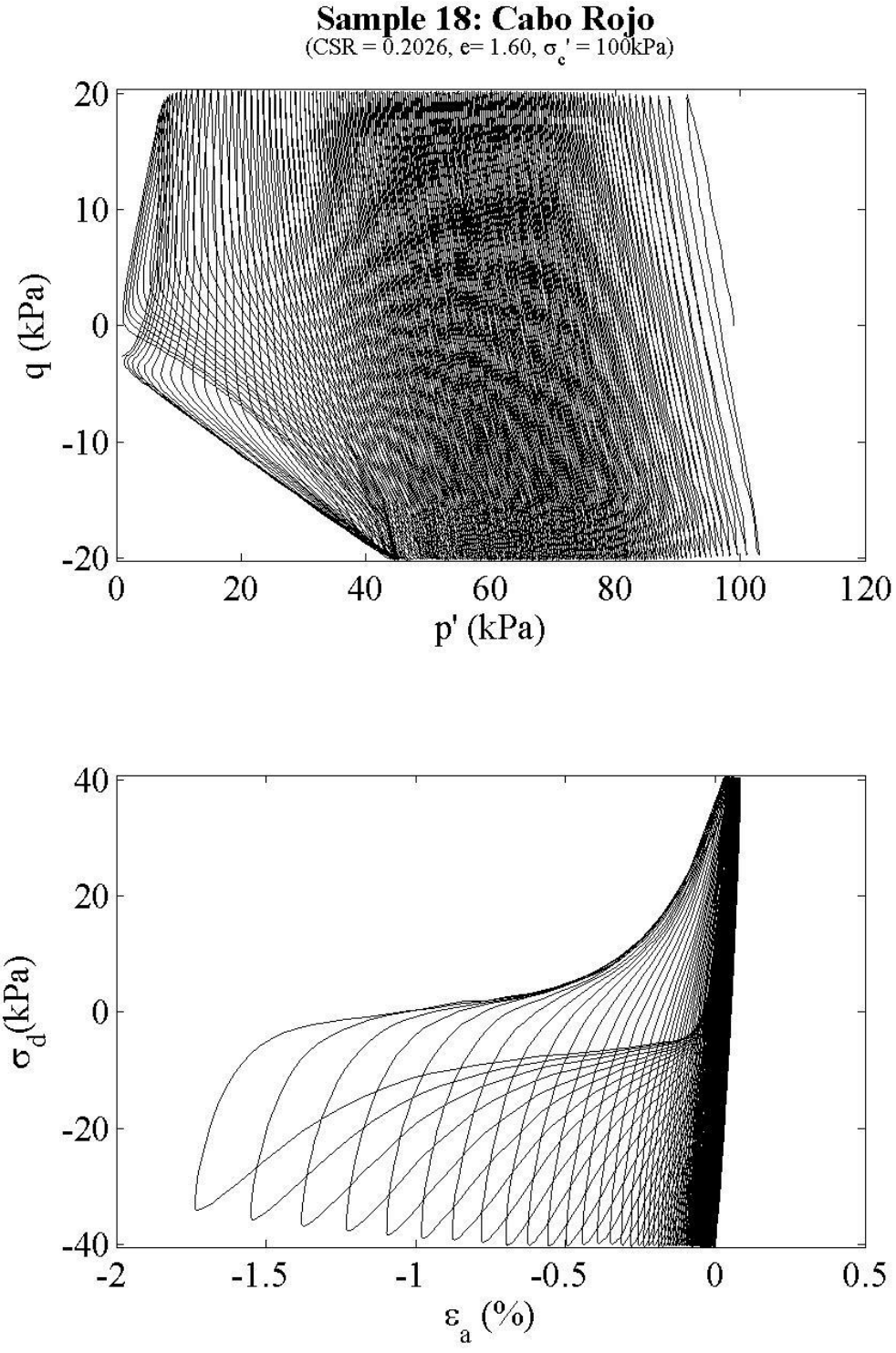

Figure 6-11: Sample 18 stress path and stress vs. strain plots

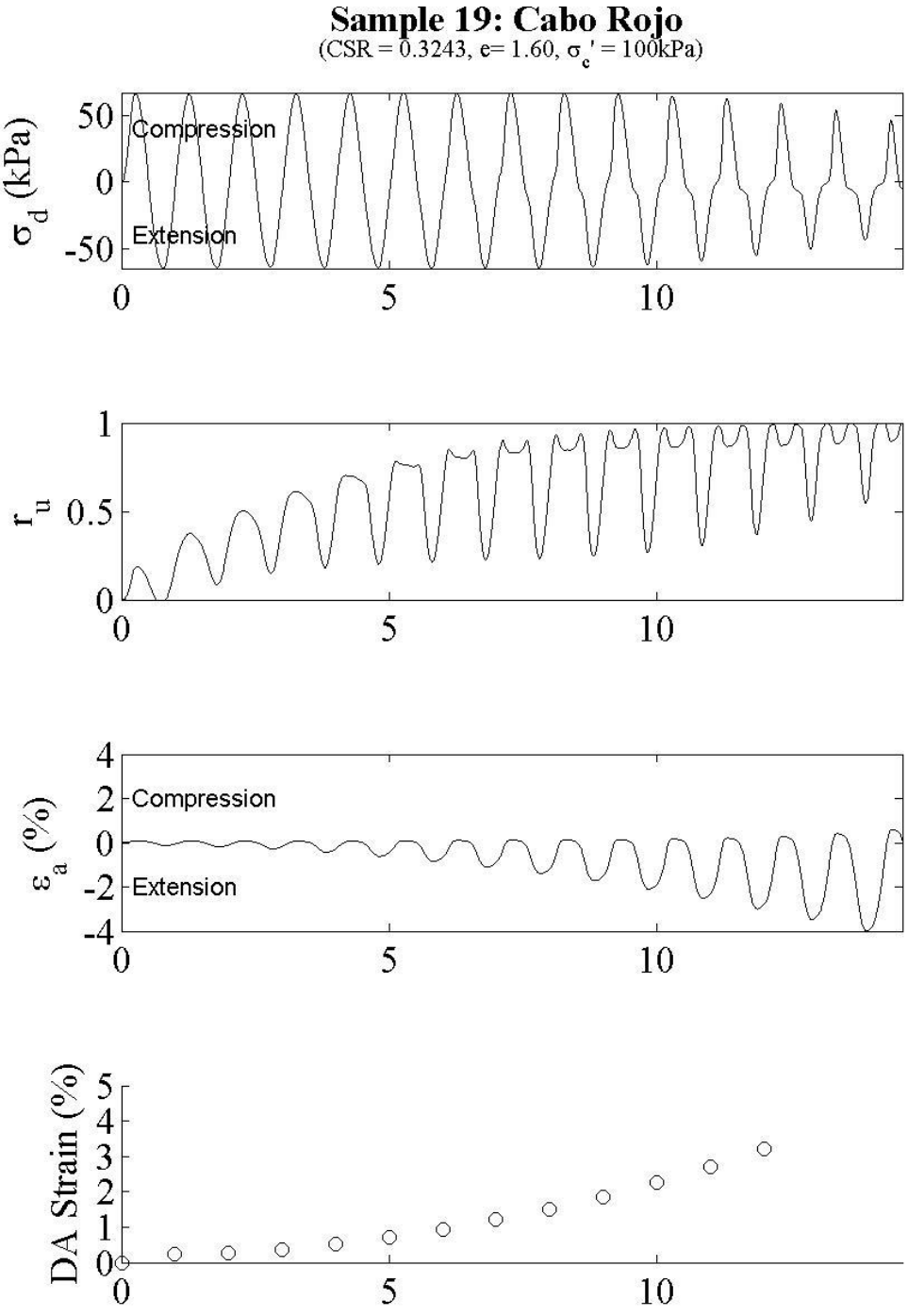

Figure 6-12: Sample 19 comparison plot

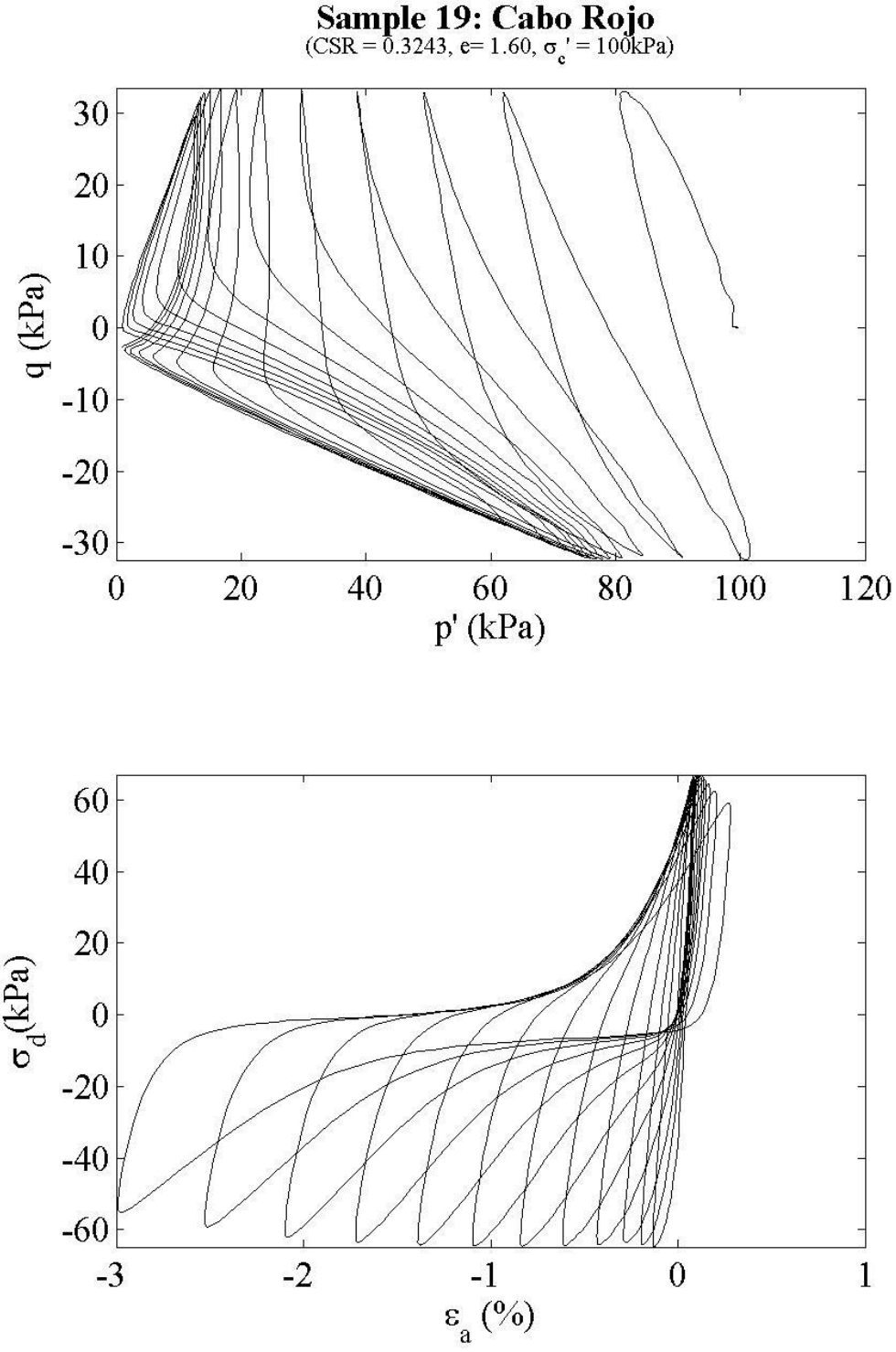

Figure 6-13: Sample 19 stress path and stress vs. strain plot

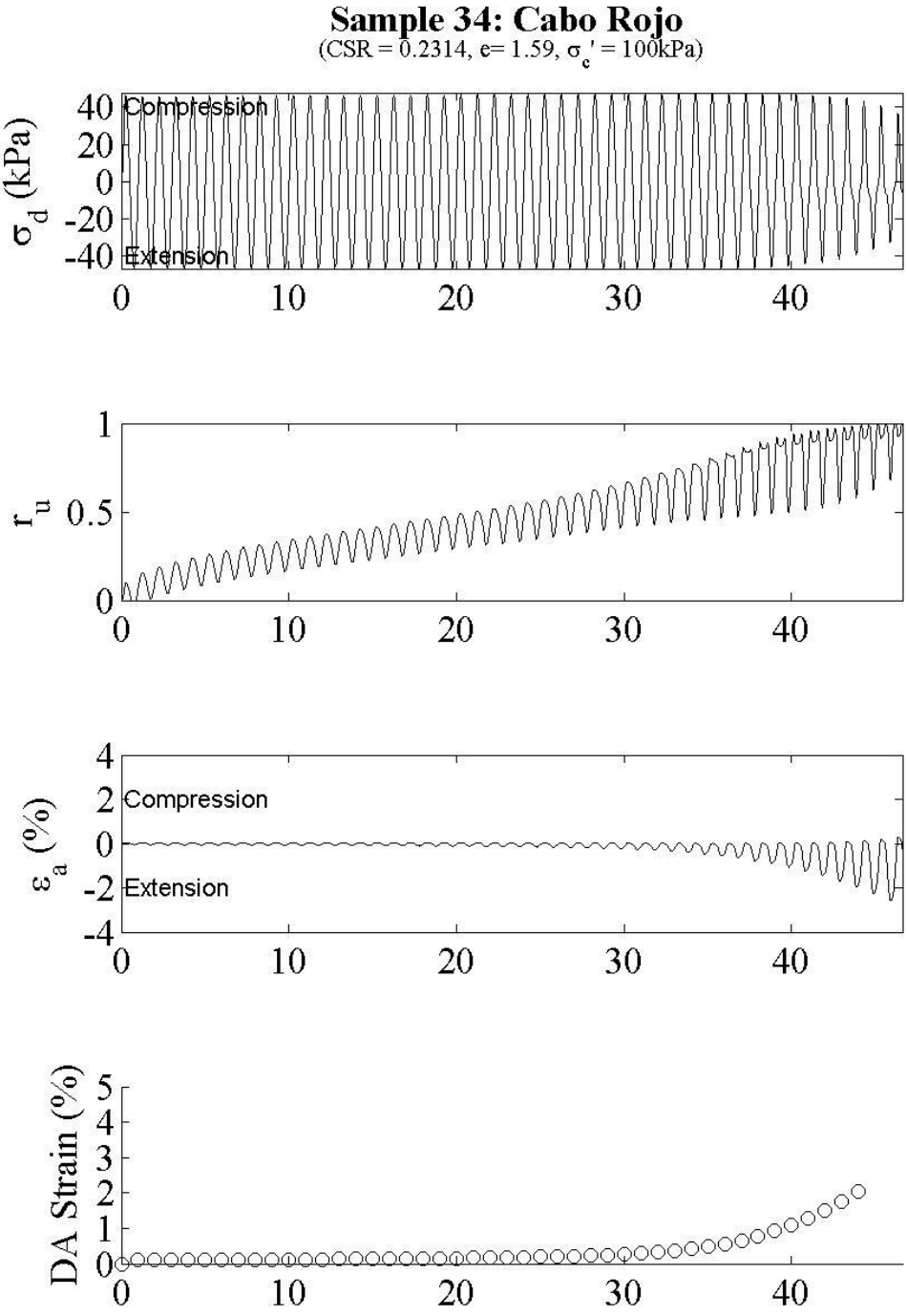

Figure 6-14: Sample 34 comparison plot

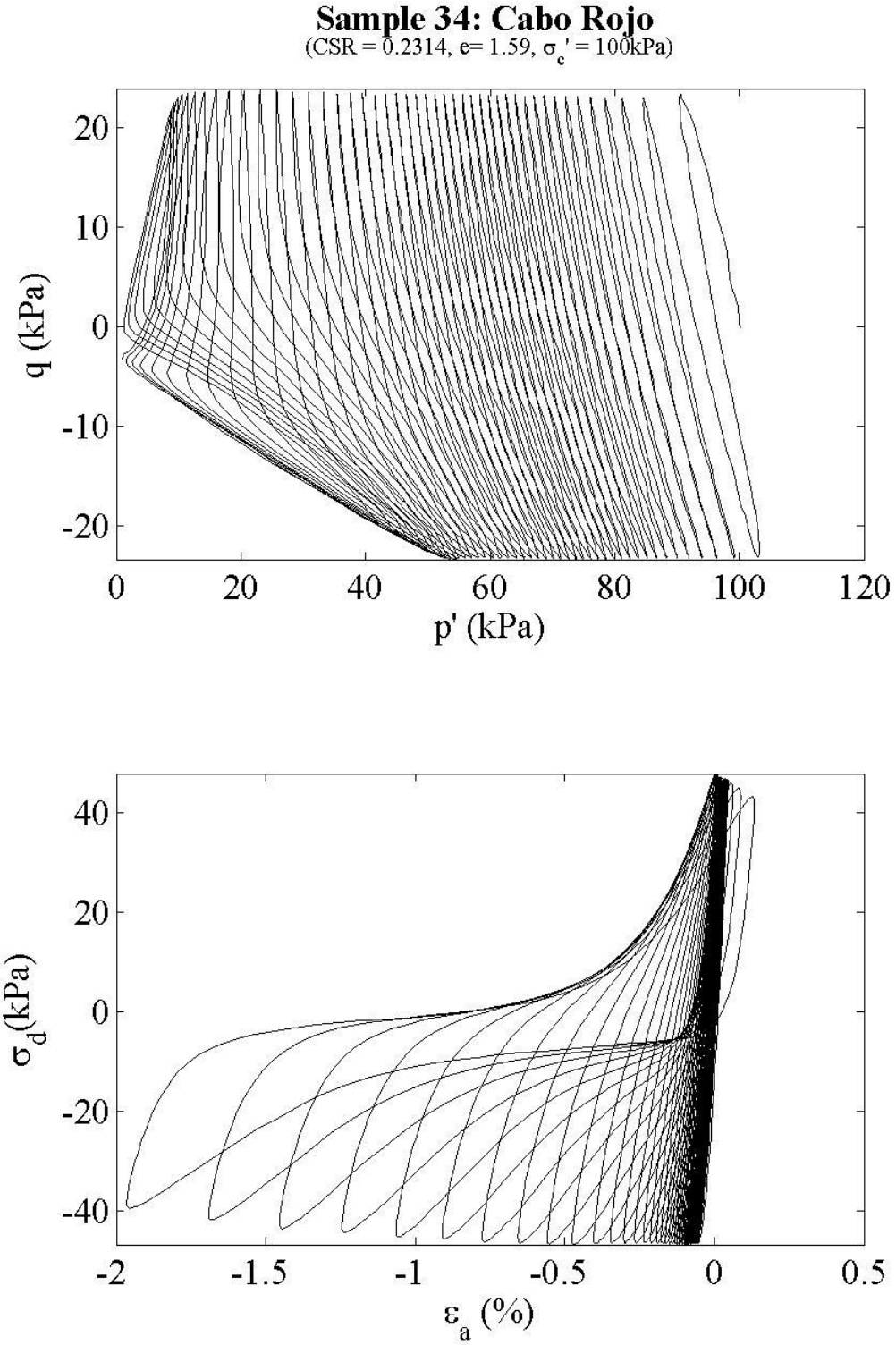

Figure 6-15: Sample 34 stress path and stress vs. strain plots

A.2 Void ratio = 1.75

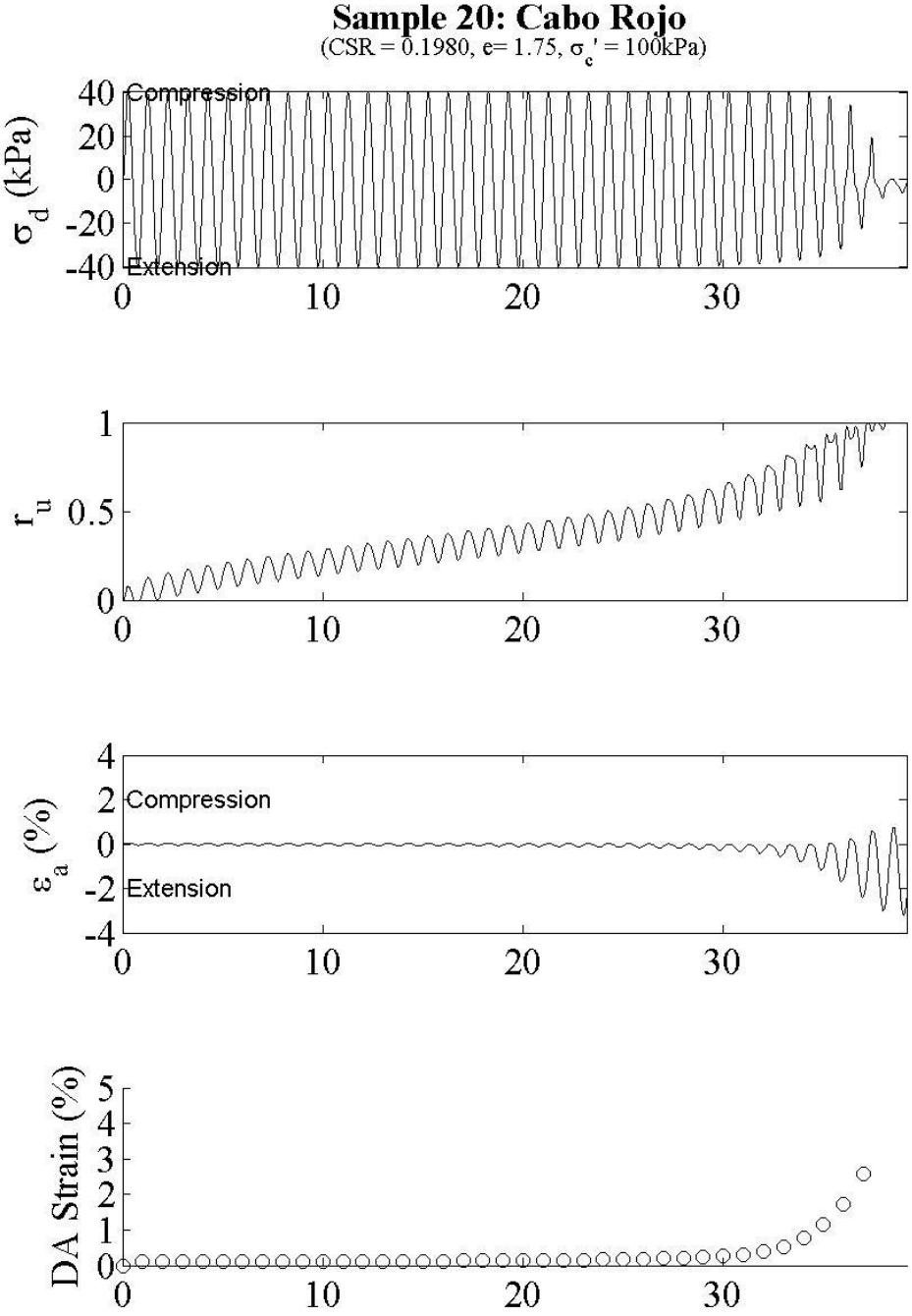

Figure 6-16: Sample 20 comparison plot

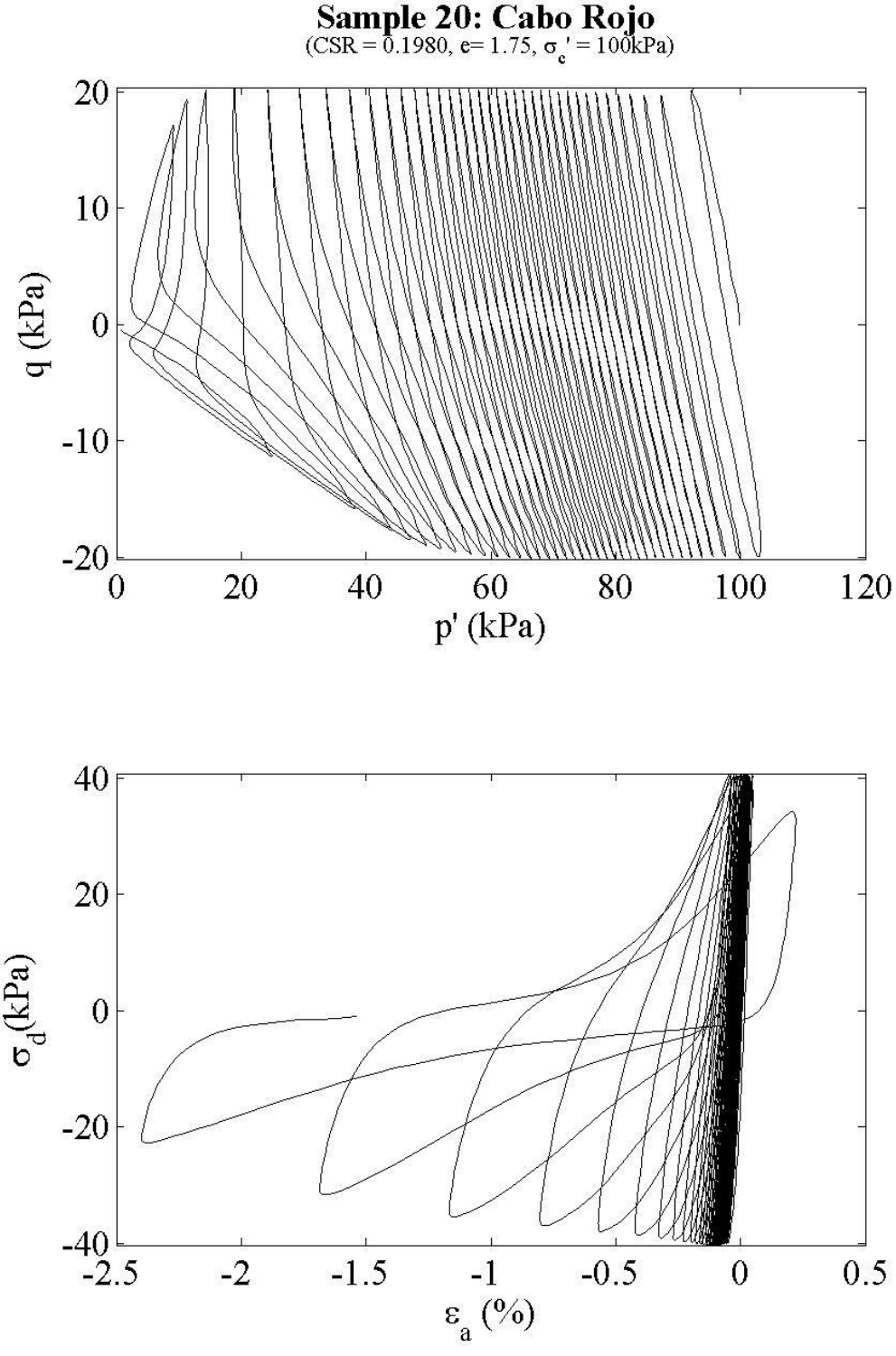

Figure 6-17: Sample 20 stress path and stress vs. strain

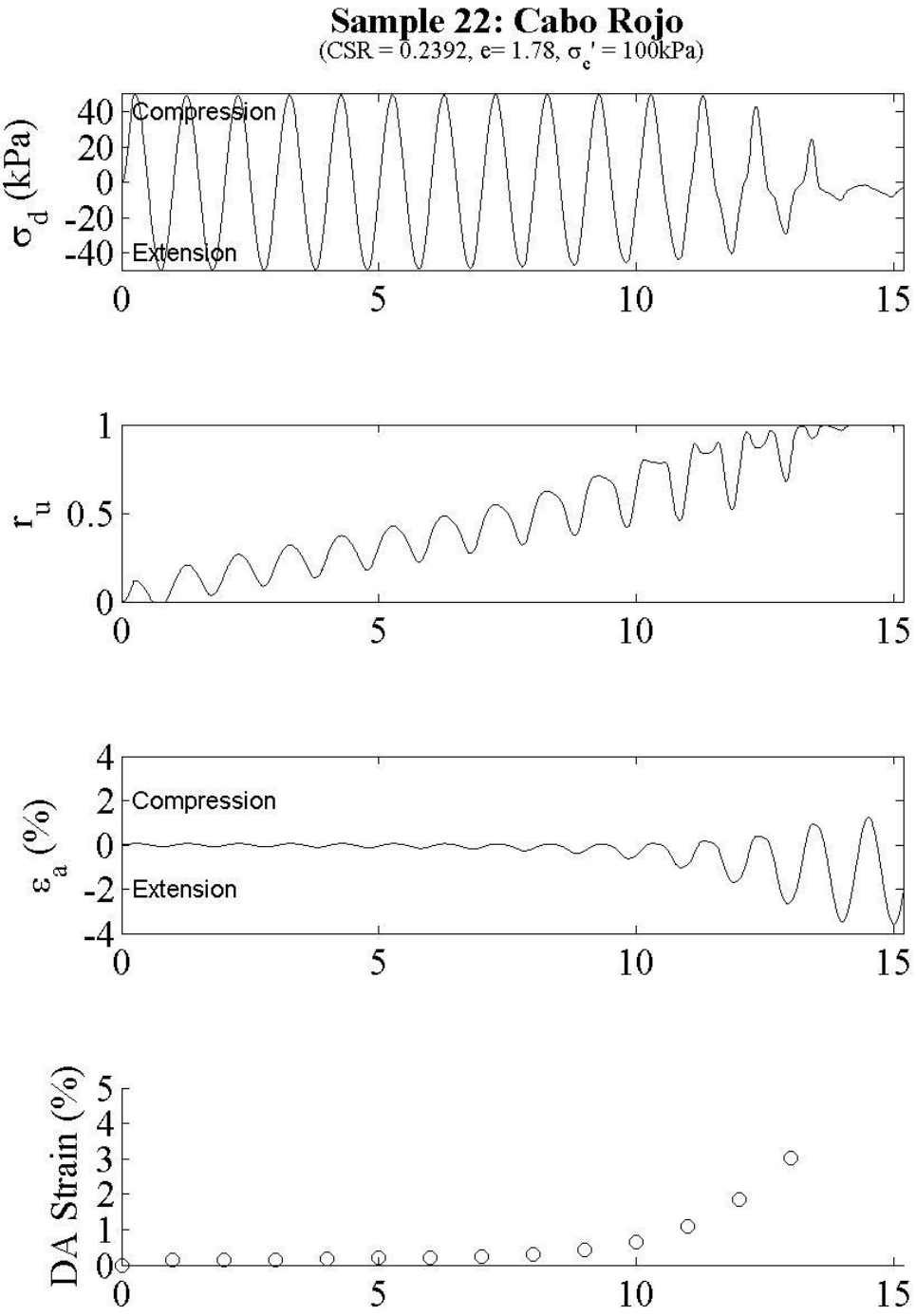

Figure 6-18: Sample 22 comparison plot

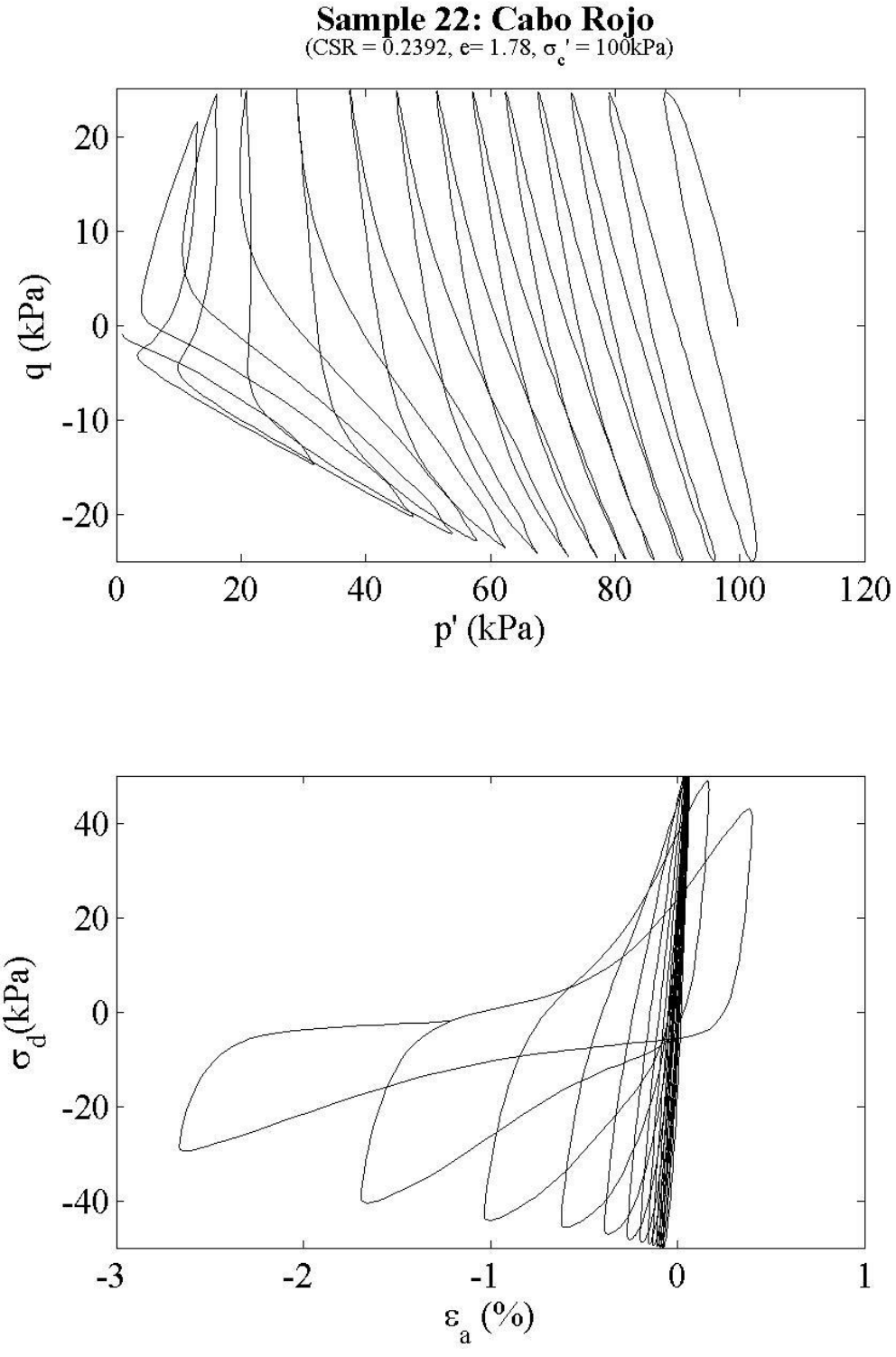

Figure 6-19: Sample 22 stress path and stress vs. strain plots

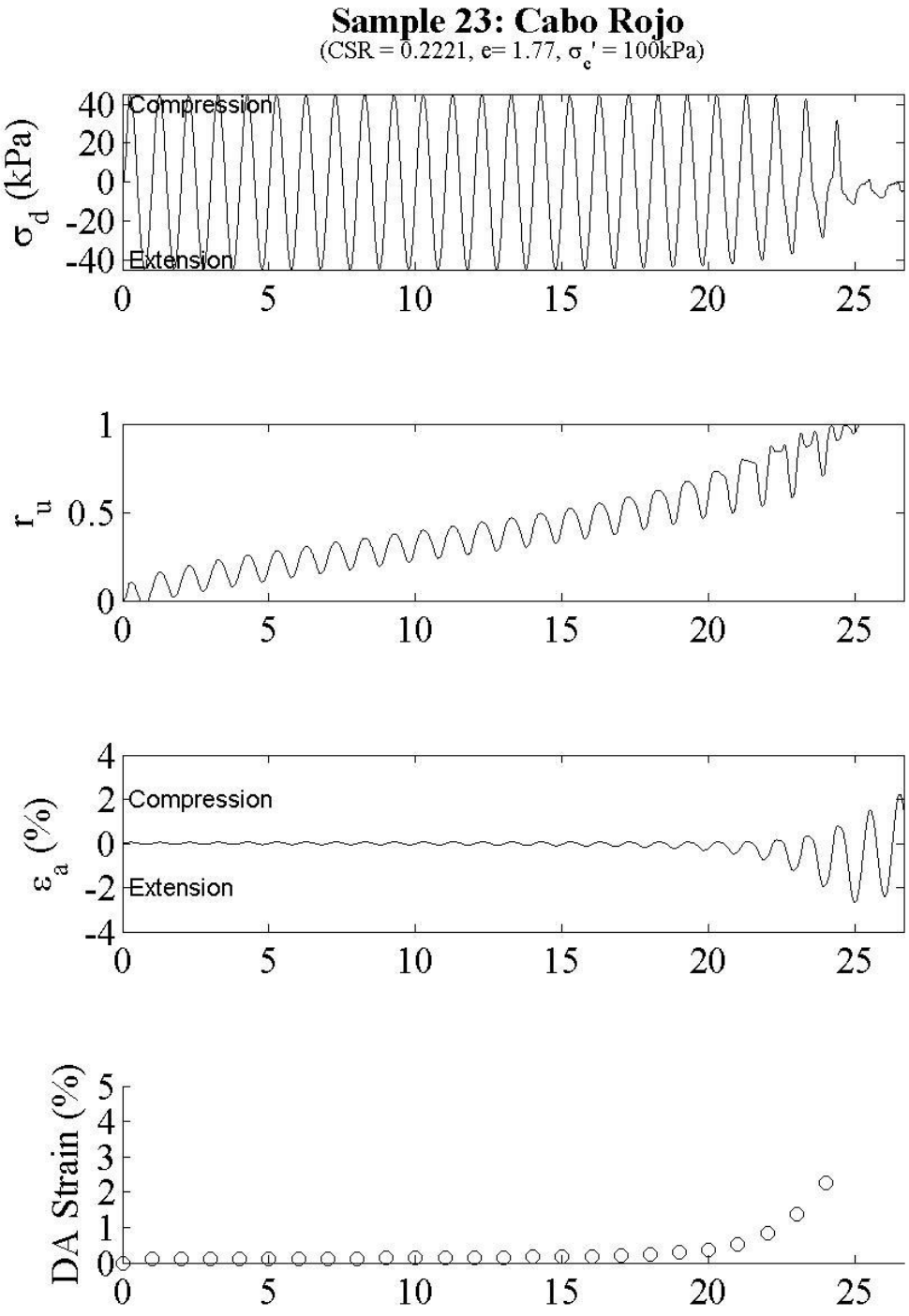

Figure 6-20: Sample 23 comparison plot

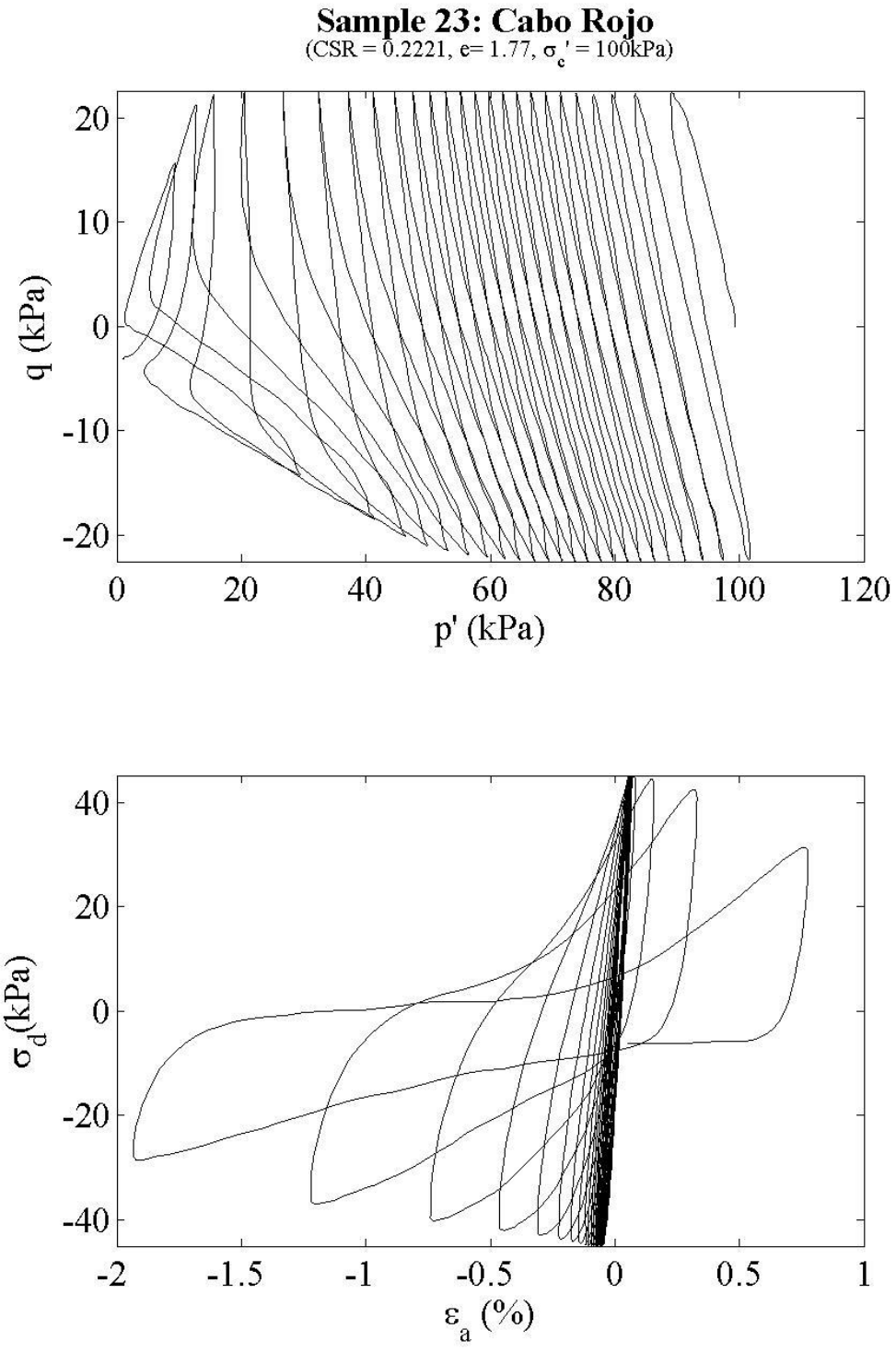

Figure 6-21: Sample 23 stress path and stress vs. strain plots

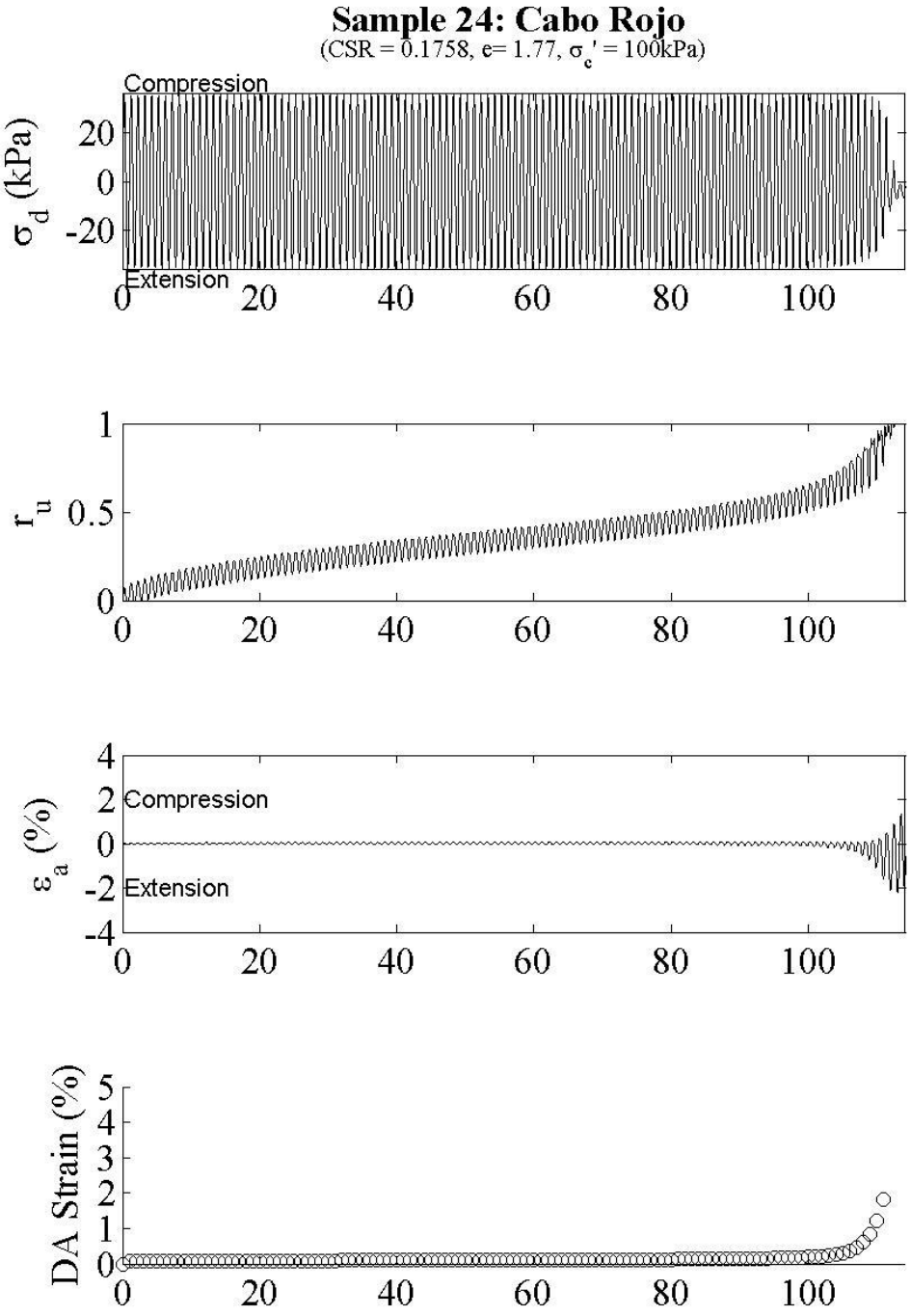

Figure 6-22: Sample 24 comparison plot

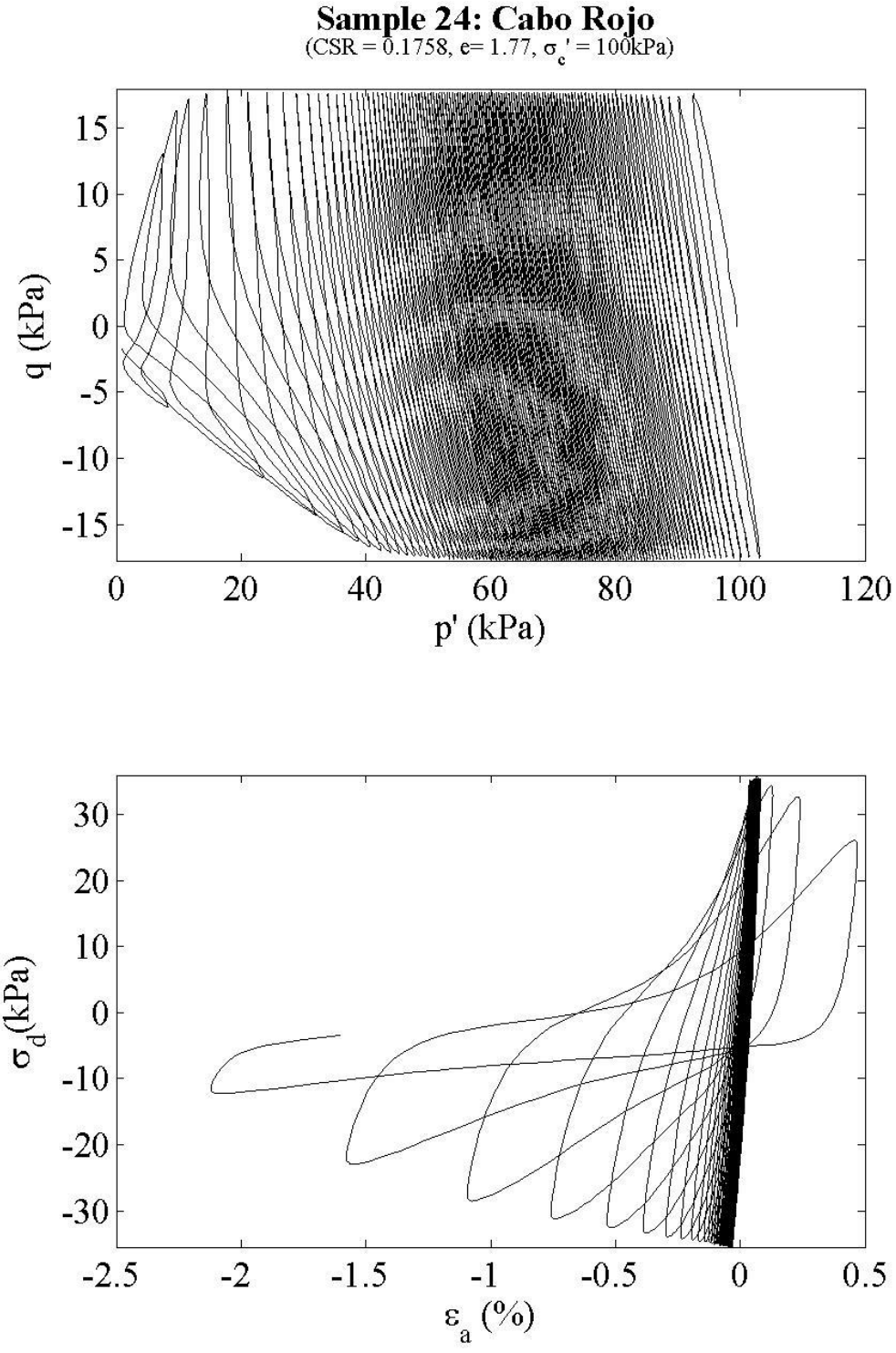

Figure 6-23: Sample 24 stress path and stress vs. strain plots

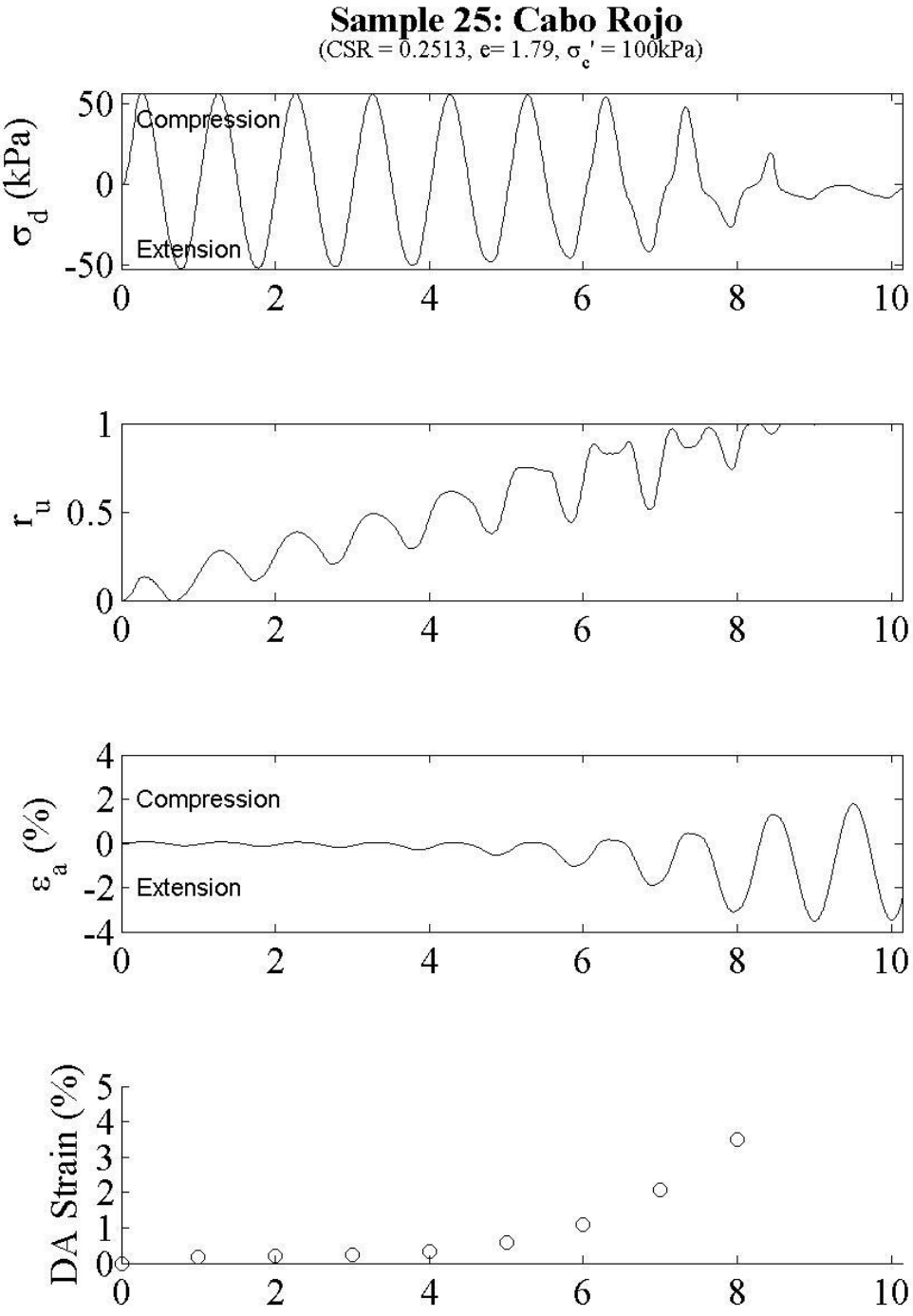

Figure 6-24: Sample 25 comparison plot

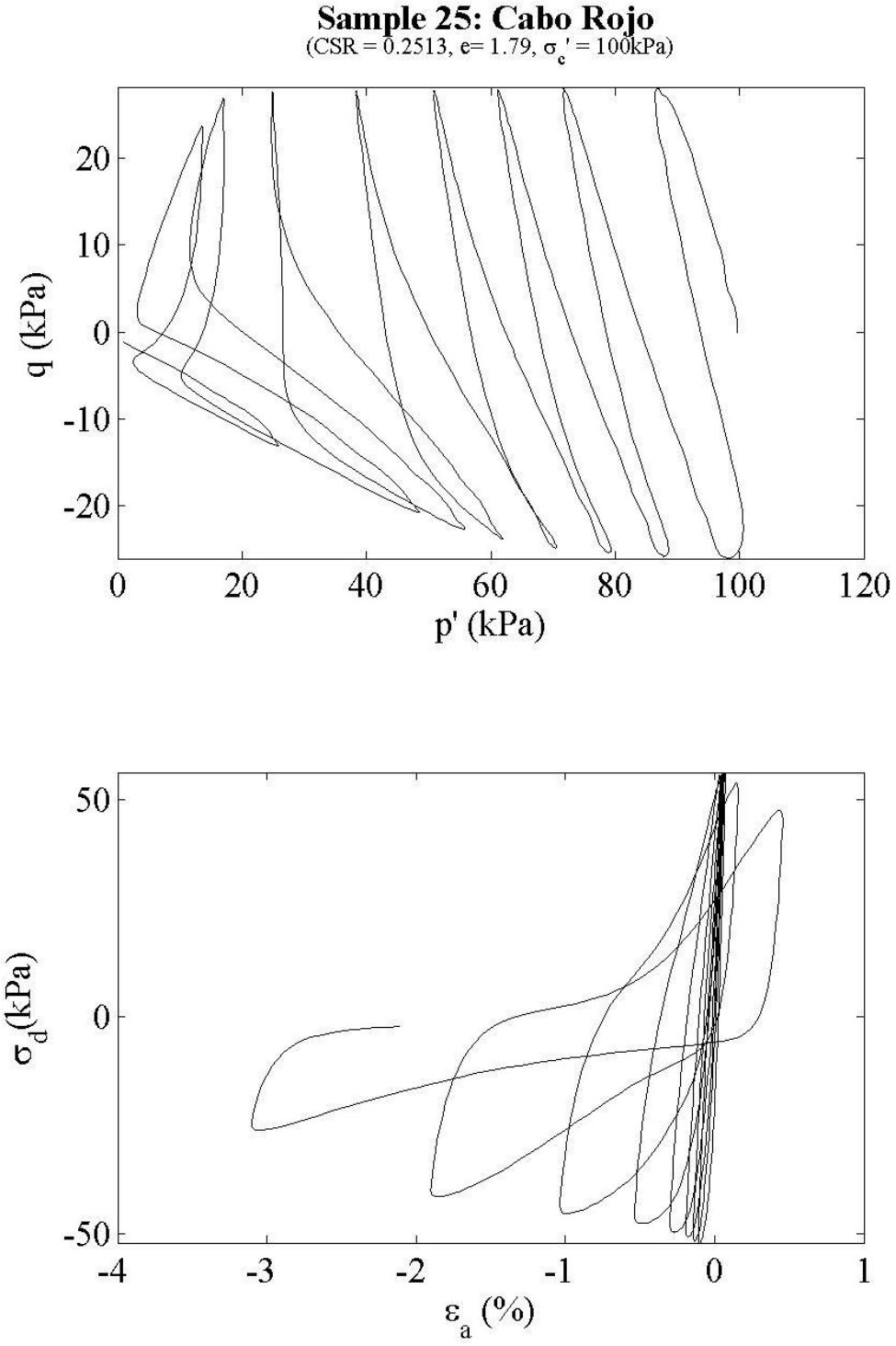

Figure 6-25: Sample 25 stress path and stress vs. strain plots

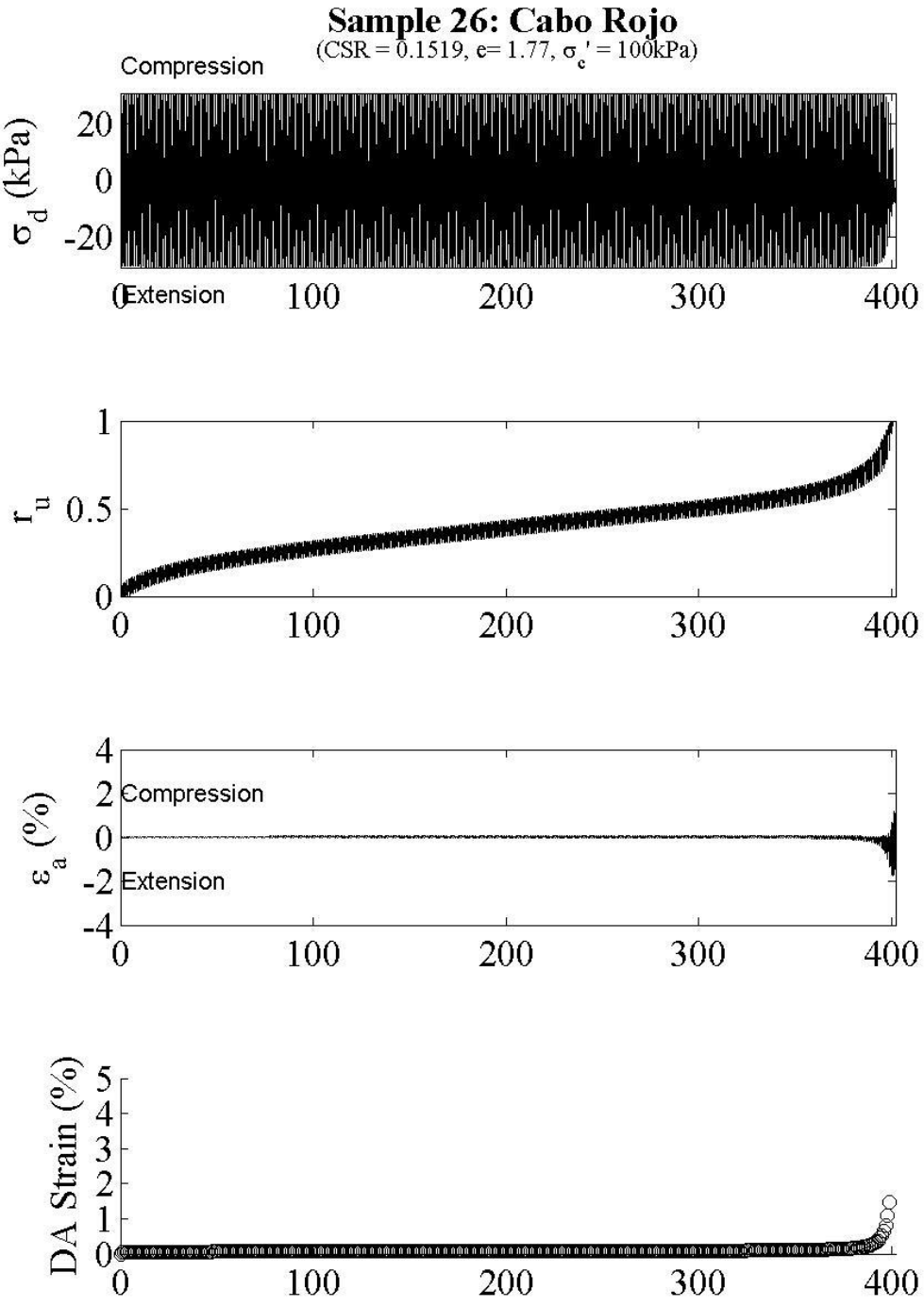

Figure 6-26: Sample 26 comparison plot

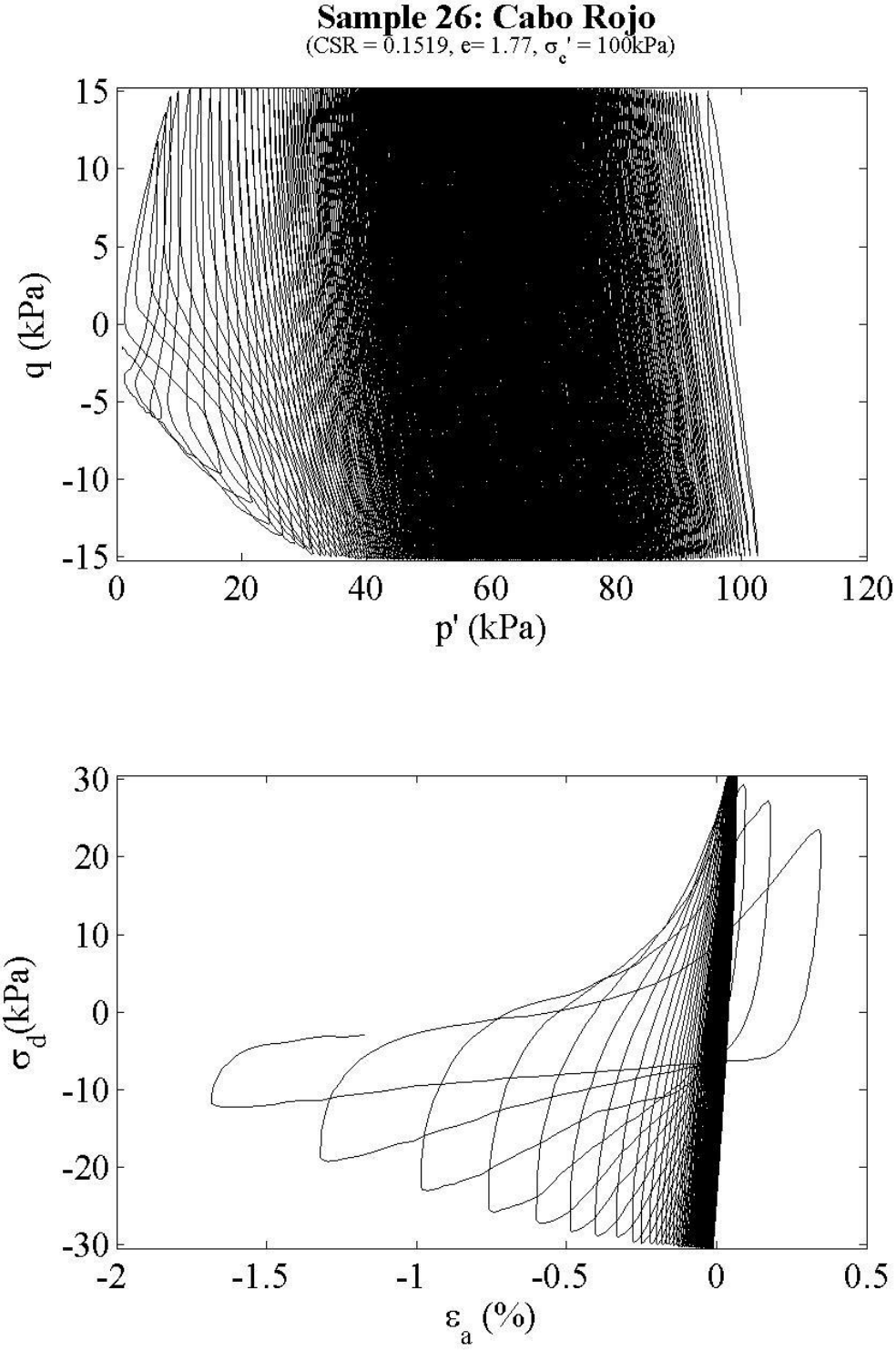

Figure 6-27: Sample 26 stress path and stress vs. strain plots

A.3 Void ratio = 1.85

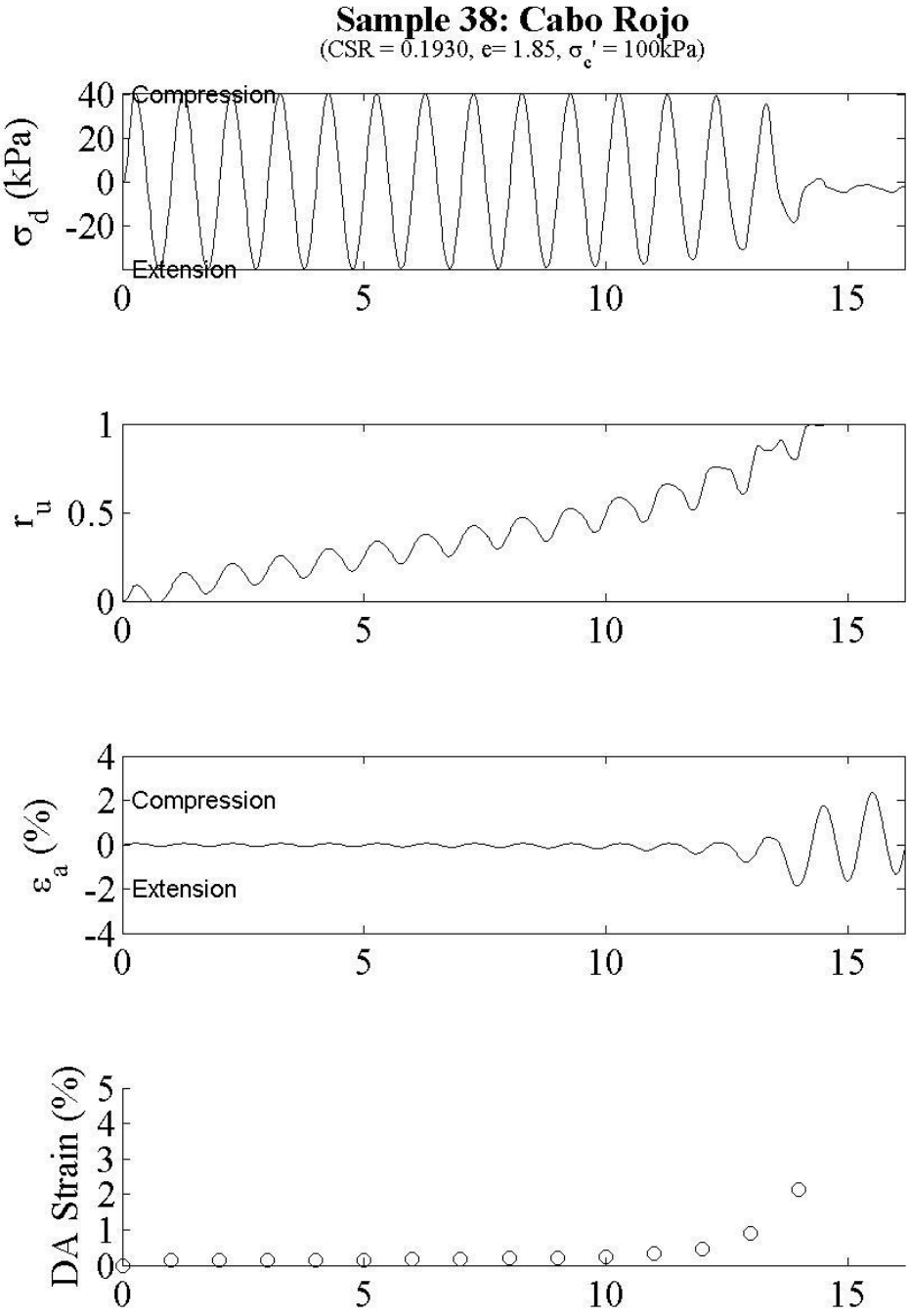

Figure 6-28: Sample 38 comparison plot

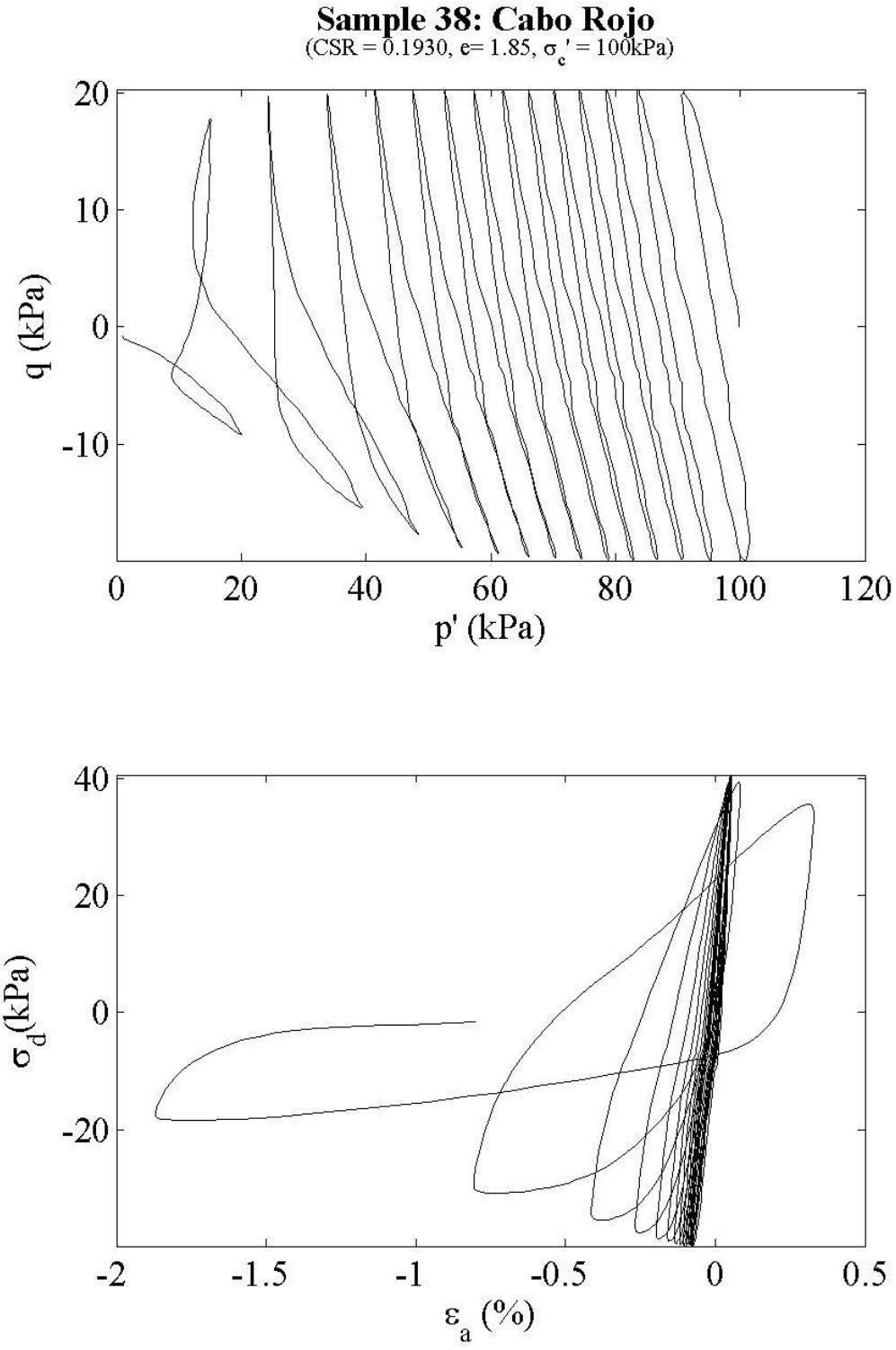

Figure 6-29: Sample 38 stress path and stress vs. strain

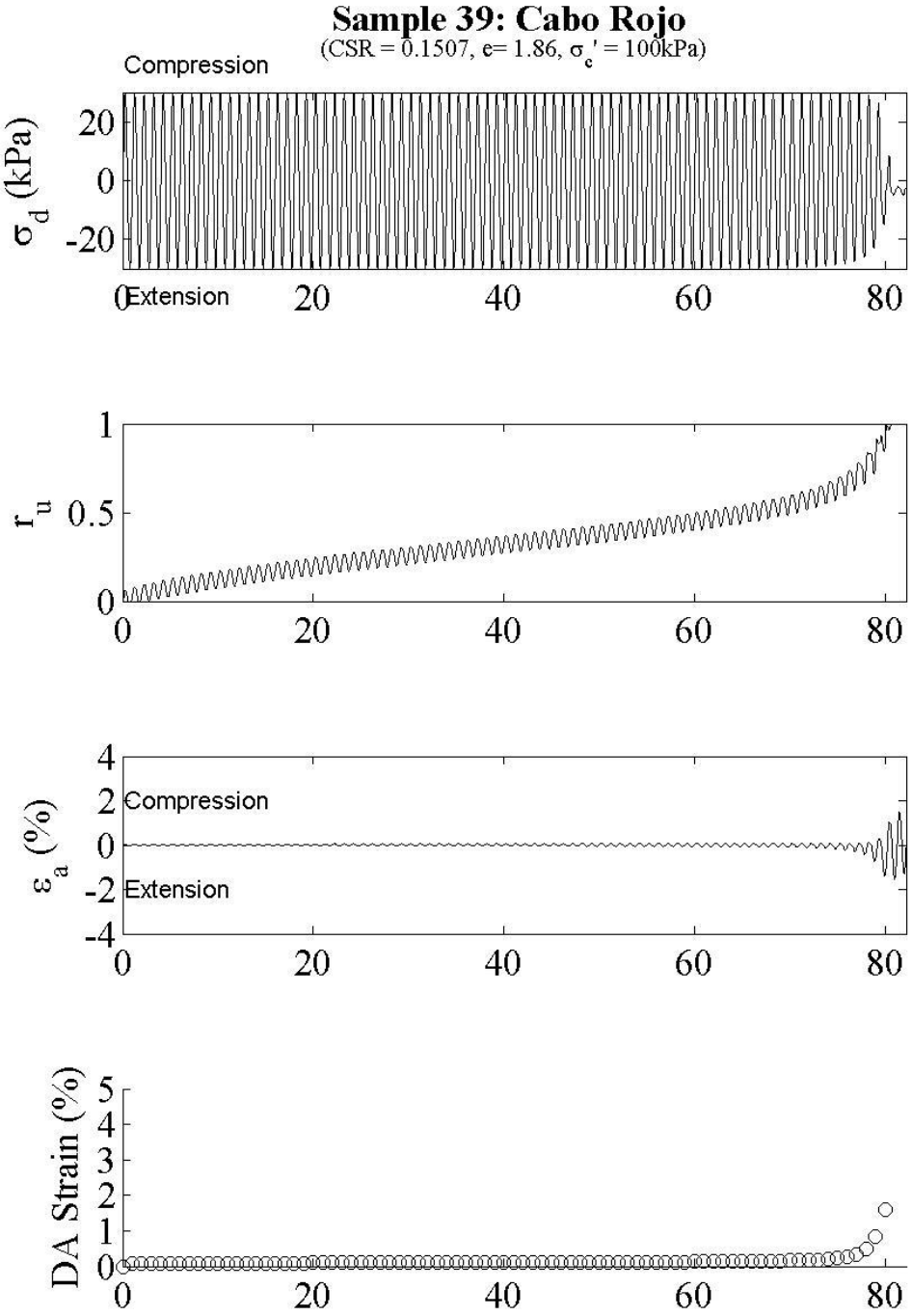

Figure 6-30: Sample 39 comparison plot

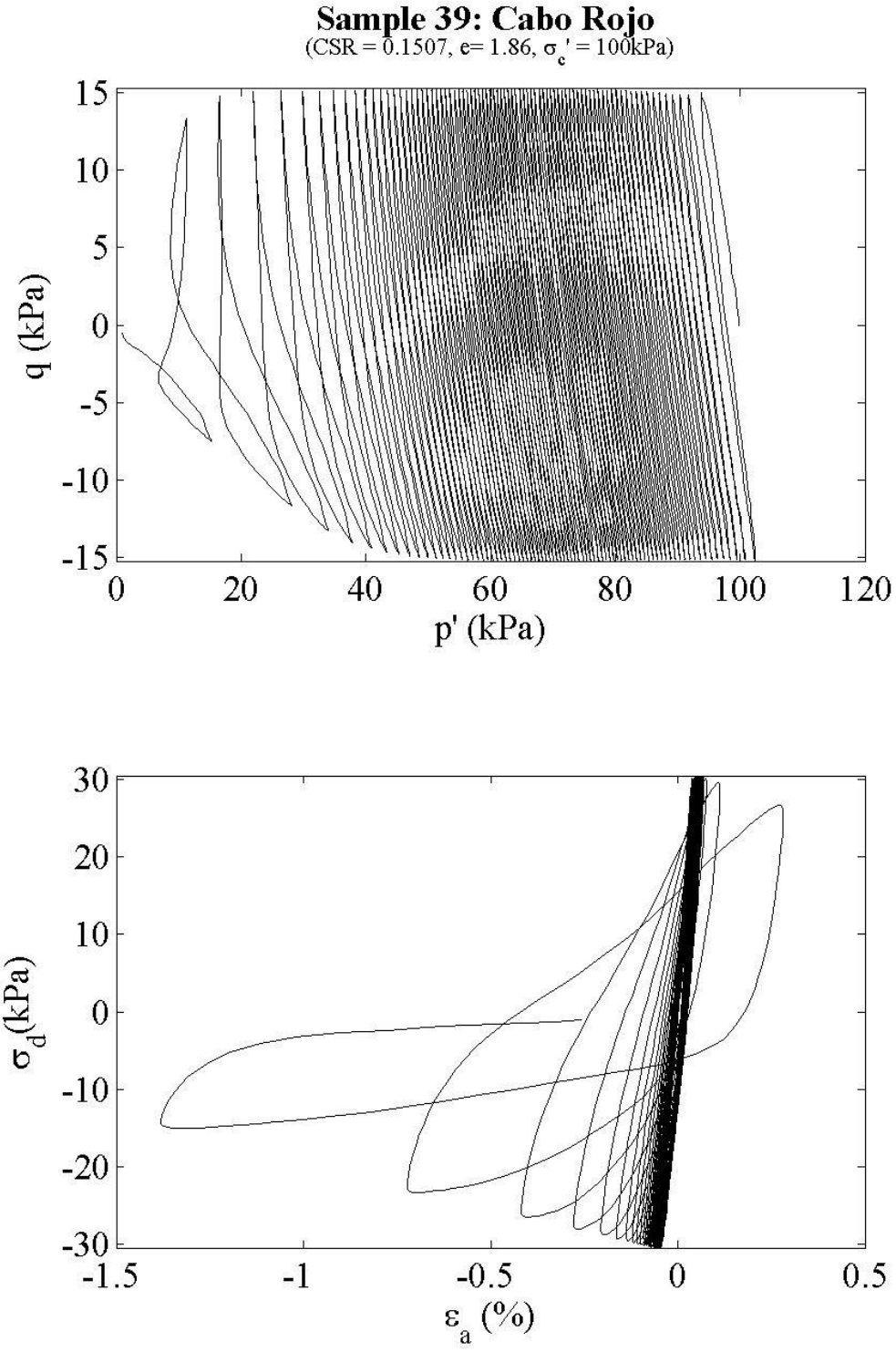

Figure 6-31: Sample 39 stress path and stress vs. strain plots

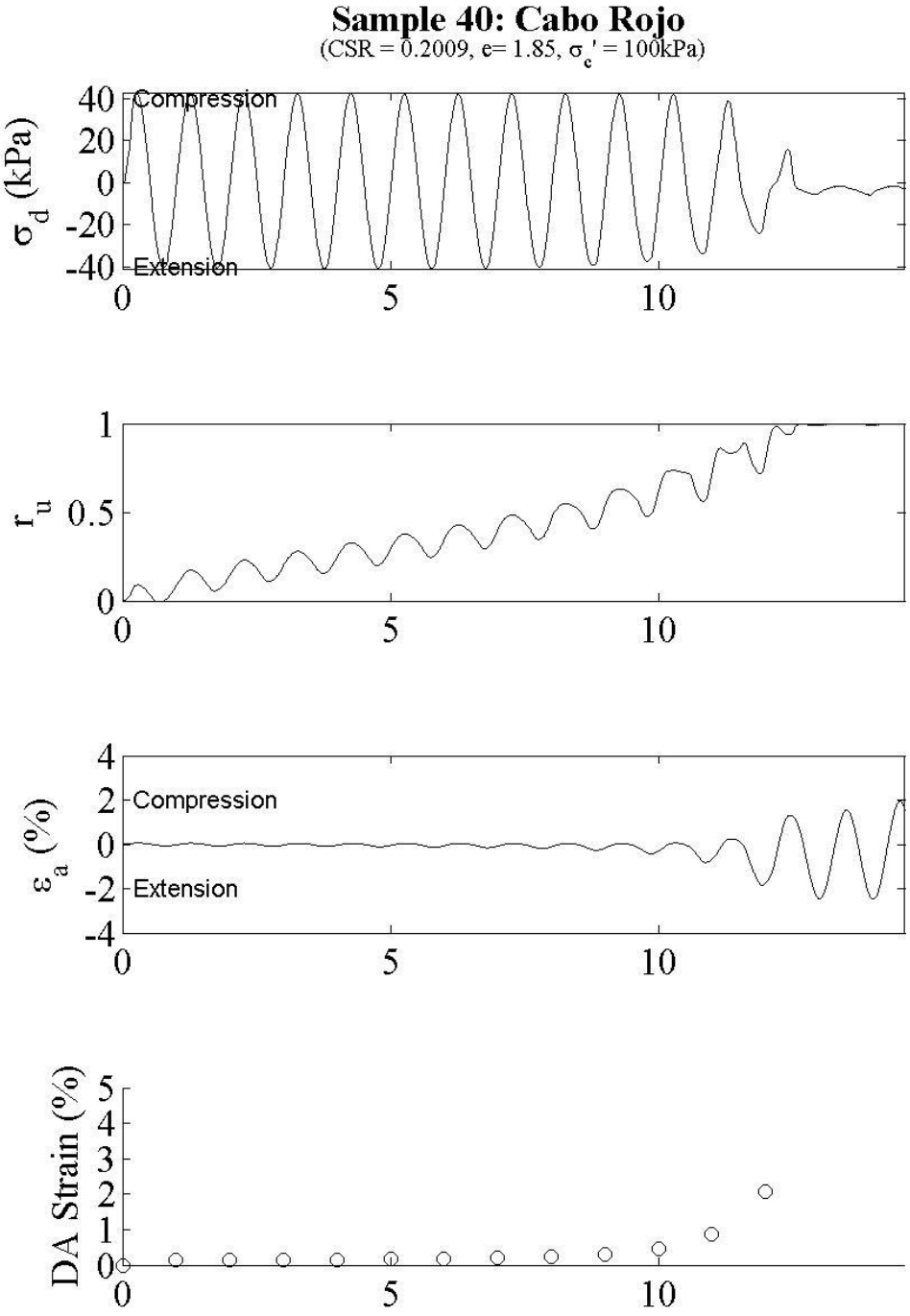

Figure 6-32: Sample 40 comparison plot

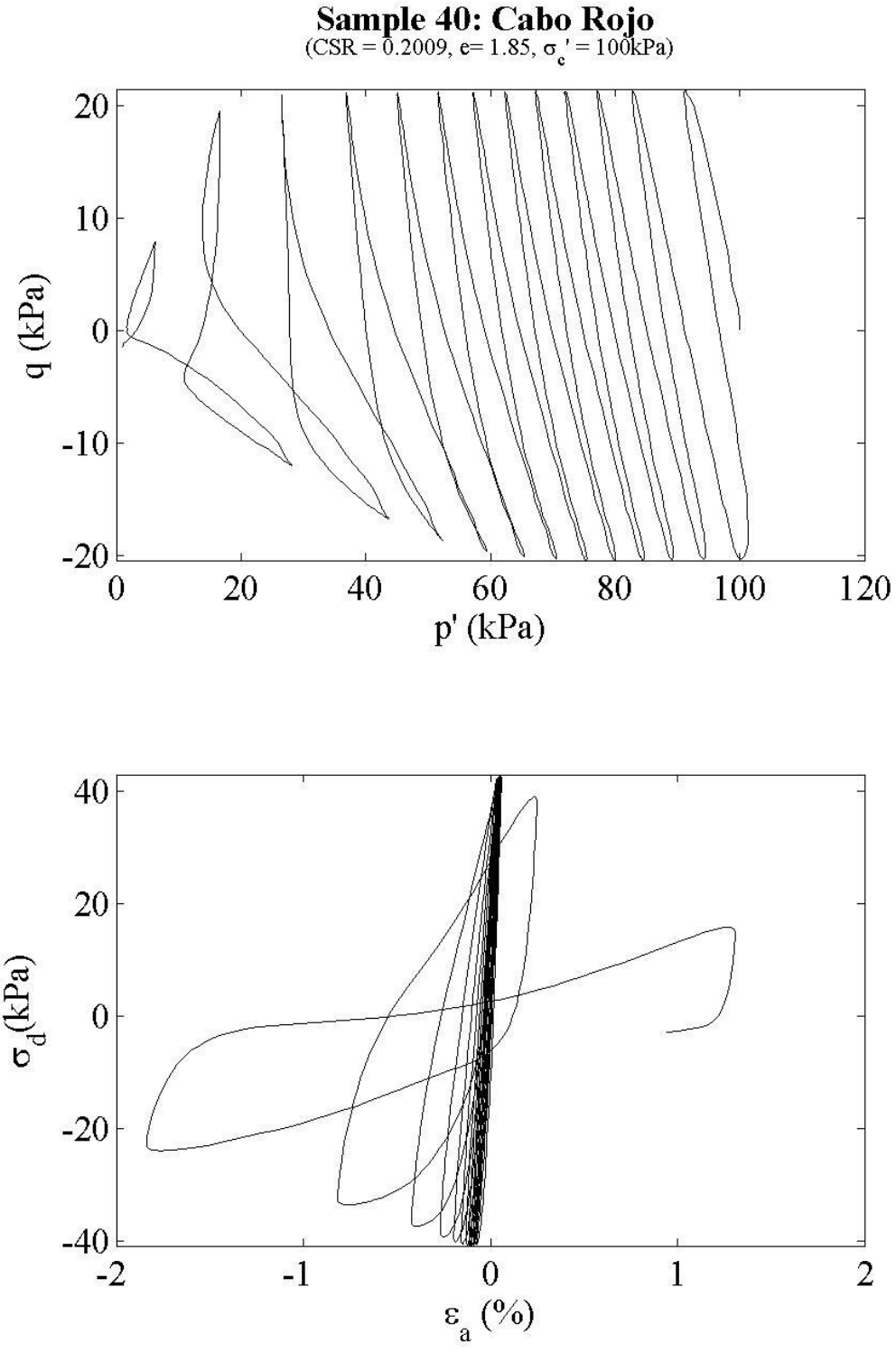

Figure 6-33: Sample 40 stress path and stress vs. strain plots

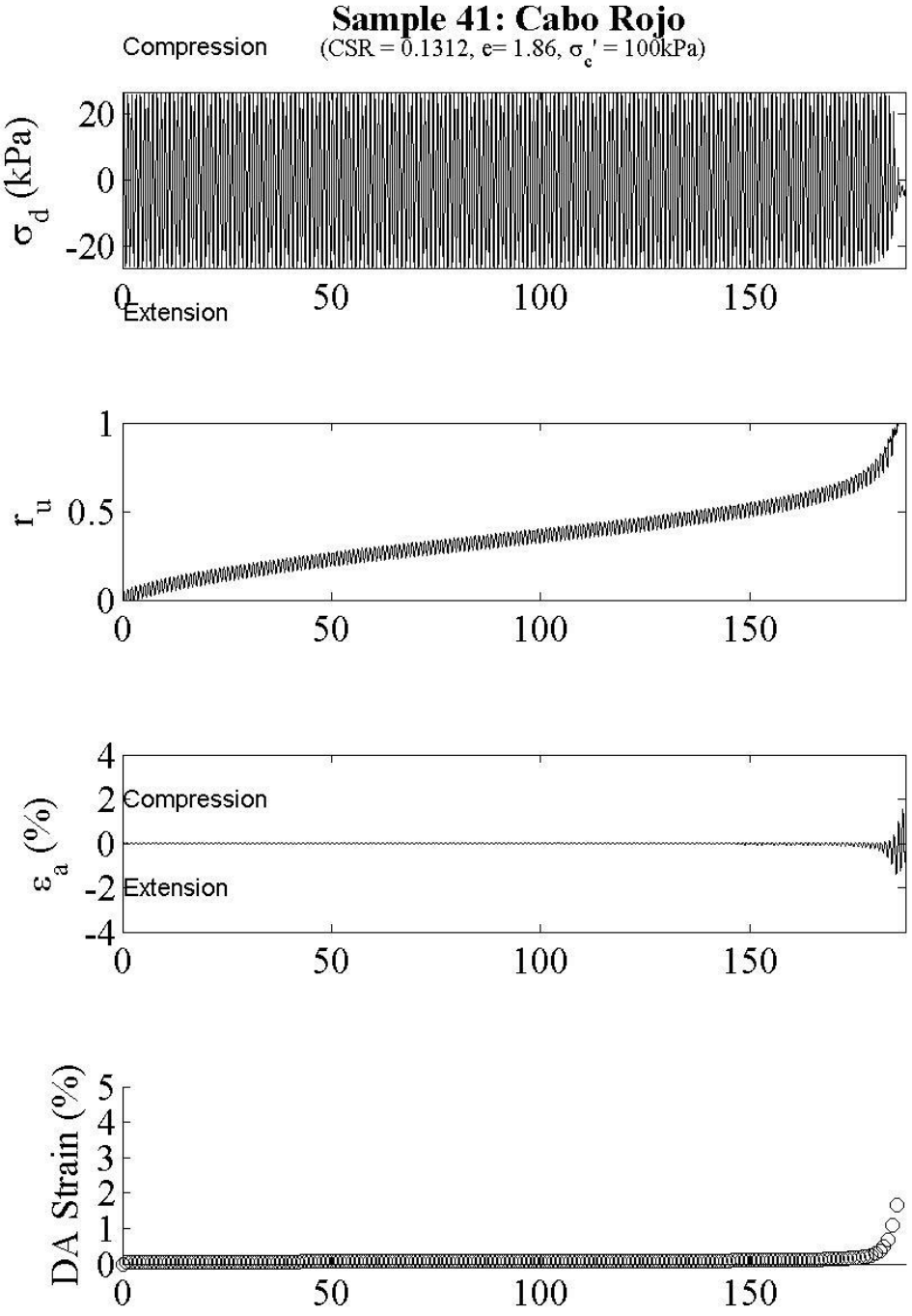

Figure 6-34: Sample 41 comparison plot

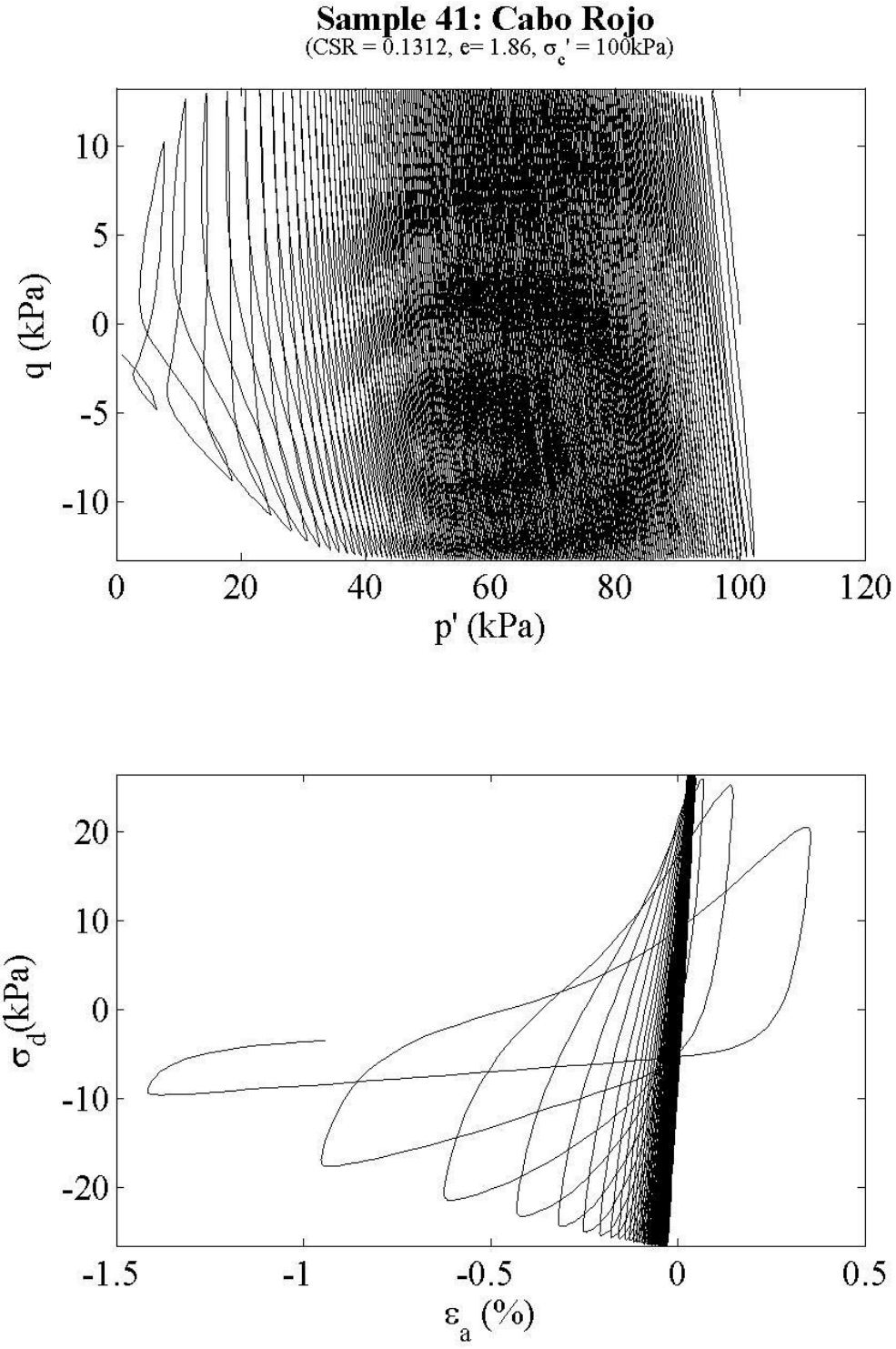

Figure 6-35: Sample 41 stress path and stress vs. strain plots

7. Appendix B: Monterey Sand Results

B.1 Void ratio = 0.76

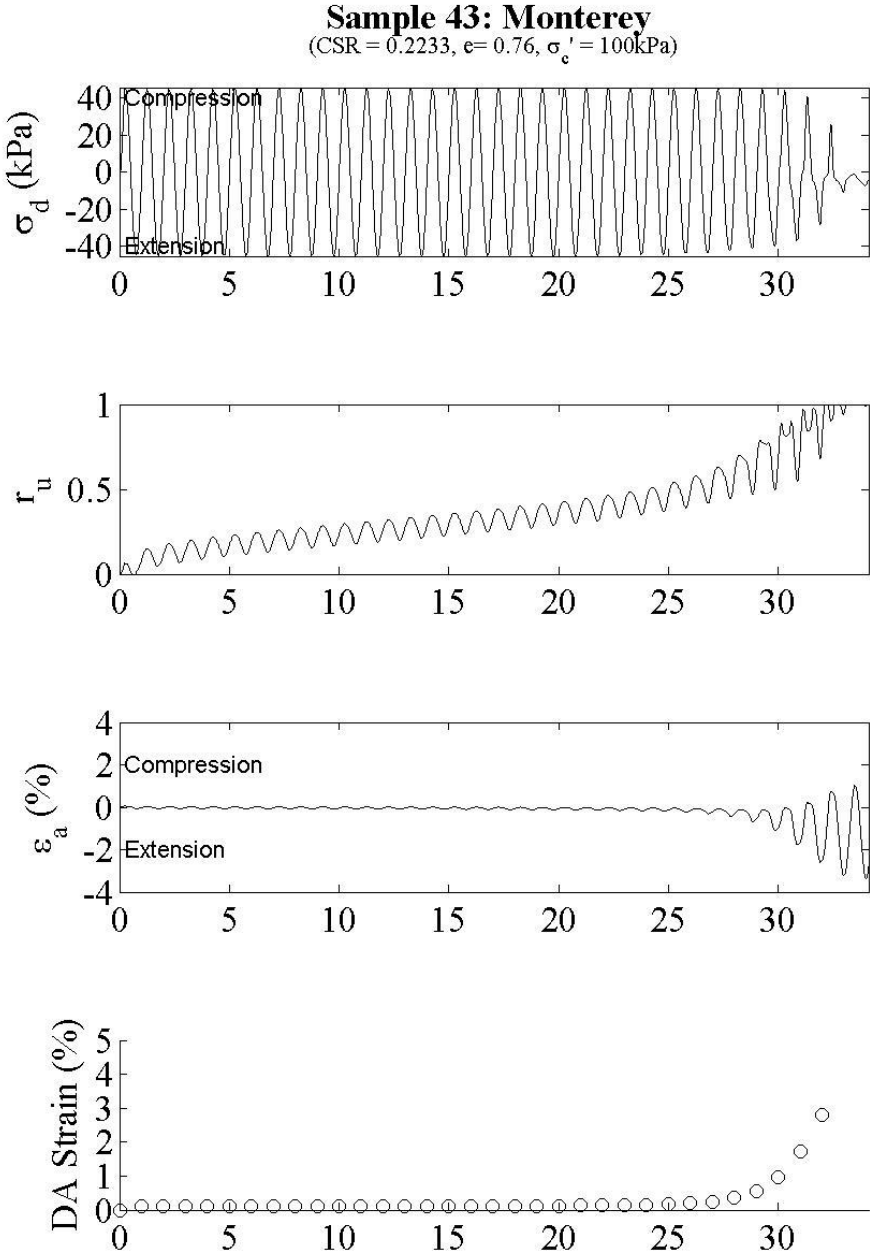

Figure 7-1: Sample 43 comparison plot

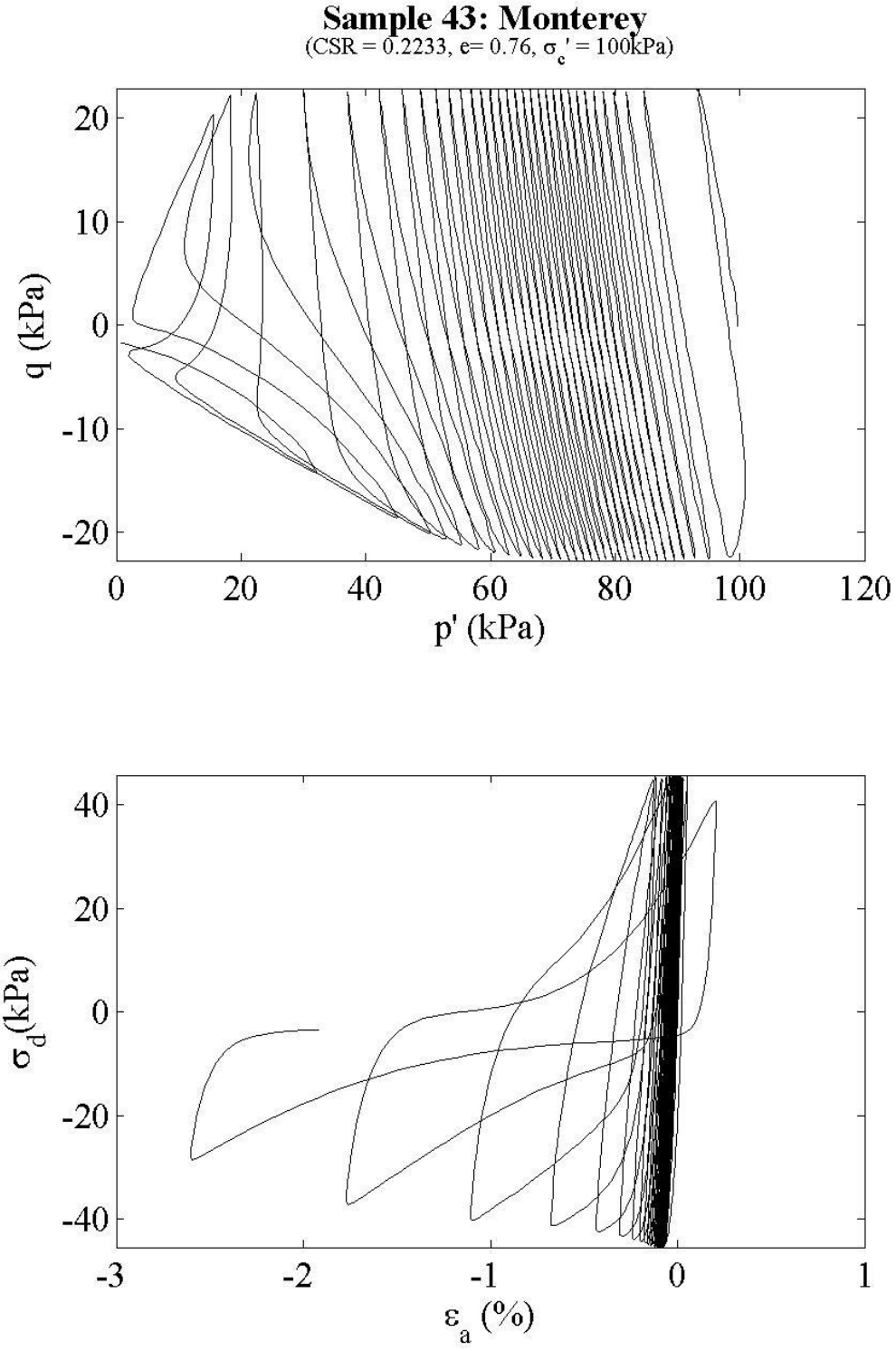

Figure 7-2: Sample 43 stress path and stress vs. strain plots

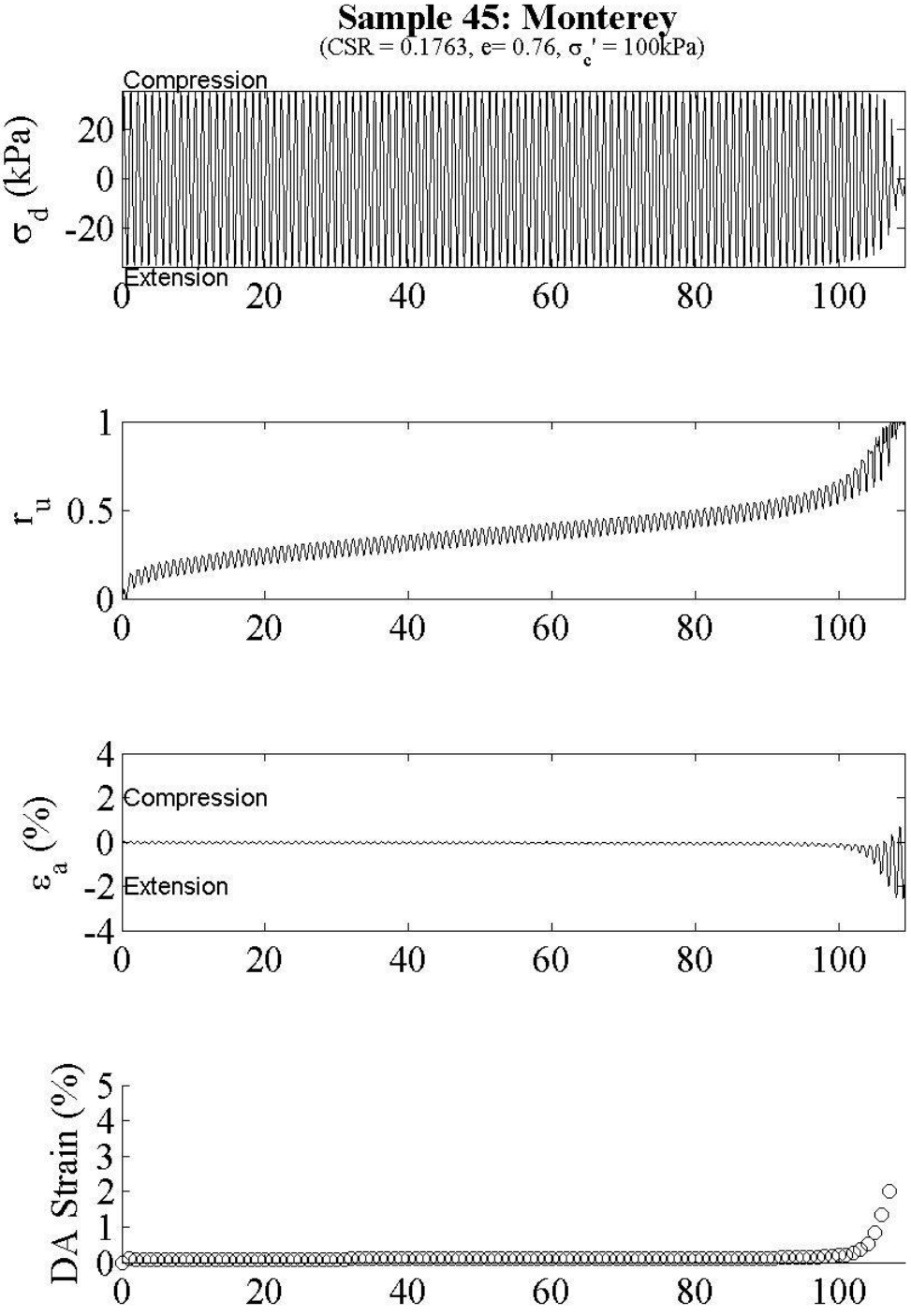

Figure 7-3: Sample 45 comparison plot

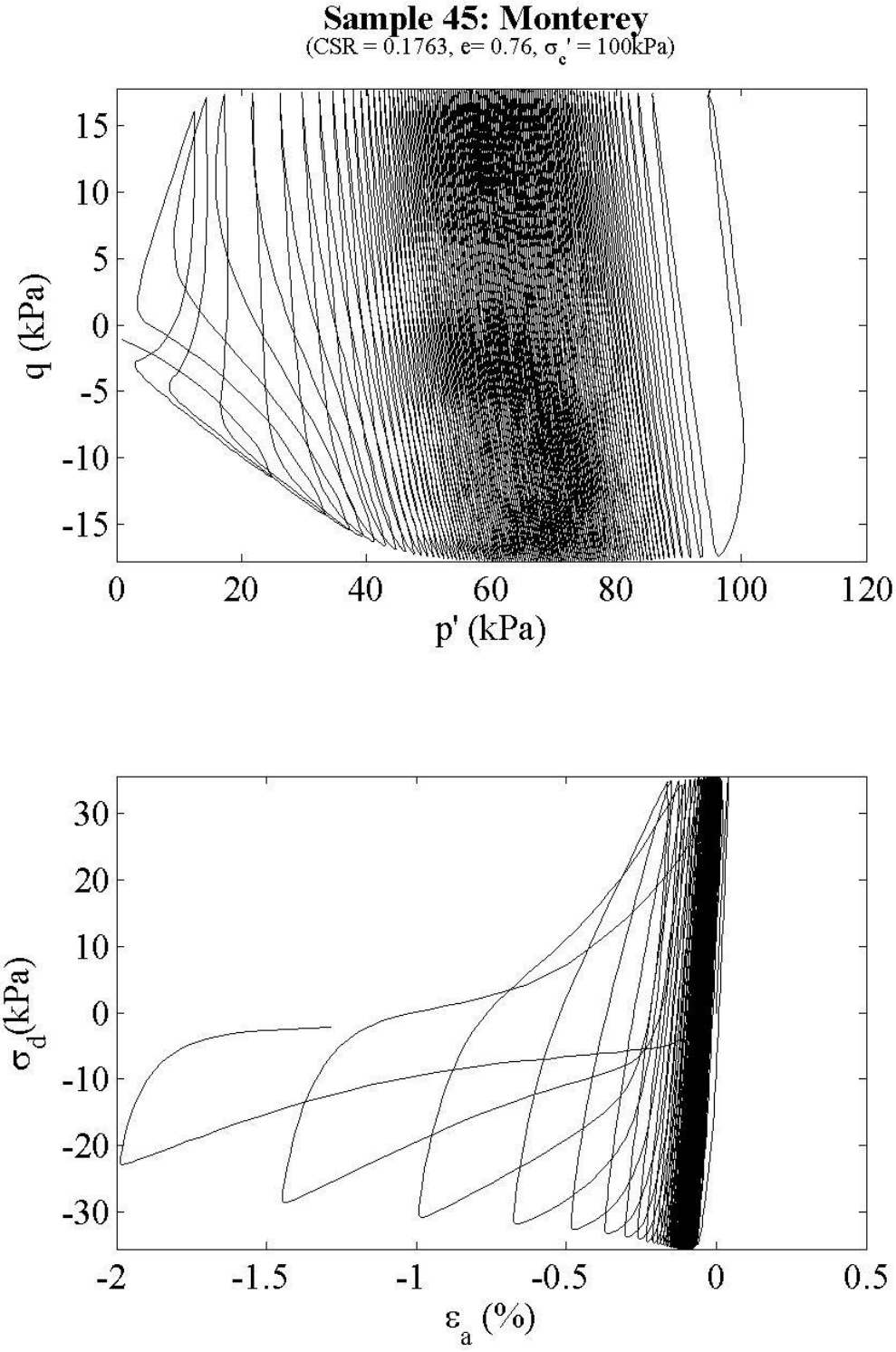

Figure 7-4: Sample 45 stress path and stress vs. strain plots

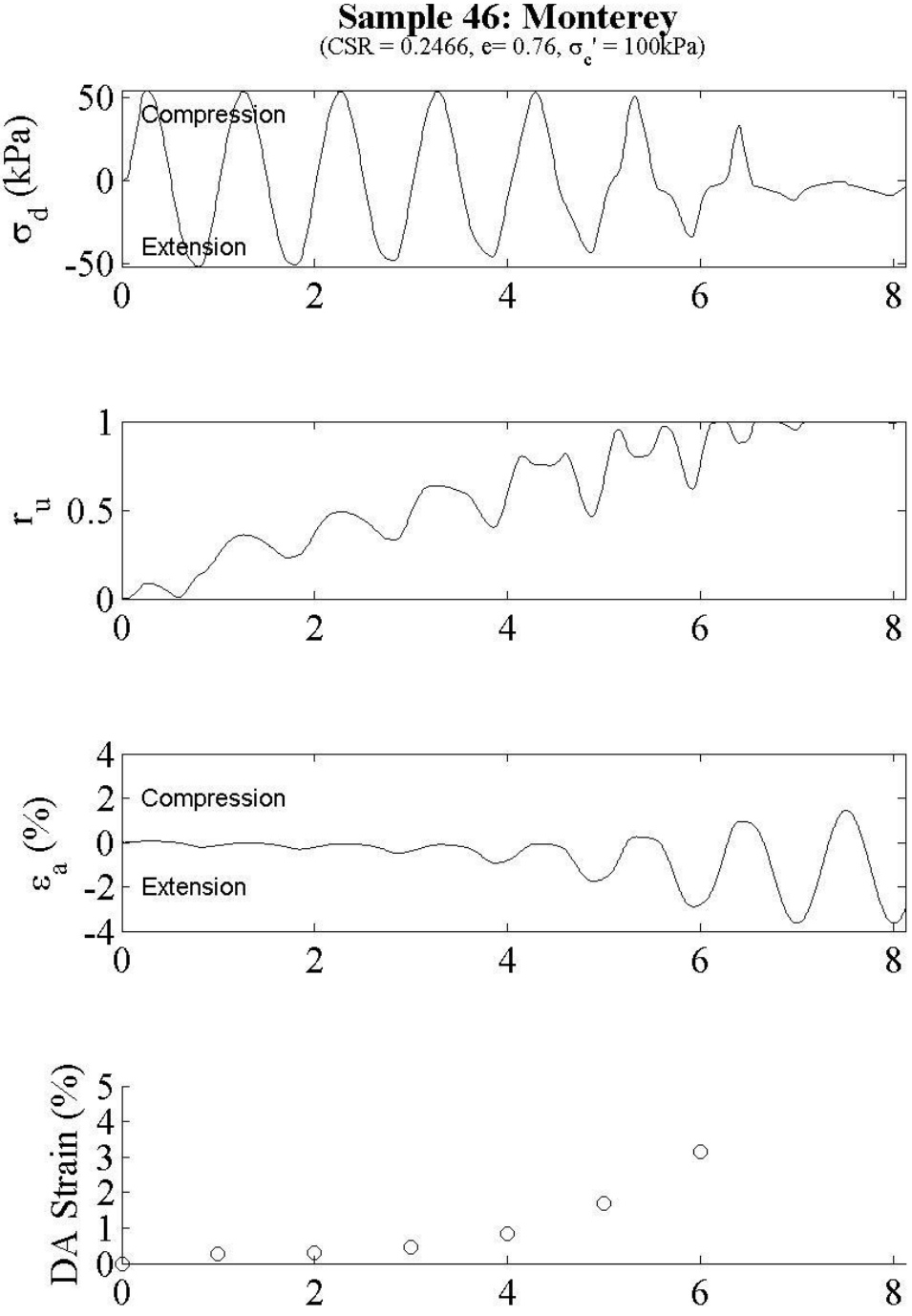

Figure 7-5: Sample 46 comparison plot

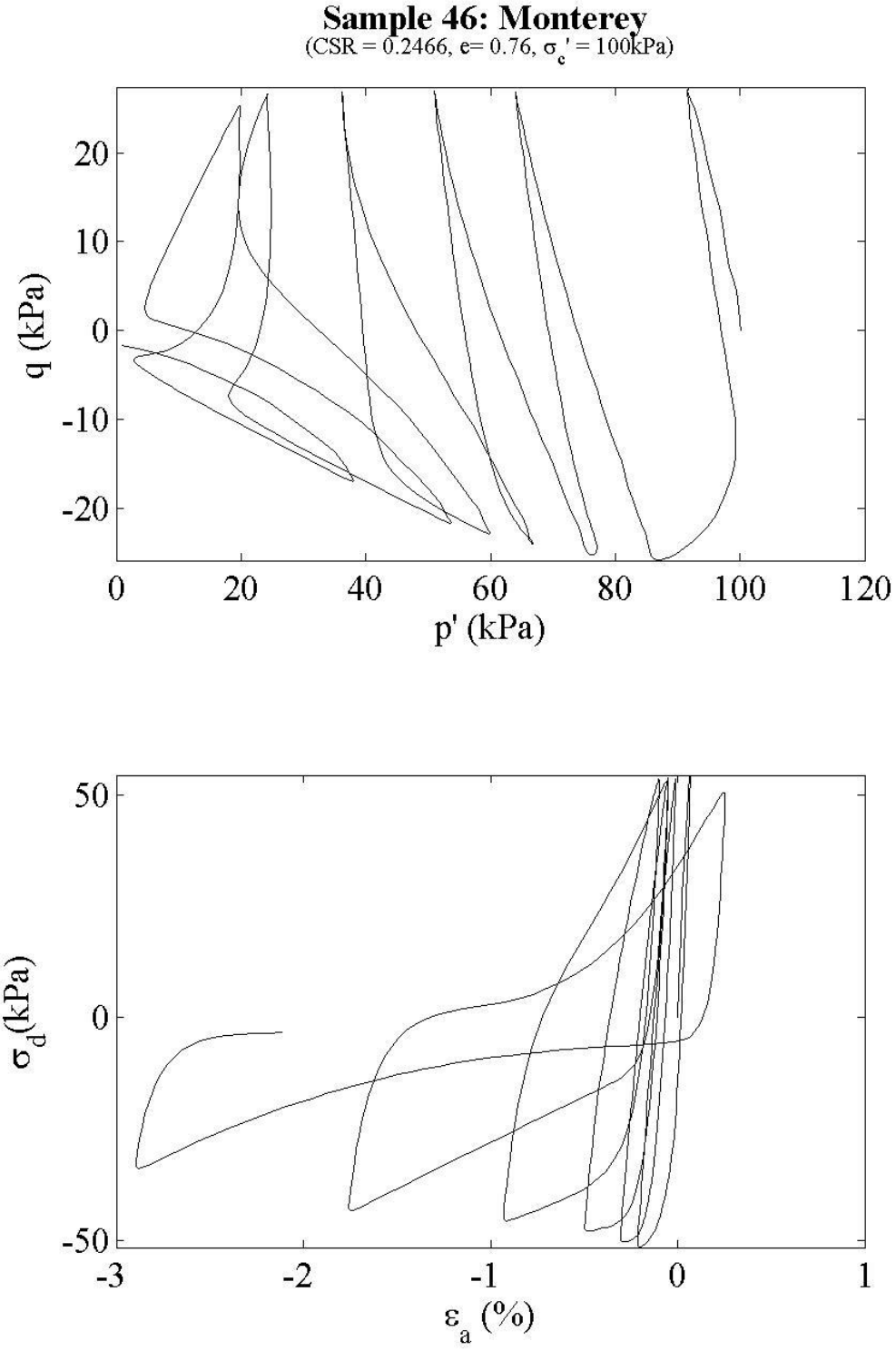

Figure 7-6: Sample 46 stress path and stress vs. strain plots

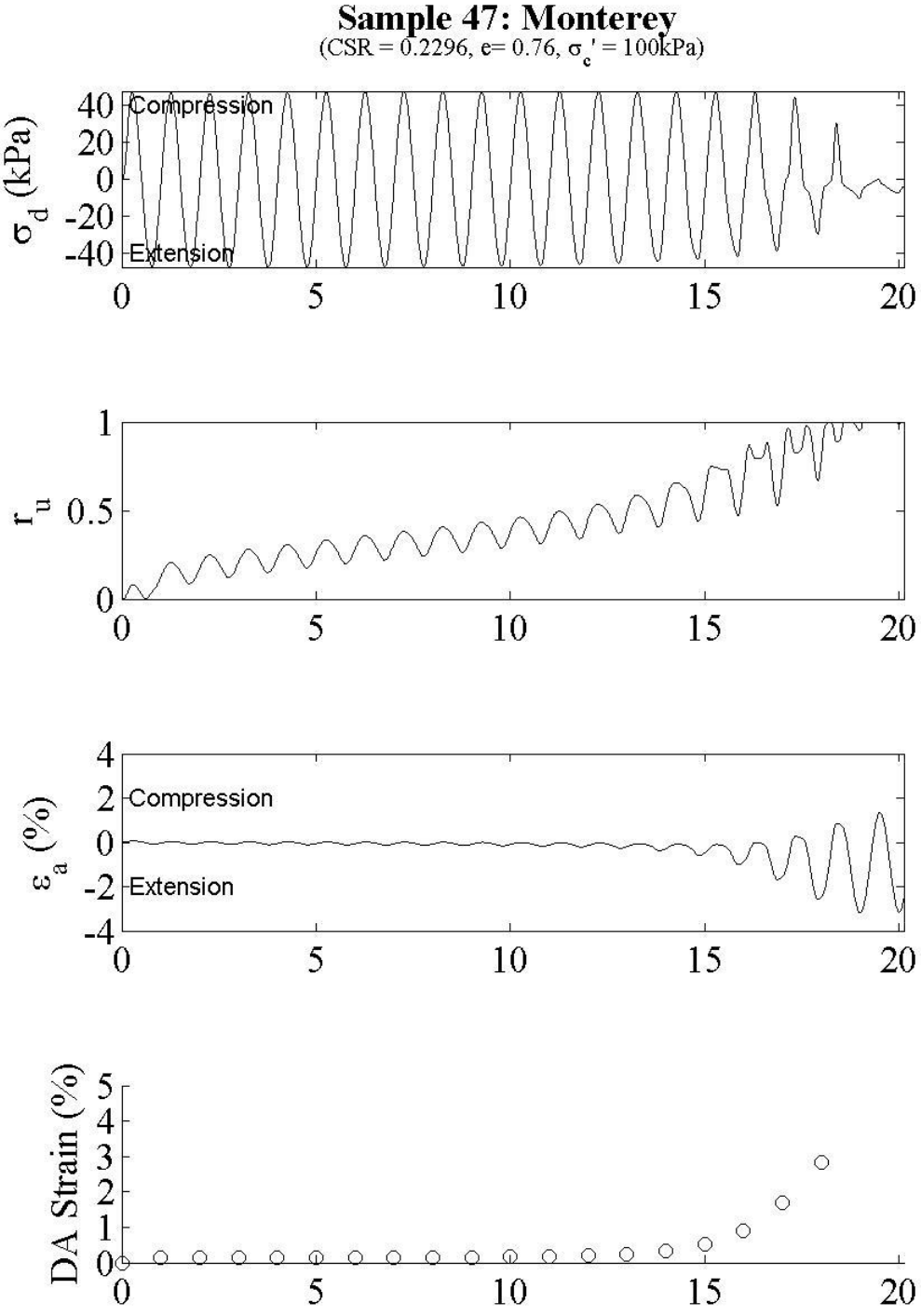

Figure 7-7: Sample 47 comparison plot

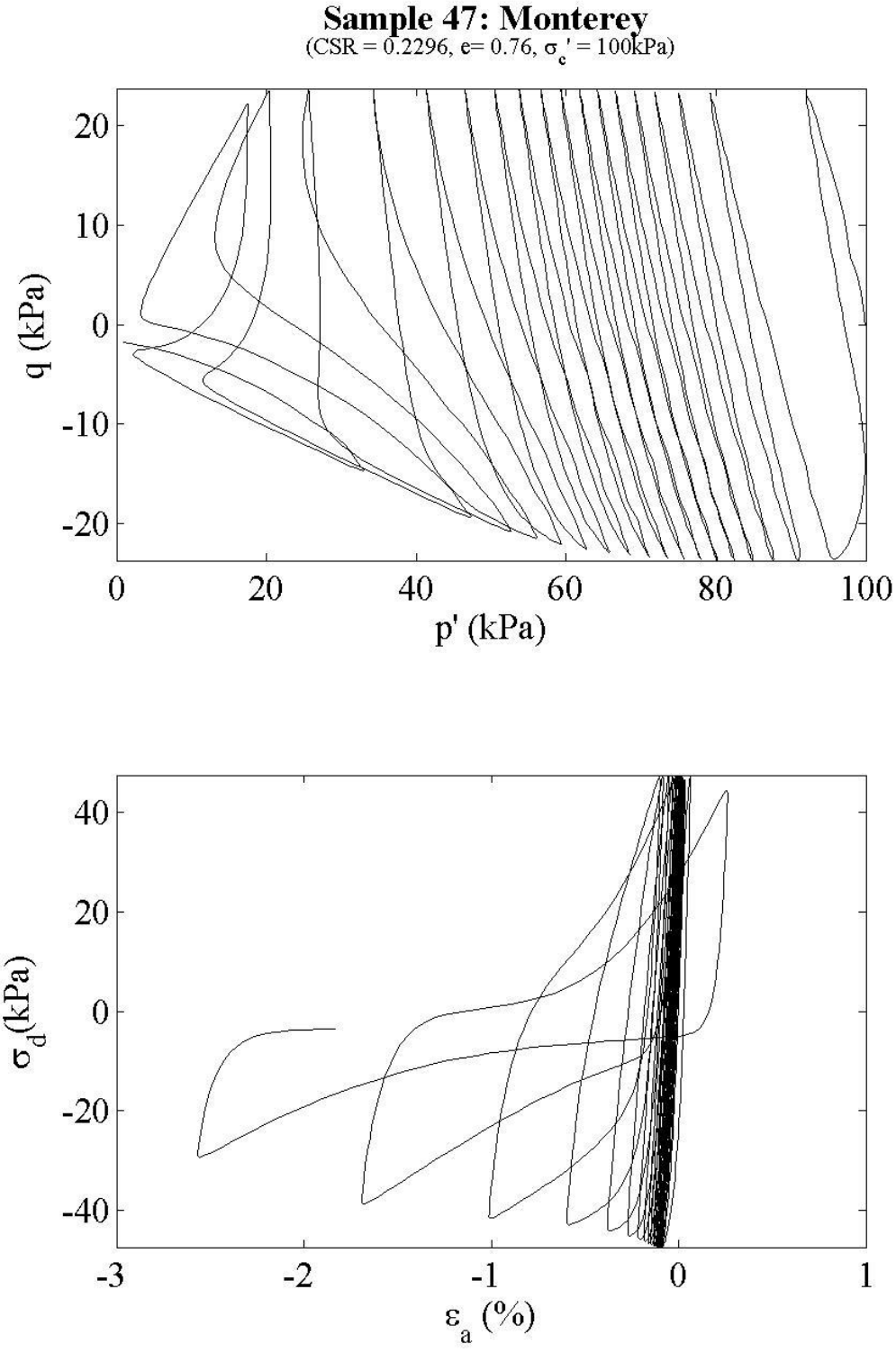

Figure 7-8: Sample 47 stress path and stress vs. strain plots

B.2 Void ratio = 0.69

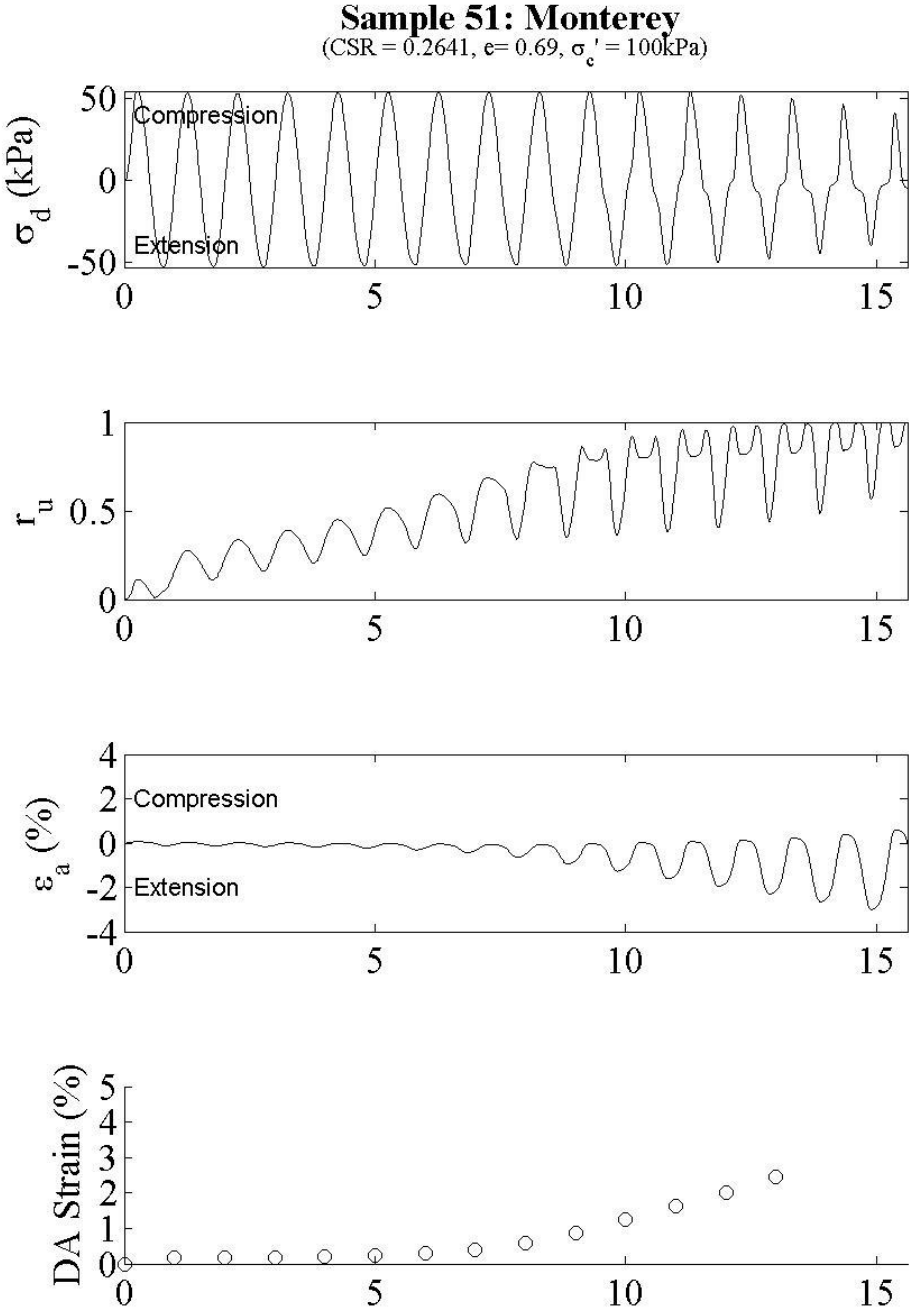

Figure 7-9: Sample 51 comparison plot

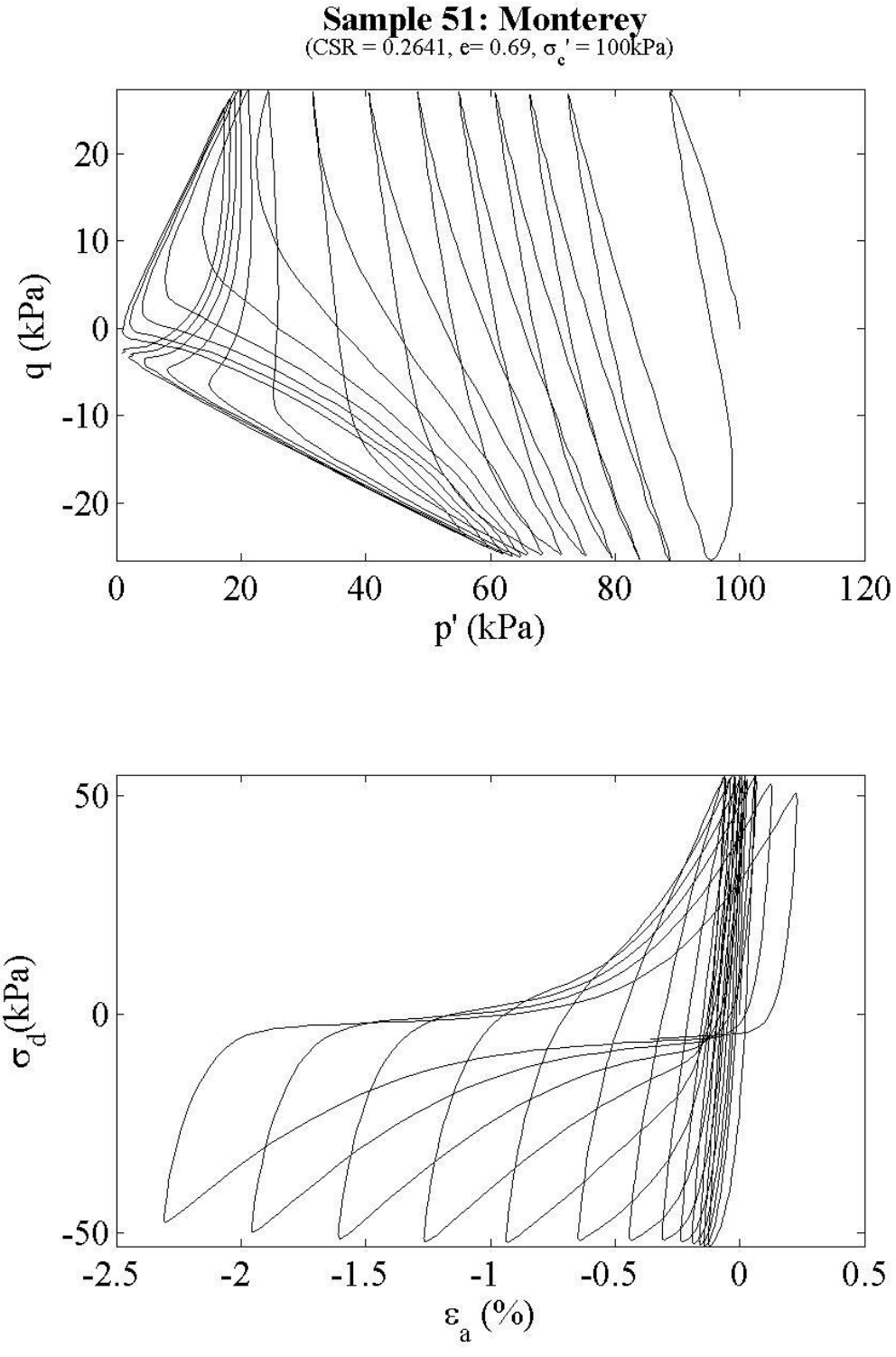

Figure 7-10: Sample 51 stress path and stress vs. strain plots

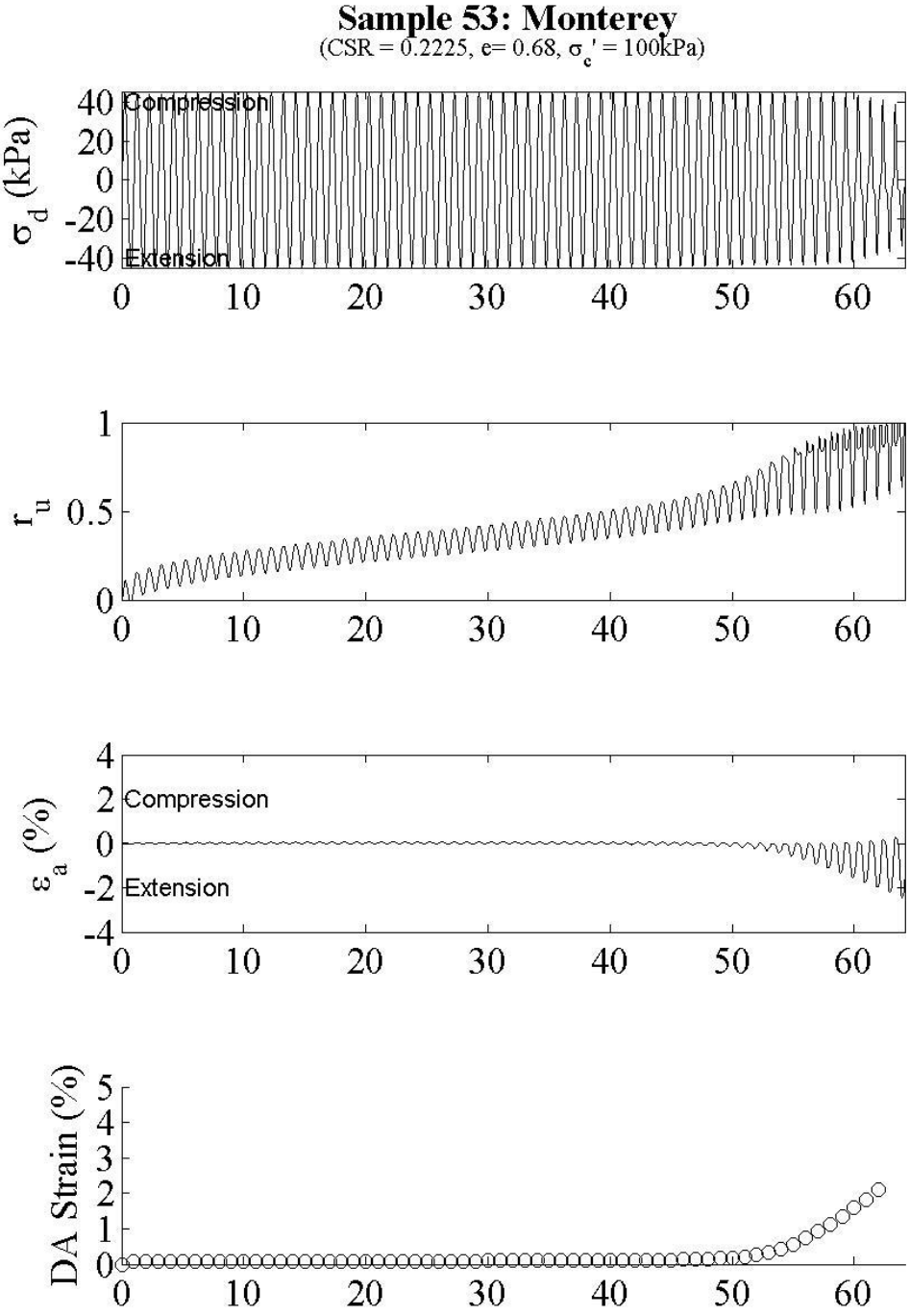

Figure 7-11: Sample 53 comparison plot

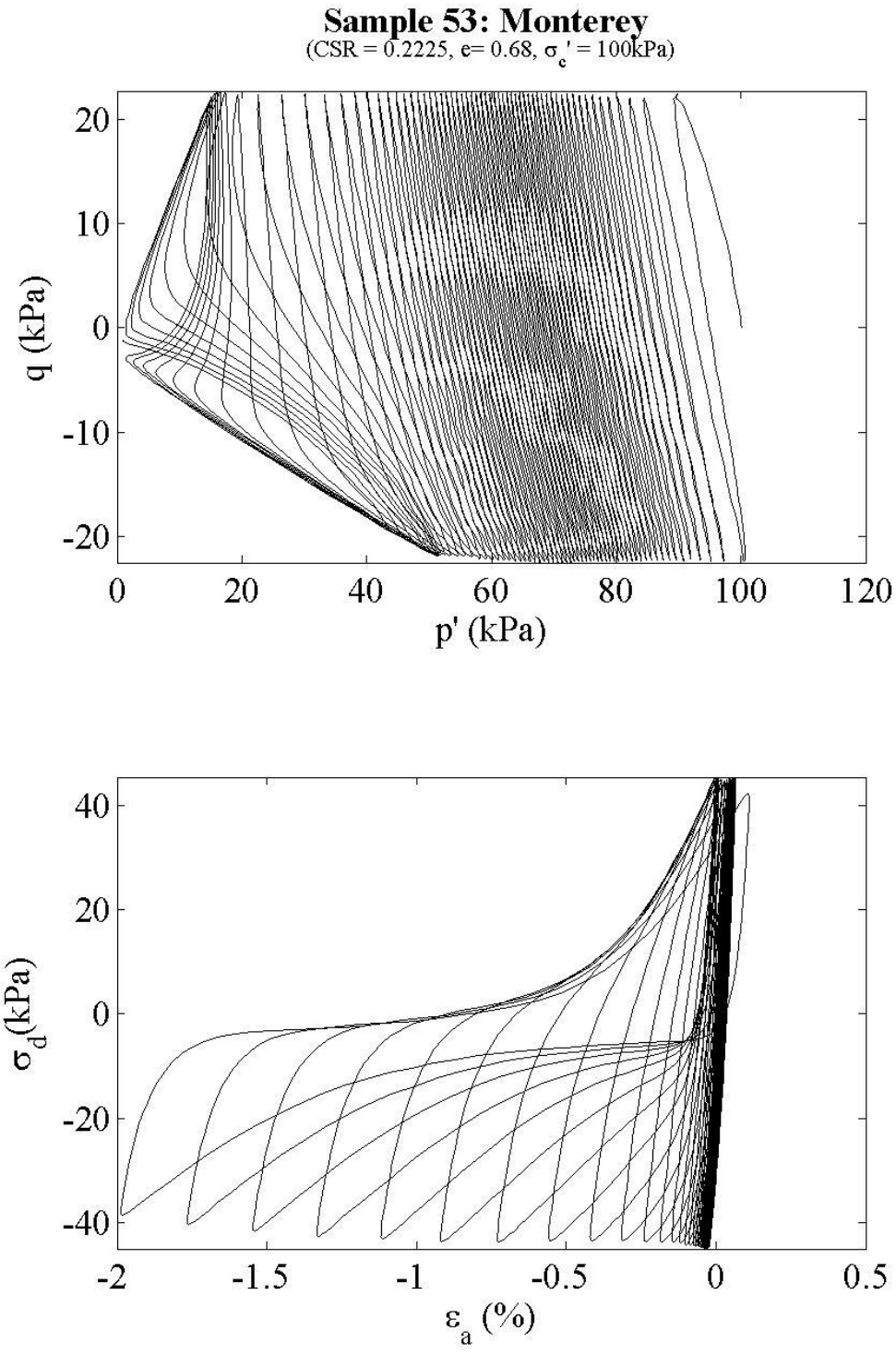

Figure 7-12: Sample 53 stress path and stress vs. strain plots

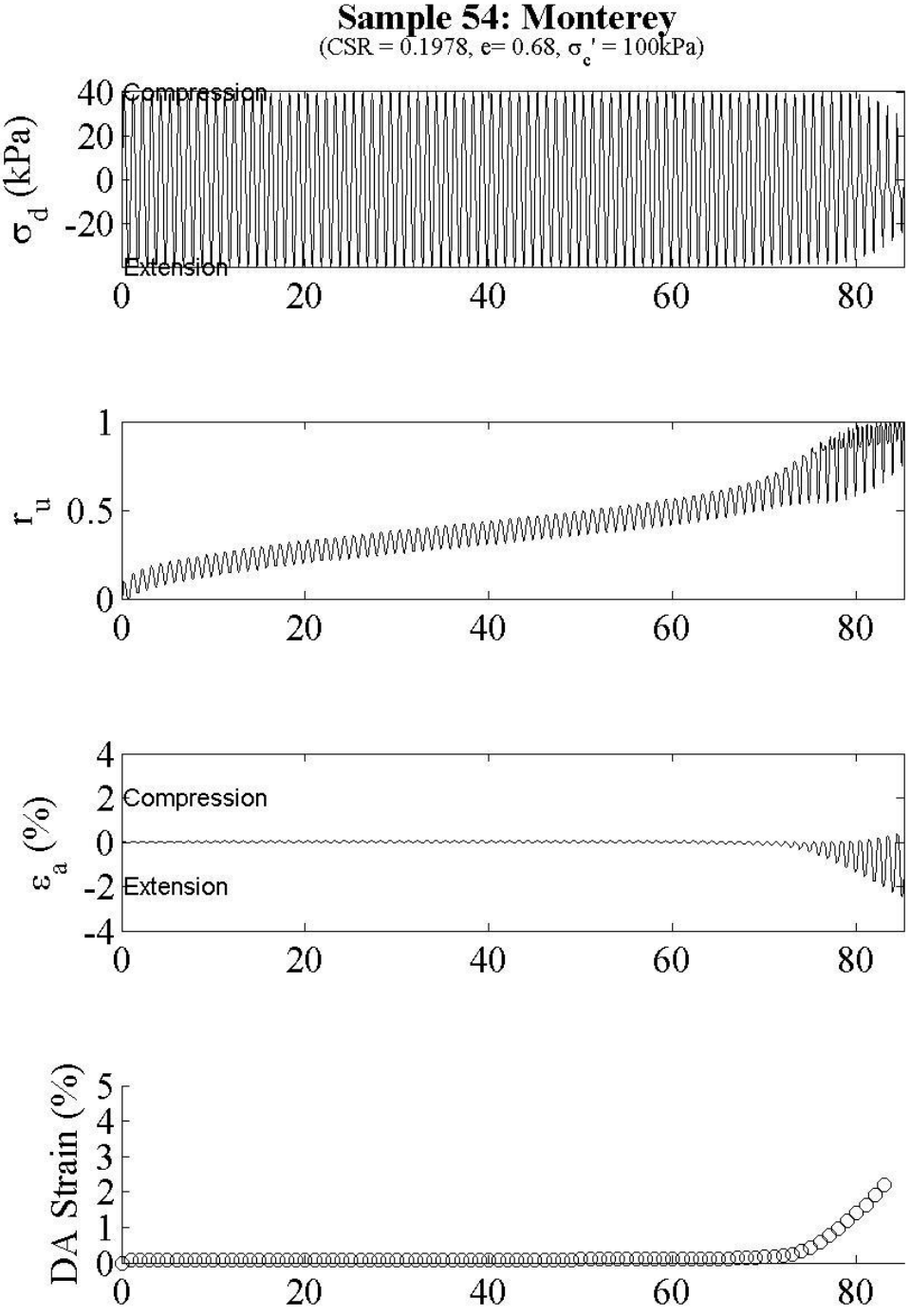

Figure 7-13: Sample 54 comparison plot

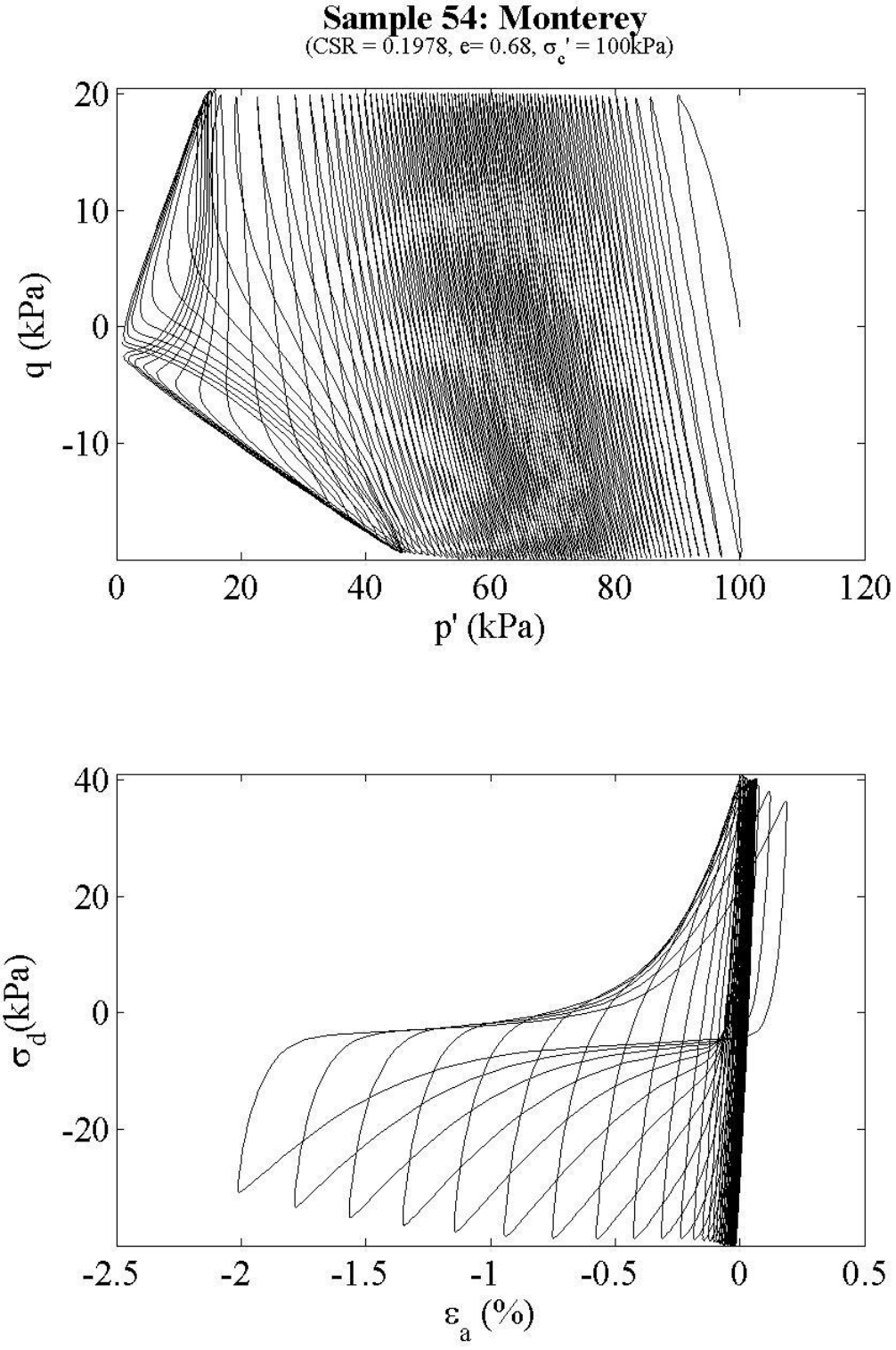

Figure 7-14: Sample 54 stress path and stress vs. strain plots

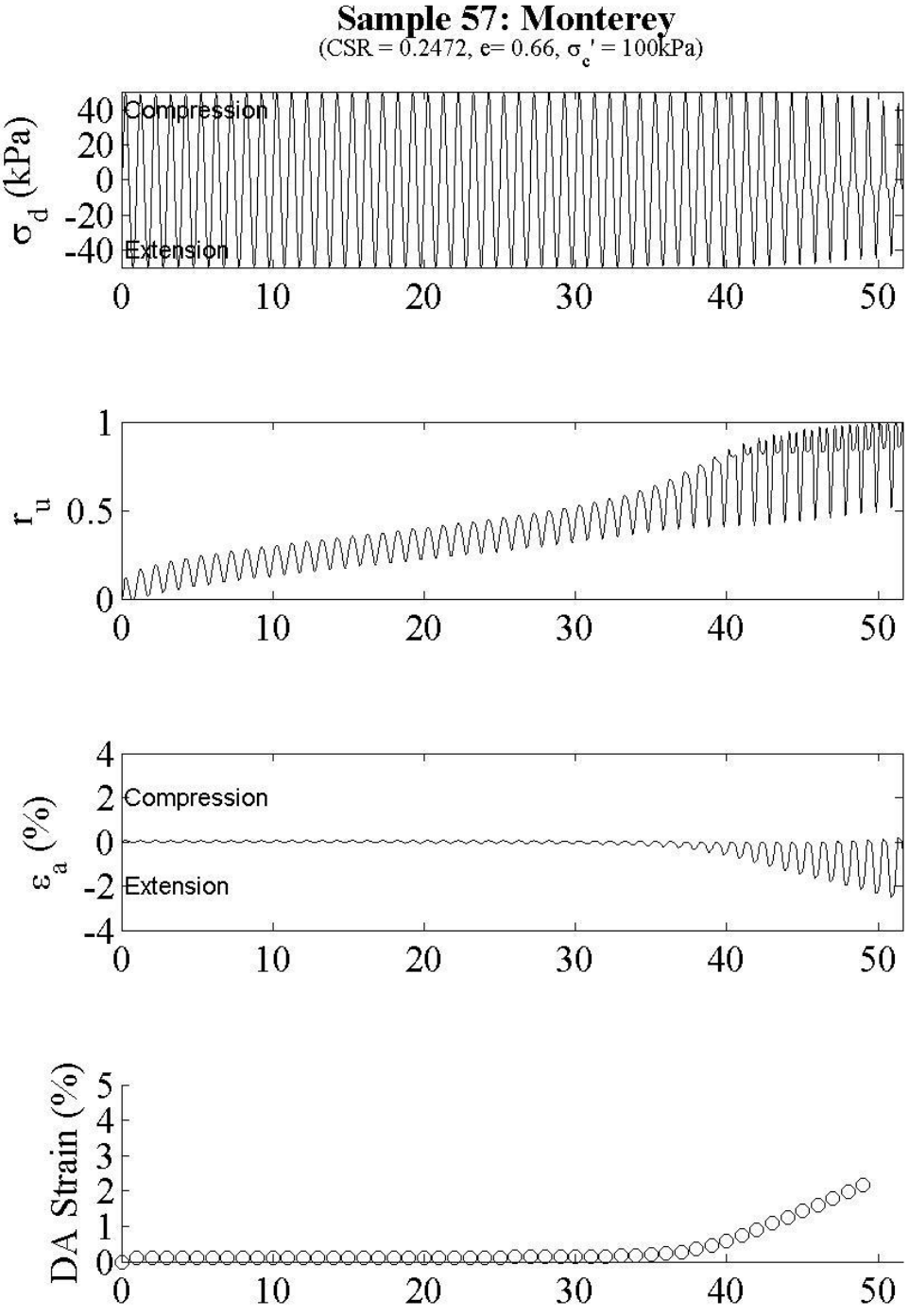

Figure 7-15: Sample 56 comparison plot

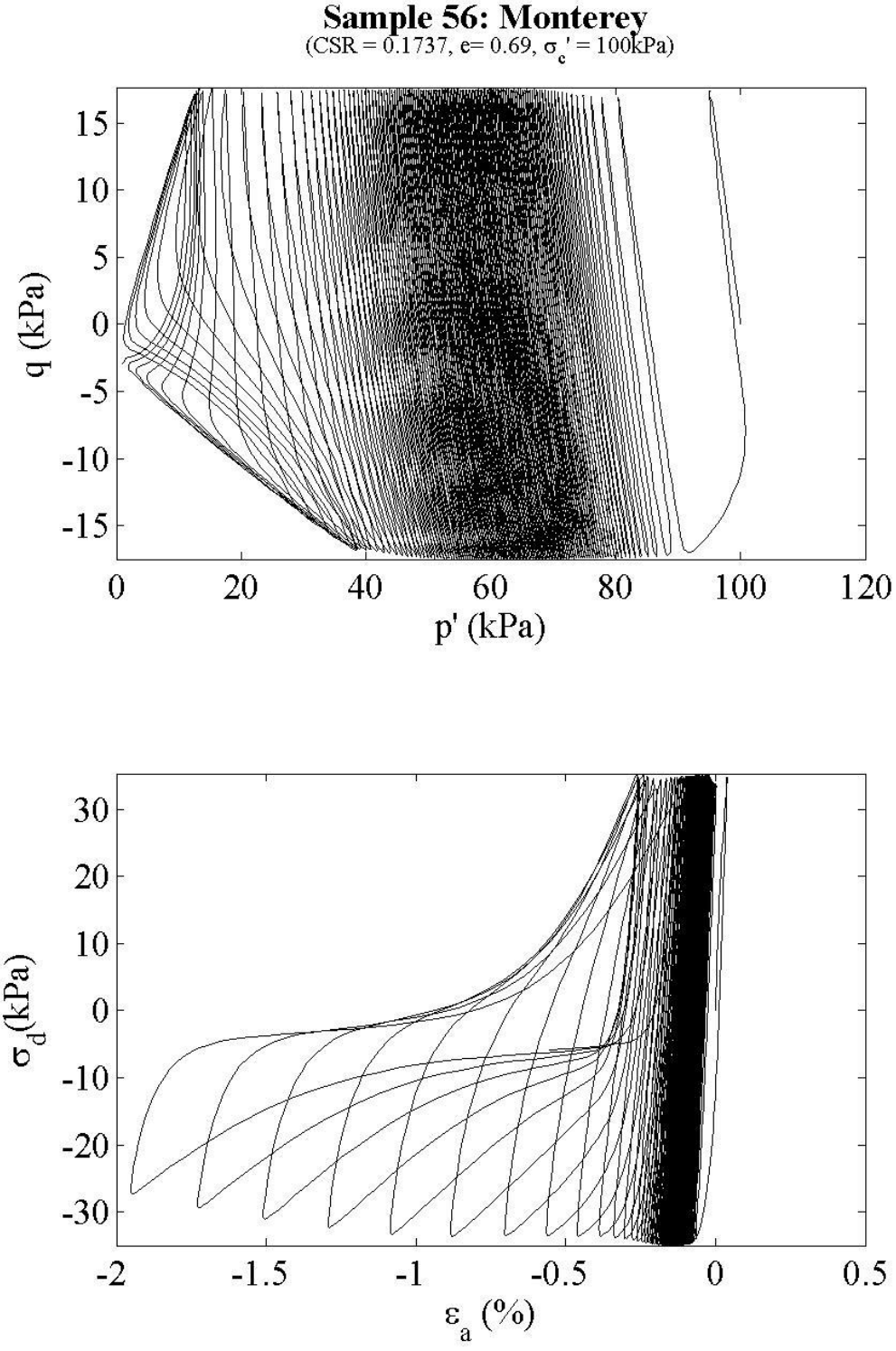

Figure 7-16: Sample 56 stress path and stress vs. strain plots

B.3 Void Ratio = 0.65

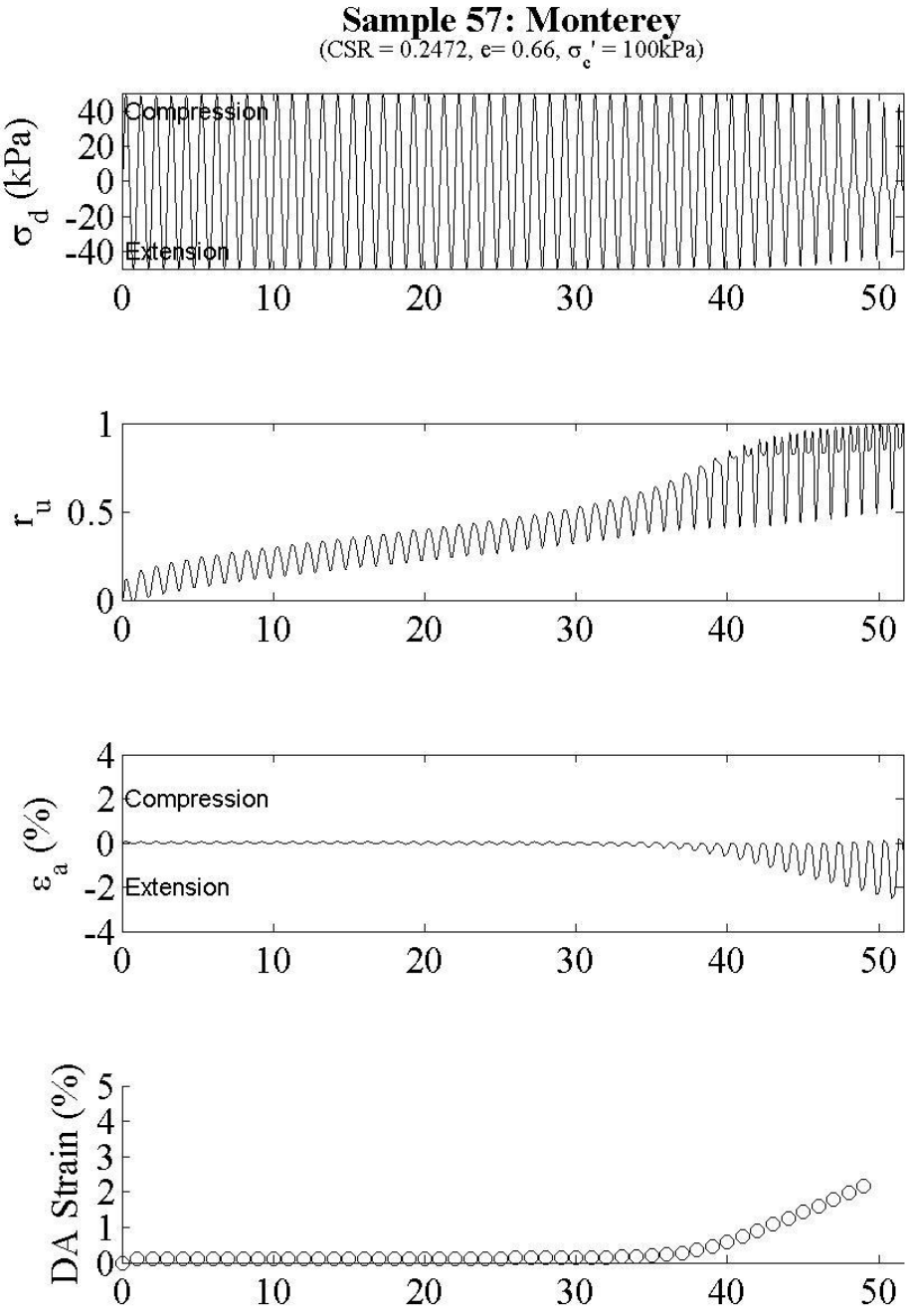

Figure 7-17: Sample 57 comparison plot

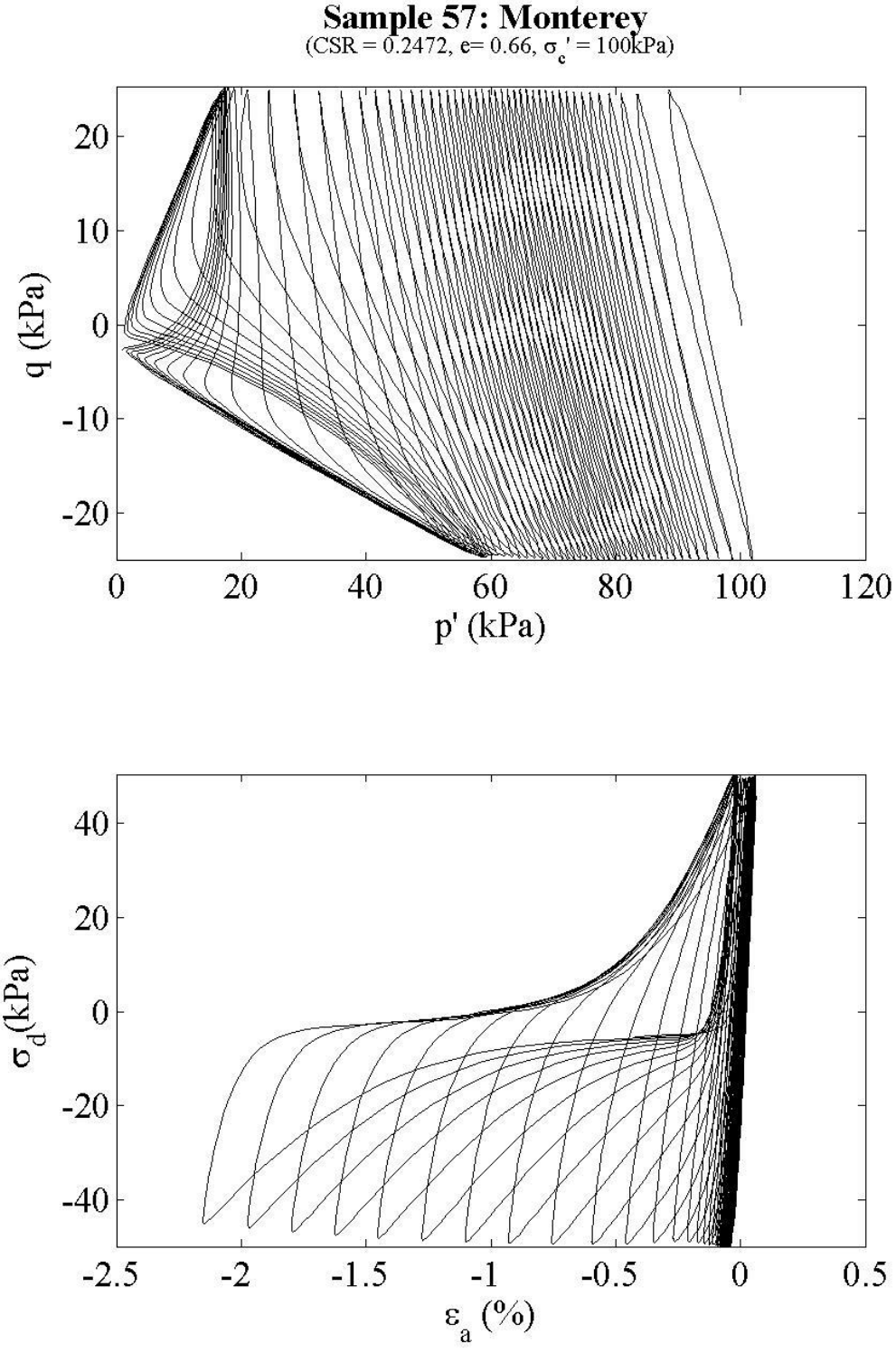

Figure 7-18: Sample 57 stress path and stress vs. strain plots

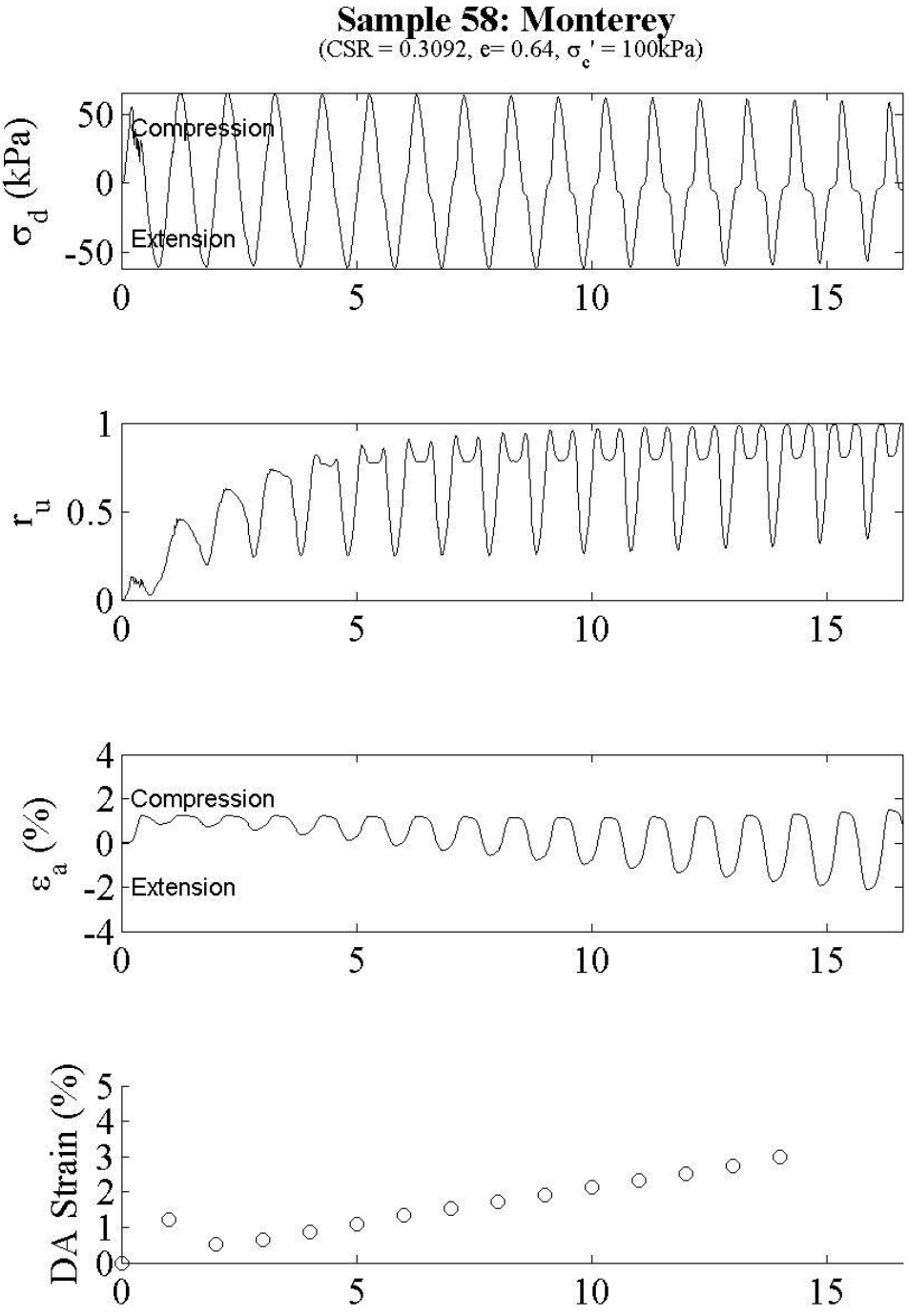

Figure 7-19: Sample 58 comparison plot

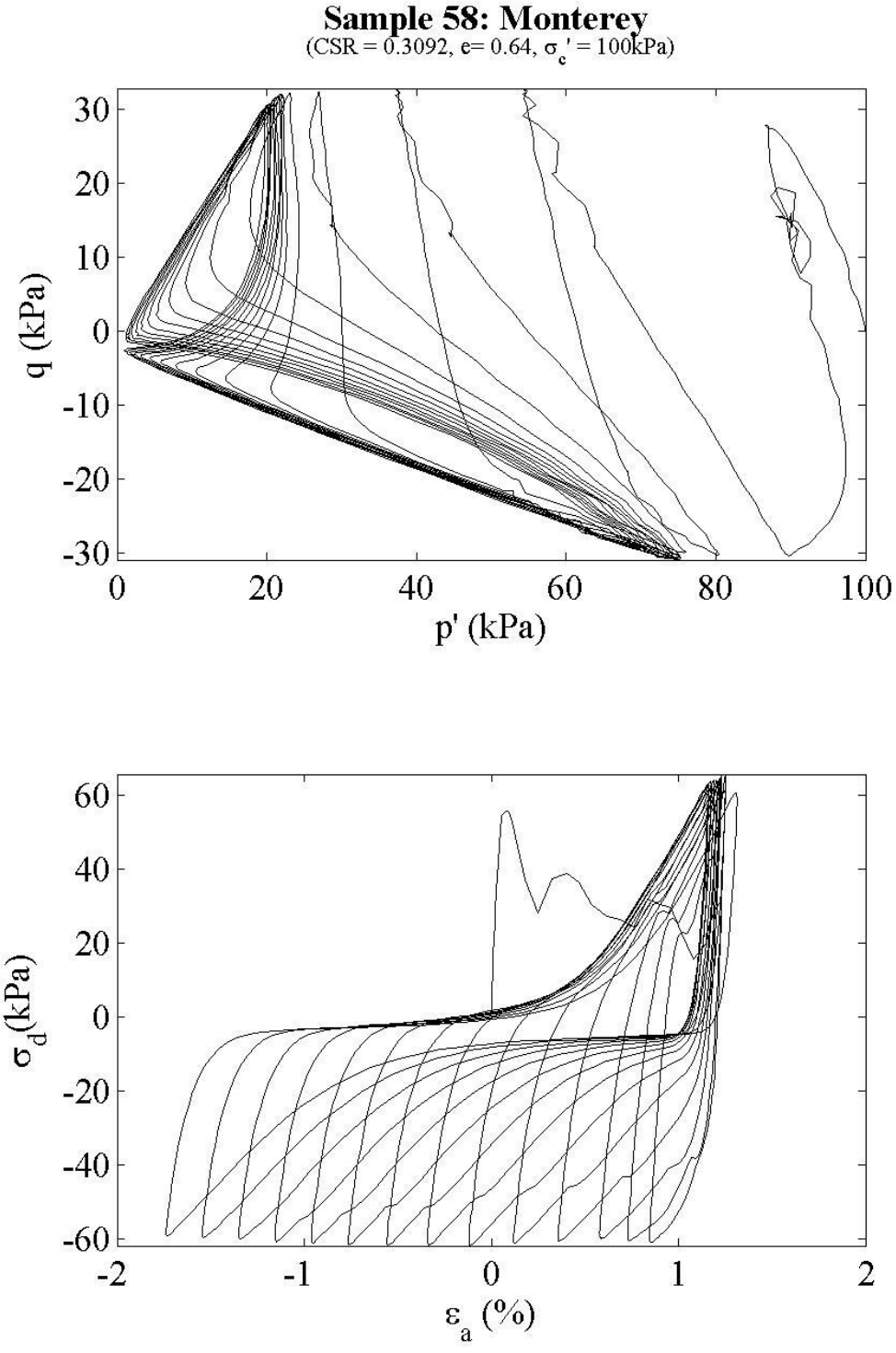

Figure 7-20: Sample 58 stress path and stress vs. strain plots

8. Bibliography

Andrus, R.D., and Stokoe, K.H. (2000). "Liquefaction resistance of soils from shear wave velocity." *Journal of Geotechnical and Geoenvironmental Engineering*, 126(11), 1015-1025.

Baxter et al. (2008). "Correlation Between Cyclic Resistance and Shear-Wave Velocity for Providence Silts." *Journal of Geotechnical and Geoenvironmental Engineering*, 134, 37-46.

Bradshaw, A.S. (2006). *Liquefaction Potential of Non-plastic Silts*. Ph.D. Dissertation, Department of Civil Engineering, University of Rhode Island.

Bray, J. D. and Sancio R. B. (2006). "Assessment of the Liquefaction Susceptibility of Fine-Grained Soils." *Journal of Geotechnical and Geoenvironmental Engineering*, 132(9), 1165-1177.

Catanño, J. A. (2006). Stress Strain Behavior and Dynamic Properties of Cabo Rojo Calcareous Sands. M.S. Thesis, Department of Civil Engineering, University of Puerto Rico.

Catanño, J. and Pando, M., (2010). "Static and dynamic properties of a calcareous sand from Southwest PR," *GeoFlorida 2010: Advances in Analysis, Modeling, & Design, Proceedings of the GeoFlorida 2010 Conference*.

Chen, Y., Zhou, Y., and Ke, H. (2008). Shear Wave Velocity-Based Liquefaction Resistance Evaluation: Semi-Theoretical Considerations and Experimental Validations. The 14th World Conference on Earthquake Engineering, October 12-17, 2008, Beijing, China.

Chillarige, A. V., Robertson, P.K., Morgenstern, N.R., and Christian, H. A. (1997). "Evaluation of the in situ state of Fraser River delta sand." Canadian Geotechnical Journal, Vol. 34, pp. 510-519.

De Alba, P., Baldwin, K., Janoo, V., Roe, G., and Celikkol, B. (1984). "Elastic-wave velocities and liquefaction potential." Geotechnical Testing Journal, Vol. 7, No. 2, pp. 77-87

Flynn, W., (1997). A comparative study of cyclic loading responses and effects of cementation of liquefaction potential of calcareous and silica sands." M.S. Thesis, University of Hawaii, Manoa.

Frydman, S., Hendron, D., Horn, H., and Steinbach, J., (1980). "Liquefaction study of cemented sand." *Journal of Geotechnical Engineering Division*, ASCE, Vol. 106, No.3, pp. 275-297.

Guadalupe-Torres, Yaurel (2013). *Unique Relationship between Small Strain Shear Modulus and Effective Stresses at Failure*. Ph.D. Dissertation, Department of Civil Engineering, University of Rhode Island.

Hanchar, Scott T. (2006) *A comparison of Bender Elements and Torsional Shear Wave Transducers*. Master's Thesis, Department of Ocean Engineering, University of Rhode Island.

Hyodo, M., Hyde, A.F.L. and Aramaki, N., (1996). "Cyclic strength and deformation of crushable carbonate sand." *Soil Dynamics and Earthquake Engineering*, 15, 1996, pp. 331-336.

Huang, Y.-T., Huang, A.-B., Kuo, Y.C., Tsai, M.-D. (2004). "A laboratory study on the undrained strength of a silty sand from central Taiwan." *Soil Dynamics and Earthquake Engineering*, 24, 2004, 733-743.

Idriss, I.M. and Boulanger, R.W., (2008). "Soil liquefaction during earthquakes." EERI-MNO 12, 235 pages.

Juang, C.H, Chen, C.J., Jiang T (2001). "Probabilistic Framework for Liquefaction Potential by Shear Wave Velocity." *Journal of Geotechnical and Geoenvironmental Engineering*, 127, 670-678.

Juang, C.H., Jiang, T., Andrus, R.D.(2002). "Assessing Probability-based Methods for Liquefaction Potential Evaluation." *Journal of Geotechnical and Geoenvironmental Engineering*, 128(7), 580-589.

Kaggawa, W.S., Poulos, H.G., and Carter, J.P., (1988). "Response of carbonate sediments under cyclic triaxial test conditions." Engineering for Calcareous Sediments. Proc. Int. Conf. Calcareous Sediments, Perth (eds R.J. Jewell and D.C. Andrews), 1, pp. 97-107. Rotterdam: Balkema

Kayen, et al. (2004). "Global Shear Wave Velocity Database for Probabilistic Assessment of the Initiation of Seismic-Soil Liquefaction." International Conference on Soil Dynamics & Earthquake Engineering, Berkeley, CA, January 7-9, 2004.

Kayen, R., Moss, R.E.S., Thompson, E.M., See, R.B, Cetin, K.O., Der Kiureghian, A., Tanaka, Y., Tokimatsu, K. (2013). "Shear-Wave Velocity-Based Probabilistic and Deterministic Assessment of Seismic Soil Liquefaction Potential." *Journal of Geotechnical and Geoenvironmental Engineering*, Vol. 139, No. 3, pp. 407-419

Kramer, S.L., Geotechnical Earthquake Engineering, Publ. Prentice Hall, 1996

Kumar, J. and Madhusudhan, B.N. (2010). "A note on the measurement of travel times using bender and extender elements." *Soil Dynamics and Earthquake Engineering* 30 (2010), 630-634.

Ladd, R.S., "Preparing Test Specimens Using Undercompaction" *Geotechnical Testing Journal*, GTJODJ, Vol. 1, No. 1, March 1978, pp. 16-23

Lee, J-S., and Santamarina, J.C. (2005). "Bender elements: Performance and signal interpretation", *Journal of Geotechnical and Geoenvironmental Engineering*, 131(9), 1063-1070.

Liu, Jungang. (2012) *Liquefaction Resistant on Monterey No. 0/30 Sand*. M.S. Thesis. Department of Civil Engineering, University of Colorado, Denver.

Mao, X. and Fahey, M., (2003). "Behaviour of calcareous soils in undrained cyclic simple shear." Geotechnique, Vol. 53, No. 8, pp. 717-727

Marcuson, W.F., III (1978). "Definition of terms related to liquefaction." *Journal of Geotechnical Engineering Division*, ASCE, 104(9), 1197-1200.

Morioka, Brennon T. (1999). *Evaluation of the Static and Cyclic Strength Properties of Calcareous Sand using Cone Penetration Tests*. Ph. D. Dissertation. Department of Civil Engineering, University of Hawaii.

Mulilis, et al (1977). "Effects of Sample Preparation on Sand Liquefaction." *Journal of Geotechnical Engineering*, 103, 91-108.

Paydar, A.N. and Ahmadi, M.M. (2013). The effect of fines type on correlation between shear wave velocity and liquefaction resistance of sand containing fines, 18th International Conference on Soil Mechanics and Geotechnical Engineering, Paris, France, 1415-1418.

Robertson, P.K. (1994). Suggested Terminology for liquefaction, 47th Canadian Geotechnical Conference, Halifax, Canada, September, 277-286.

Robertson, P.K., Sasitharan, S., Cunning, J.C., Sego, D. C. (1995) "Shear-wave Velocity to Evaluate In-situ State of Ottawa Sand." *Journal of Geotechnical Engineering* 1995, 121: 262-273.

Robertson, P.K., and Wride, C.E. (1998). "Evaluating cyclic liquefaction potential using the Cone Penetration Test." *Canadian Geotechnical Journal*, 35(3), 442-459.

Robertson, P.K., Woeller, D. J., and Finn, W. D. L., (1992). "Seismic cone penetration tests for evaluating liquefaction potential under cyclic loading." *Canadian Geotechnical Journal*, Vol. 29, pp. 686-695

Sandoval, E. A., and Pando, M.A. (2012). "Experimental assessment of the liquefaction resistance of calcareous biogenous sands." *Earth Sciences Journal*. Vol. 16, No. 1, pp. 55-63

Seed, H.B. (1979). "Soil liquefaction and cyclic mobility evaluation for level ground during earthquakes", *Journal of Geotechnical Engineering Division*, 105(GT2), 201-225.

Seed, H.B., and Idriss, I.M (1971). "Simplified procedure for evaluating soil liquefaction potential." *Journal of Soil Mechanics and Foundations*. 97(9), 1249-1273.

Seed, H.B., Tokimatsu, K., Harder, L.F., and Chung, R.M. (1985). "The influence of SPT procedures in soil liquefaction resistance evaluations". *Journal of Geotechnical Engineering*, 111(12), 1425-1445.

Semple, R.M. (1988). "The Mechanical Properties of Carbonate Soils." Proceedings, International Conference on Calcareous Sediments, Perth, West Australia, 807-836.

Sharma, S.S., and Ismail, M.A., (2006). "Monotonic and cyclic behavior of two calcareous soils of different origins." Journal of Geotechnical and Geoenvironmental Engineering, ASCE Vol. 132, No. 12, pp. 1581-1591.

Silver, M.L., Chan, C.K., Ladd, R.S., Lee, K.L., Tiedemann, D.A., Townsend, F.C., Valera, J.E., Wilson, J.H. (1976). Cyclic Triaxial Strength of Standard Test Sand. Journal of Geotechnical Engineering Division, ASCE. Vol. 102, No. GT5, May 1976, pp. 511-523.

Tokimatsu, K., Yamazako, T., and Yoshimi, Y. (1986). "Soil liquefaction evaluations by elastic shear moduli." *Soils Foundation*, Vol. 26, No. 1, pp.25-35

Tokimatsu, K., and Uchida, A. (1990). "Correlation between liquefaction resistance and shear wave velocity." *Soils and Foundations*, 30(2), 33-42.

Wang, J. H., Moran, K., and Baxter, D.P. (2006). "Correlation between the Shear Wave Velocity and the Liquefaction Resistance of Offshore Saturated Sands and Silts." *Journal of Geotechnical and Geoenvironmental Engineering* 2006, 132, 1574-1580.

Youd, et al (2001). "Liquefaction Resistance of Soils: Summary Report From the 1996 NCEER and 1998 NCEER/NSF Workshops on Evaluation of Liquefaction Resistance of Soils." *Journal of Geotechnical and Geoenvironmental Engineering*, April 2001, 127, 297-313.

Yunmin, C., Han, H. and Ren-peng, C. (2005). "Correlation of shear wave velocity with liquefaction resistance based on laboratory tests." *Soil Dynamics and Earthquake Engineering* 25 (2005) 461-469.

Zhou, Y.-G., Chen, Y.-M., and Ke, H. (2005). "Correlation of liquefaction resistance with shear wave velocity based on laboratory study using bender element." J. Zhejiang Univ., Sci, 6A (8), 131-145.

Zhou, Y. G., and Chen, Y.M. (2007). "Laboratory Investigation on Assessing Liquefaction Resistance of Sandy Soils by Shear Wave Velocity." *Journal of Geotechnical and Geoenvironmental Engineering*, ASCE, August 2007, 133, 959-972.